Molecular Models in ab Initio Studies of Solids and Surfaces: From Ionic Crystals and Semiconductors to Catalysts†

JOACHIM SAUER

Central Institute of Physical Chemistry, Academy of Sciences, Rudower Chaussee 5, Berlin 1199, German Democratic Republic

Contents

Dr. Sauer was born in Hosena, Germany, in 1949. He graduated from the Department of Chemistry of Humboldt-University in Berlin (German Democratic Republic) and received his Dr. rer. nat. degree (equivalent to Ph.D.) in 1974. He dealt with quantum chemical calculations on electronic and spectroscopic properties as well as on intermolecular interactions of conjugated systems and their radical ions. In 1977 Dr. Sauer joined the Central Institute of Physical Chemistry of the Academy of Sciences of the GDR where he established theoretical research on intermolecular interactions in adsorption and catalytic processes. His favorite subject is zeolites. Beginning in 1978 he spent several periods with Dr. Rudolf Zahradnik and his co-workers at the Heyrovsky Institute of the Czechoslovak Academy of Sciences in Prague. Presently he is heading a research team in applied quantum chemistry. He is broadly interested in nonempirical quantum chemical methods and their application in chemistry with emphasis on two subjects, intermolecular interactions and surface science (adsorption and catalysis). In 1982 Dr. Sauer was awarded the "Friedrich-Wöhler-Preis" of the Chemical Society of the GDR, and in 1985 he received the Dr. sc. nat. degree from the Academy of Sciences of the GDR. He is author or coauthor of 75 scientific papers.

I. Introduction

The tremendous increase of interest in the chemistry and physics of solids and their surfaces is connected with recent progress in advanced technologies. Electronic devices, selective catalysts, and adsorbents, as well as materials designed to meet novel demands, are at the leading edge of these advances. It has become clear that numerous important phenomena are due to deviations from the infinite periodic structure of ideal solids: doping and defects in semiconductors and other types of solids, local interactions in metal–semiconductor systems and metal–support catalysts; structures in amorphous and glassy solids, formation of surface complexes and surface reactions on irregularly distributed sites; and, last but not least, solid-state reactions.

A prerequisite for an advance in this field was the development of highly sophisticated and powerful ex-

---

†Dedicated to Rudolf Zahradník on the occasion of his 60th birthday.

perimental techniques, in particular spectroscopic methods, for investigating solids and their surfaces on a molecular scale. Examples are high-resolution solid-state magic-angle spinning NMR spectroscopy[1,2] and scanning tunnel microscopy (STM, Nobel prize 1986).[3] However, the results obtained have raised many questions at the atomic level that are a major challenge to theoreticians: Which atomic structures produce a given effect? How do local effects show up in bulk properties? What is the geometry of a site of interest and what properties does it have? What is the nature of the bonds between the atoms involved and how large are the forces acting between them? These questions can be answered provided that methods are used that yield reliable total energies and, moreover, reliable energy changes for changed positions of the nuclei. In other words, the methods must yield reliable potentials for the motion of the nuclei.

Quantum chemical ab initio methods[4-9] met such requirements. For molecules in the gas phase, ab initio calculations have become an alternative to experiments for determining accurately structures, vibrational frequencies, and electronic properties as well as intermolecular forces and molecular reactivities.[4-9] It would be most valuable if predictions of local structures and properties of active sites of solids could be made with similar accuracy and reliability, since they are frequently not, or not directly, accessible by experiments. What complicates the application of quantum chemical methods to solid-state problems is, on the molecular scale, the infinite dimension of solids. This complication becomes particularly serious for ab initio techniques.

One way to overcome the difficulties is to adopt finite models such as clusters of atoms or ions, real or hypothetical molecules, that can be treated by the same ab initio methods applied to molecules. This means to confine the explicit treatment to those atoms and interactions of significance for the effect under study but to neglect or to only approximately include influences of the environment by suitably chosen boundary conditions. Hence, this "molecular" approach is particularly suited to tackle local phenomena, e.g. to describe active sites of catalysts or impurity centers in semiconductors, but it also helps to extend knowledge on structure and bonding of crystals and on their bulk properties.[10] It is the subject of this paper.

The molecular approach is alternative to the way solid-state physicists look at the problems (see, e.g., ref 10 and 11). They start from the idea of an ideally periodic solid and exploit the translation symmetry of a crystal. Quantum chemical methods doing the same are named *crystal orbital* (CO) methods.[12] They provide the accurate limit for calculations on finite models and, hence, help to understand the approximations connected with the molecular approach. Unfortunately, CO methods use a language different from the language of molecular orbital (MO) theory well-known to chemists. Hoffmann,[13] however, has recently offered a nice translation. There are two problems with CO calculations. First, they are computationally much more demanding than calculations on finite models. Second, local effects such as impurities or defects must be treated as quasi-periodic assuming rather large pseudo unit cells.

The above requirements are met not only by conventional quantum chemical ab initio methods but also by the most recent variants of density functional methods.[14,15] These "first-principle" methods share with ab initio methods the feature that they avoid empirical relationships or adjustable parameters, but they make different approximations (local density approximation) and, unlike the ab initio methods, their accuracy cannot be improved beyond the limits of this approximation. Nevertheless, they reached a level of sophistication allowing calculation of total energies for molecules[16-18] and solids[11,19-22] with sufficient accuracy to make structure predictions. Hence, density functional methods also solve the class of solid-state problems addressed in this paper. There are examples within both the "molecular" and the "physical" approach. Having no own experience with density functional methods, I do not look at them in the same detail as I look at ab initio methods, and I only try to assess their performance by comparing some results for molecules and solids with ab initio results.

The exclusion of semiempirical methods from this review (except for a few remarks in section III.D) may be criticized. We owe to semiempirical methods much of our skill of selecting models. There is no space for a detailed description, and reference is made to previous reviews.[23-26] Their undoubted success (see ref 13 for a recent example) is limited to the calculation of one-electron energies (ionization potentials, electron affinities, excitation energies), charge distributions, and electronic properties. However, the local structure and local interactions (i.e., nature and properties of the bonds involved) must be known to specify the geometry and the parameters entering a semiempirical calculation. Structure information is obtained in an indirect way only, by calculating the properties of a defect, impurity, or some other site and comparing the results for different models and geometries with observed parameters. Similar remarks apply to the widely used SW–Xα methods[27] as well as to semiempirical band structure calculations of solid-state physics.[10,28-30]

This review starts from the presumption that one would like to perform a quantum chemical calculation on a solid by ab initio methods. Section II gives a short survey of relevant approximations and, on the basis of knowledge for molecules, makes an attempt to convey to the reader what type of results and degree of accuracy he may (or should not) expect from ab initio calculations. Section III explains why the physical approach to solve the problem, the crystal orbital technique, becomes computationally so complicated that it is presently not broadly applicable. In section IV rules are heuristically derived on how to select a good molecular model or cluster model and how to keep boundary effects at a minimum. Use is made of these rules to systematize different suggestions for "embedding" procedures. Sections V–VII give an account of the achievements of ab initio calculations on cluster models and molecular models for different types of solids.

II. Prologue: Ab Initio Computational Methods

Ab initio methods, also called nonempirical methods, provide a solution to the Schrödinger equation on the basis of well-defined approximations such as Born–

Oppenheimer separation, variational principle, and perturbation theory (see, e.g., ref 31) without any empirical data, relationships, or adjustable parameters. Ab initio does not necessarily mean *accurate*, but it is an important feature of ab initio methods that it is known how the approximations can be gradually lifted to approach the accurate limit.

A. Survey of Approximations

The electronic properties of a molecular system and its energy E_R are obtained as a solution of the electronic part of the Schrödinger equation for a configuration $\mathbf{R}$ of the nuclei:

$$\mathcal{H}(\mathbf{r}, \mathbf{R}) \ \Psi_{\mathbf{R}}(\mathbf{r}) = E_{\mathbf{R}}\Psi_{\mathbf{R}}(\mathbf{r}) \qquad \text{(II.1)}$$

The n-particle wave function $\Psi_{\mathbf{R}}(\mathbf{r})$ describes the motion of the electrons in the field of the (fixed) nuclei. Due to the electron–electron interaction term in the Hamiltonian, this equation cannot be solved without large approximations. It is the aim of computational quantum chemistry to suggest approximate methods of solution and to investigate their range of applicability. Almost all procedures rely on the so-called Hartree–Fock (HF) or self-consistent field (SCF) approximation. It assumes that the motion of an electron within the molecular system depends only on the *average* potential of all electrons and it is also known as model of independent particles. The real motions of the electrons, however, as described by the exact wave function are "correlated". The energy difference between the exact result and the Hartree–Fock approximation is called the correlation energy. Inclusion of electron correlation on a reasonable level is much more demanding than a SCF solution. Roughly speaking, for the same system the computational effort is at least 1 order of magnitude larger (vide infra, II.C).

The HF approximation assumes that the n-particle wave function $\Psi(\mathbf{r})$ can be written as an antisymmetrized product of one-electron functions $\psi_i(\mathbf{r}_1)$ (Slater determinant):

$$\Psi(\mathbf{r}_1, \mathbf{r}_2, ..., \mathbf{r}_n) = \frac{1}{\sqrt{n!}} \begin{vmatrix} \psi_1(\mathbf{r}_1) & \psi_2(\mathbf{r}_1) \cdots & \psi_n(\mathbf{r}_1) \\ \vdots & & \\ \psi_1(\mathbf{r}_n) & & \psi_n(\mathbf{r}_n) \end{vmatrix} \quad \text{(II.2)}$$

One-electron functions are called orbitals. If one looks for the set of n orbitals that yields the lowest energy of a molecular system in the sense of the variational principle, one finds that they are determined by the equations

$$F(\mathbf{r}_1) \ \psi_i(\mathbf{r}_1) = E_i\psi_i(\mathbf{r}_1) \qquad \text{(II.3)}$$

called HF equations. The orbitals $\psi_i(\mathbf{r}_1)$ are named molecular orbitals, and the Fock operator, F, is given by

$$F(\mathbf{r}_1) = h(\mathbf{r}_1) + g(\mathbf{r}_1) \qquad \text{(II.4)}$$

The one-electron part $h(\mathbf{r}_1)$ comprises the *differential* operator of the kinetic energy and the potential of the nuclei. The electron–electron interaction term, $g(\mathbf{r}_1)$, takes the form of an effective one-electron operator and describes the mean potential created by the electrons of the system. It consists of two parts, Coulomb and exchange potential, respectively

$$g(\mathbf{r}_1) = j(r_1) - k(\mathbf{r}_1) \qquad \text{(II.5a)}$$

with

$$j(\mathbf{r}_1) = \sum_{k=1}^{n} \int \frac{|\psi_k(\mathbf{r}_2)|^2}{|\mathbf{r}_2 - \mathbf{r}_1|} \, d\mathbf{r}_2 \qquad \text{(II.5b)}$$

and

$$k(\mathbf{r}_1) \ \psi(\mathbf{r}_1) = \delta_{s_k s}\sum_{k=1}^{n} \psi_k(\mathbf{r}_1) \int \frac{\psi_k(\mathbf{r}_2) \ \psi(\mathbf{r}_2)}{|\mathbf{r}_2 - \mathbf{r}_1|} \, d\mathbf{r}_2 \quad \text{(II.5c)}$$

The multiplier $\delta_{s_k s}$ arises from summation over the spin coordinates (which are suppressed in this paper wherever possible). It is 0 when the spin functions belonging to the orbitals ψ and ψ_k are different, and it equals 1 when the same spin function is assigned to both ψ and ψ_k. $j(\mathbf{r}_1)$ and $k(\mathbf{r}_1)$ are *integral* operators that depend on the solutions ψ_k of eq II.3. Hence, the HF equations are *integrodifferential equations* that must be solved iteratively until the potential $g(\mathbf{r}_1)$ is "self-consistent". Their solution by numerical integration is feasible only for highly symmetric potentials. Besides atoms, numerical solutions have been achieved for diatomics only. Even the water molecule still poses a not yet surmounted barrier. Therefore, further approximations are necessary, and virtually all solutions for molecules are based on the so-called *algebraic approximation*. By expansion of molecular orbitals ψ_i into a finite series of basis functions $\chi_i(\mathbf{r})$

$$\psi_i(\mathbf{r}_1) = \chi(\mathbf{r}_1)c_i = (\chi_1(\mathbf{r}_1), \chi_2(\mathbf{r}_1), ..., \chi_m(\mathbf{r}_1))\begin{pmatrix} c_{1i} \\ c_{2i} \\ \vdots \\ c_{mi} \end{pmatrix} \quad \text{(II.6)}$$

the integrodifferential equations in (II.3) are transformed into matrix equations (Roothaan equations)[32]

$$\mathbf{FC} = \mathbf{SCE} \qquad \text{(II.7)}$$

with the Fock and overlap matrices

$$\mathbf{F} \equiv \langle \chi | F\chi \rangle \qquad \mathbf{S} \equiv \langle \chi | \chi \rangle \qquad \text{(II.8)}$$

(We use brackets $\langle | \rangle$ as short-hand notation for integration over the coordinates of an electron, $\mathbf{r}_1$.) The HF solutions are given as m column vectors $\mathbf{c}_i$ of coefficients referring to a chosen basis set χ:

$$\mathbf{C} = (\mathbf{c}_1, \mathbf{c}_2, ..., \mathbf{c}_m) \qquad E_{ij} = E_i\delta_{ij} \qquad \text{(II.9)}$$

The one-electron density function, $\rho(r)$, is represented for this basis set by the matrix

$$\mathbf{R} = \sum_{k}^{n}\mathbf{c}_k\mathbf{c}_k^{+} \qquad \text{(II.10)}$$

where the summation is over all orbitals k occupied in the electronic state considered. The Fock matrix attains the form

$$F_{\mu\nu} = \langle \mu | h\nu \rangle + G(\mathbf{R})_{\mu\nu} \qquad \text{(II.11)}$$

with the two-electron part

$$G(\mathbf{R})_{\mu\nu} = \sum_{\rho}\sum_{\sigma}R_{\rho\sigma}[\langle \mu\nu|\rho\sigma \rangle - \langle \mu\rho|\nu\sigma \rangle] \quad \text{(II.12)}$$

The analytical form of the basis functions is chosen such that differentiation and integration can be easily done analytically. Boys[33] opened the area of modern computational quantum chemistry when he suggested atom-centered Gaussian-type functions (GTF):

$$g(\alpha, A, l) = N_{\alpha,l} x_A{}^i y_A{}^j z_A{}^k e^{-\alpha r_A^2} \qquad (II.13)$$

(A refers to the atom, $i + j + k = 0$ for s-type functions, 1 for p-type functions, ...)

From the computational point of view the bottleneck is now the large number (millions for a small molecule, but billions for a typical case considered in this review) of integrals over the basis function that have to be computed, stored, and reread in each iteration.

$$\langle \mu\nu|\rho\sigma \rangle = \int \chi_\mu{}^*(\mathbf{r}_1)\, \chi_\nu(\mathbf{r}_1)\, \frac{1}{r_{12}}\, \chi_\rho{}^*(\mathbf{r}_2)\, \chi_\sigma(\mathbf{r}_2)\, d\mathbf{r}_1\, d\mathbf{r}_2$$

$$(II.14)$$

Formally, their number grows as m^4 (in practice less). Hence, m should be as small as possible. One generally accepted way to achieve this is the use of fixed linear combinations of several GTF as basis functions in molecular calculations.

$$\chi_\mu(\mathbf{r}_1) = \sum_j c_{j\mu} g_j(\mathbf{r}_1) \qquad (II.15)$$

The coefficients of the "primitives" in these "contracted" GTF (CGTF) are transferred from calculations on atoms. Moreover, much effort is directed (i) to reduce for a given expansion the number of integrals to be stored and (ii) to find for a given purpose an optimal expansion as short as possible. Most basis sets are derived in atomic calculations due in part to the chemists' feeling that in molecules one can still identify slightly distorted atoms pointing to the historical root of the algebraic approximation, namely the LCAO expansion (linear combination of atomic orbitals).

Since selection of an appropriate basis set is critical for an ab initio study to be successful, a short account will be given of the classification and performance of basis sets. A basis set is called "minimal" (MB) if a single CGTF is employed for each type of atomic orbital occupied in the ground state of the respective atom. If more than one function is employed for each atomic orbital, the basis set is named "double ζ" (DZ), "triple ζ" (TZ), and so on. This nomenclature originates from the use of Slater-type orbitals (STO) having the radial dependence $r^{-\zeta r}$ as basis sets. A DZ basis set employs two different ζ exponents to describe, e.g., a 1s orbital. Consequently, minimal basis sets are also named single-ζ (SZ). Since inner shells are little affected by ordinary chemistry, effective basis sets use only one CGTF for the inner shell but two CGTF for the valence-shell orbitals. They are called split-valence (SV) or valence double-ζ (VDZ) basis sets. A significant gain in flexibility is achieved by inclusion of polarization functions in the basis set. Polarization functions correspond to atomic orbitals with higher azimuthal quantum numbers than those corresponding to atomic orbitals occupied in the ground states of atoms. A typical case is the "double-ζ plus polarization" (DZP) set that includes d functions on first- and second-row atoms, e.g., on C or Si, and p functions on H (see, e.g., ref 34). Its composition, according to common notation, is [6, 4, 1/4, 2, 1/2, 1] where the number of contracted s, p, d functions are given and specifications for atoms from different periods of the periodic table are made in decreasing order separated by a slanted stroke. Particularly widespread are the basis sets suggested by the Pople group:[7] STO-3G (minimal), 3-21G and 4-31G (split-valence), 6-31G* and 6-31G** (split-valence

augmented by polarization functions; the first star indicates a set of d functions on non-hydrogen atoms while the second star refers to a set of p functions on hydrogen atoms), and 6-311G** (single-ζ core, triple-ζ valence and polarization functions on all atoms). The STO-3G(*) and 3-21G(*) sets have sets of d functions added to second-row (or higher) elements only. In notations like 3-21+G or 6-31++G** the first plus stands for an additional set of diffuse s and p functions on non-hydrogen atoms while the second plus refers to a diffuse s Gaussian on hydrogen. In the STO-3G set each STO of a minimal set is represented by three primitive GTF, while in the n-k1G sets the CGTF of each core orbital consists of n primitives and the valence shell orbitals are split into one CGTF consisting of k primitives and a single set of GTF. The sp parts of the basis sets from the Pople group have the added constraint that each s Gaussian shares with the corresponding set of the three p_x, p_y, and p_z Gaussians the same exponent ($\alpha_s = \alpha_p$). This is called the "shell structure" and greatly reduces the integral and gradient (vide infra) computation times at the expense of some loss in flexibility.

A survey of basis sets available and specific comments on their selection for a particular problem can be found in reviews of Dunning and Hay,[34] Ahlrichs and Taylor,[35] Huzinaga,[36] and Davidson and Feller.[37]

A substantial reduction of the number of two-electron integrals can be achieved, in particular for elements from higher periods, when in the process considered the core electrons can be assumed as being inert and replaced by an effective core (EC) potential (sometimes also called "pseudopotential" or "model potential"; all three terms will be used as synonyms in this paper). As long as these EC potentials do not contain adjustable parameters and are derived in a nonempirical way, the methods are still "ab initio", although they contain an additional approximation requiring testing. Note that EC potentials should be used together with basis sets specially adapted to them. Details can be found in previous reviews[37,38] in this journal, in particular in Appendix C of ref 38.

To determine bond angles and distances is one of the main tasks of computational quantum chemistry. Powerful methods have been developed[39,40] to locate minima on the energy hypersurface with respect to the nuclear coordinates of a molecule, which correspond to molecular equilibrium structures. These methods require the repeated calculation of the first derivatives of the energy, $E_R = E(X_1, ..., X_{3N})$, with respect to the nuclear coordinates of the N nuclei chosen here as the full set of $3N$ Cartesian coordinates:

$$g_i(X_1, ..., X_{3N}) = \partial E(X_1, ..., X_{3N})/\partial X_i \quad (II.16)$$

In early days of computational quantum chemistry the gradient components, g_i, had to be evaluated by numerical differentiation, i.e., as finite differences between energy values calculated for small displacements, Δ, of the nuclear coordinates from the reference structure, X^e, and the energy value of the reference structure:

$$g_i \approx [E(X_i = X_i{}^e + \Delta) - E(X_i = X_i{}^e)]/\Delta \quad (II.17)$$

Starting with the work of Pulay, analytical formulas were derived for calculation of gradients and, subsequently, also of higher derivatives of the energy (see reviews in ref 39, 41, and 42 and the references therein).

TABLE 1. Typical Results for Molecular Geometries and Vibrational Frequencies

	SCF approximation			correlation included/	
	MB	SV/DZ	DZP	large basis sets	ref
bond distances[a,b]	(+) 5	(-) 2	(-) 2	0.3-0.5	49[c]
bond angles[a]	10	5[d]	3	1	49[c]
	STO-3G	3-21G	6-31G*	MP2/6-31G*	ref
distances[a] (A-H/A-B)[e]					
A,B first-row atoms only[e]	2.3/3.1	1.1/2.4	1.2/2.8	0.9/2.3	50, 51
A,B up to second-row atoms[e]	5.2/6.2	1.6/6.7	1.4/2.2		52, 53
A,B up to third- and fourth-row atoms[e]	6.7/4.1	4.0/10.4			54
angles[a]					
first-row atoms only	3.1	2.1	1.4	1.4	50, 51
up to second-row atoms	2.1	1.6	1.3		52, 53
	MINI-1	3-21G	6-31G*	MP2/6-31G*	ref
harmonic freq.[f] %	7.3[g]	12[h]	11-13	8	55, 56
harmonic freq.[j] %	4.6[g]	7.5[h]	8-11	5	56

[a] Mean absolute deviation (picometers, degrees) from experiment. [b] The sign in parentheses indicates a tendency to overestimate (+) or to underestimate (-) the bond distance. [c] Cf. ref 37. [d] Larger errors for lone-pair atoms. [e] The first entry refers to A-H bonds; the second entry, separated by a slanted stroke, to A-B bonds. [f] Mean relative deviation from observed frequencies (percent). [g] Data from ref 57 and 58. [h] Data from ref 55. [j] Mean relative deviation (percent) from experimental *harmonic* frequencies.

The advantages of analytical derivative methods are increased numerical precision and increased computational efficiency. For example, the time required for the analytical evaluation of all gradient components is equal, within a factor of 2 or 3, to the time needed to calculate the SCF energy. For special types of basis sets, e.g., the 3-21G set, vide infra, efficient codes are available[43,44] that yield the gradients in a time equal or less than the time needed to compute the SCF energy.[40] In contrast, numerical differentiation (eq II.17) requires the computation of $3N - 6$ SCF energies. For a ten atomic molecule this means a computation time 8-24 times longer than that of the analytical derivative methods.

Analytical derivatives also greatly facilitate the calculation of vibrational spectra.[45,46] The harmonic force constants f_{ij} are defined as second derivatives of the energy with respect to the Cartesian coordinates at the equilibrium position $\mathbf{X}_e$:

$$f_{ij} = \left.\frac{\partial^2 E(X_1, ..., X_{3N})}{\partial X_i \, \partial X_j}\right|_{X=X_e} \quad (II.18)$$

They can be either computed directly from analytical formulas for the second derivatives (which are available in the more advanced quantum chemical programs like GAUSSIAN86,[44] CADPAC,[47] and HONDO 6.5[48]) or readily obtained as finite differences of analytically determined gradients.

$$f_{ij} \approx [g_i(X_j = X_j^e + \Delta) - g_i(X_j = X_j^e)]/\Delta \quad (II.19)$$

While analytical gradient calculations are almost always feasible as long as the computer resources available allow one to carry out the energy calculation, this is no longer true for analytical second-derivative calculations. Computational times for a single run may become prohibitively long, and additional space on disk is necessary.

B. Typical Results of SCF Calculations for Molecules

That the results calculated by a series of basis sets of increasing size converges against the HF limit (i.e., the result obtained by solving eq II.3 exactly) is true only for sufficiently long expansions. In contrast, for
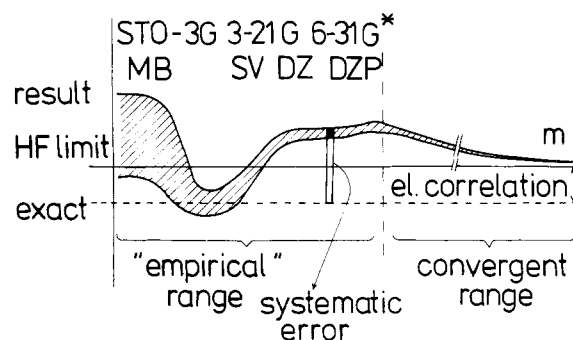

Figure 1. Error of ab initio HF results (e.g., bond lengths) as function of the number of basis functions, m. (Note, however, that for any basis set the energy is above the HF limit.)

basis sets of limited size that one can only afford to employ in many applications, there is no regular dependence of the result on the size of basis set (cf. Figure 1). Rather, due to error compensation, different basis sets perform differently for different purposes. Hence, there is an "empiric" range where the qualification of the user comes into play. In the best case, deviations from the HF limit or experimental results are systematic and increments can be deduced to make reliable predictions in other cases.

This is not the place to analyze the performance of basis sets in SCF calculations in general. We will rather offer a short account of what we have gathered from several compilations and our own experience. Table 1 attempts to summarize typical results of SCF calculations for the prediction of structures and vibrational frequencies using minimal (MB), double-ζ or valence double-ζ (DZ/SV), and polarized basis sets (DZP). While in the upper part of the table we quote what has been gathered from a large number of calculations for a broad variety of basis sets,[37,49] in the lower part we add specific information for Pople's basis sets. Minimal basis sets are connected with a rather large uncertainty, but different basis sets behave differently. While STO-3G is pretty good for molecules containing first-row atoms, it gets increasingly worse when higher elements are present. The MINI-1 basis set from Huzinaga's laboratory[59-62] yields bond distances that are systematically too long by 4.5-7.5% and 5-10% for A-H and A-B bonds, respectively (mean absolute de-

viations 7.5 and 11.5 pm for A–H and A–B bonds, respectively).[59-62,57] Moreover, it yields excellent bond angles. There are also indications,[57-62] though evidence is not too extended, that it can compete with the 3-21G basis set in vibrational frequency calculations. Qualitatively correct geometries and vibrational frequencies can be obtained at the SCF level provided that a carefully chosen DZP basis set is used. The economic and popular 6-31G* basis set is defined for first- and second-row elements only and is not completely satisfactory. It is typical for polarized basis sets that too short bond distances and too large harmonic vibrational frequencies are obtained at the SCF level.

As far as the charge distribution is concerned, dipole moments are too large at the SCF level, typically 10–30% for DZP basis sets (mean absolute deviation 0.35 D).[63] For minimal basis sets mean absolute deviations of 0.65 D have been observed.[63] However, due to fortunate error compensation some minimal basis sets may yield much better results. For example, dipole moments calculated with the STO-3G basis set are nearly as close to experimental data as are 6-31G* results.[7] Nonpolarized SV or DZ basis sets are not recommended; they tend to overestimate the charge separation and yield too large dipole moments.

Among energy data, ionization potentials rank high in solid-state theory as they are directly connected with concepts of bonding and electronic properties of solids. A wealth of experimental data is available. Most frequently, calculations are based on Koopmans' theorem, which equates (for closed-shell systems only[64,65]) the ionization energies with the negative of the orbital energies. Under this assumption typically too high values are obtained provided that sufficiently extended basis sets, e.g., DZP, are used, while too low values result if an independent SCF calculation is performed for the cation (reorganization effect).[6] The reorganization effect is partially cancelled (frequently, not always) by the correlation effect. Hence, rather large errors (up to 1–2 eV) may be met for ionization energies calculated at the SCF level, in particular when minimal or nonpolarized basis sets are used.

For reaction energies, reliable results (±20 kJ/mol) can be expected at the SCF level only when the reaction preserves the number and type of electron pairs as well as the spatial arrangement of the nearest-neighbor pairs.[66] To this class belong the so-called isodesmic reactions (retention of the number of bonds of a given formal type) and protonation or deprotonation processes.[6] An example of an isodesmic reaction is the condensation reaction

$$2 \text{-(-O)}_3\text{SiOH} \rightarrow \text{-(-O)}_3\text{SiOSi(O-)}_3 + \text{H}_2\text{O}$$
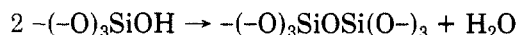
which plays an important role in the chemistry of silica and zeolites and has been recently studied by SCF calculations (6-31G* basis set).[67] Deprotonation energies of hydroxyl groups on surfaces of zeolites and related catalysts have been calculated by SCF methods and used as a measure of their Brönsted acidity[68,69] (cf. section VII.D).

$$\text{-(-O)}_3\text{SiOH} \rightarrow \text{-(-O)}_3\text{SiO}^- + \text{H}^+$$
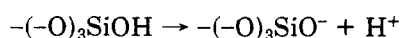
The quoted error of ±20 kJ/mol refers to neglected correlation effects and assumes that at least DZP basis sets are employed (further augmented by diffuse s, p functions if anions are involved). For smaller (SV, DZ)

basis sets the error may increase up to ±80 kJ/mol.[6] Minimal basis sets are not recommended.

C. Electron Correlation

Electron correlation effects, which are neglected in the Hartree–Fock (HF) approximation, can be taken into account by configuration interaction (CI) methods.[31] The exact wave function is constructed as superposition of the HF determinant (cf. eq II.2; a short-hand notation is adopted here specifying diagonal elements only and omitting normalization factors)

$$\Psi^{HF}(\mathbf{r}_1, ..., \mathbf{r}_n) = |\psi_1(\mathbf{r}_1), ..., \psi_i(\mathbf{r}_i), ..., \psi_j(\mathbf{r}_j), ..., \psi_n(\mathbf{r}_n)| \tag{II.20}$$

and all determinants $\psi_{ijk...}^{abc...}$ obtained by substituting an increasing number of occupied molecular orbitals i, j, k, ..., by virtual (unoccupied) orbitals a, b, c, ...

$$\Psi = \Psi^{HF} + \Psi_S + \Psi_D + \Psi_T + \Psi_Q + ... \tag{II.21}$$

S, D, T, Q, ..., label superpositions of all determinants of a given type, i.e., singly, doubly, triply, and quadruply substituted determinants. E.g.

$$\Psi_D = \sum_{i \leq j}^{occ} \sum_{a \leq b}^{uno} C_{ij}^{ab} \Psi_{ij}^{ab} \tag{II.22}$$

with

$$\Psi_{ij}^{ab}(\mathbf{r}_1, \mathbf{r}_2, ..., \mathbf{r}_n) =$$
$$|\psi_1(\mathbf{r}_1), ..., \psi_a(\mathbf{r}_i), ..., \psi_b(\mathbf{r}_j), ..., \psi_n(\mathbf{r}_n)| \tag{II.23}$$

Although the exact solution of the Schrödinger equation, in principle, can always be approached by taking *all possible substitutions* into account, such "full CI" calculations are hardly feasible for systems with more than about 10 electrons and basis sets larger than DZP even in the days of supercomputers.[70,71]

It is the major concern of present-day computational quantum chemistry to find effective methods for treating electron correlation in an approximate way. All the methods rely on some idea of how to make the expansion (II.17) shorter and how to confine it to certain types of substitutions. Inclusion of triples, Ψ_T, is already the frontier of present research. Admittedly, looking from the outside, the broad variety of methods suggested and the vast collection of acronyms in use among quantum chemists are at least as frustrating as all the acronyms used to label highly specialized spectroscopic techniques. As will emerge from later sections of this review, inclusion of electron correlation in ab initio calculations on solid-state problems is still exceptional. We skip therefore a systematic account of the methods available and mention only the most important correlation effects in solid-state and surface studies and common possibilities to treat them. It is useful to distinguish *dynamical* and *nondynamical* correlation effects since they require different approximations.

(1) Nondynamical Correlation Effects. The one-determinant Hartree–Fock ansatz provides a qualitatively wrong picture of the electronic structure. Due to energetical near-degeneracy of two or several determinants, a superposition of them is necessary to obtain a satisfactory zero-order approximation. A textbook example is the wrong dissociation limit that the one-determinant ansatz yields for the homolytic fission of chemical bonds (see, e.g., ref 31). Consider,

for example, a H_2 molecule with atomic orbitals χ_a and χ_b at nuclei H_a and H_b. In the closed-shell HF approximation both electrons are described by the same molecular orbital ψ_1 and differ only by their spin functions, α and β (σ is the spin coordinate):

$$\Psi_1(\mathbf{r}_1, \mathbf{r}_2) = |\psi_1(\mathbf{r}_1)\,\alpha(\sigma_1)\,\psi_1(\mathbf{r}_2)\beta(\sigma_2)| \quad (II.24)$$
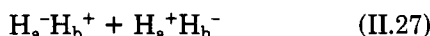
The orbital expansion coefficients (cf. eq II.6) are given by symmetry.

$$\psi_1(\mathbf{r}) = c_1(\chi_a(\mathbf{r}) + \chi_b(\mathbf{r})) \quad (II.25)$$

Substituting eq II.25 into eq II.24 yields (neglecting the spin part and normalization constants)

$$\Psi_1(\mathbf{r}_1, \mathbf{r}_2) = \chi_a(\mathbf{r}_1)\,\chi_a(\mathbf{r}_2) + \chi_b(\mathbf{r}_1)\,\chi_b(\mathbf{r}_2) +$$
$$\chi_a(\mathbf{r}_1)\,\chi_b(\mathbf{r}_2) + \chi_b(\mathbf{r}_1)\,\chi_a(\mathbf{r}_2) = \Phi^{ion} + \Phi^{cov} \quad (II.26)$$

I.e., the HF wave function gives equal weight to situations that may be described as "ionic"

$$H_a^-H_b^+ + H_a^+H_b^- \quad (II.27)$$

$$\Phi^{ion} = \chi_a(\mathbf{r}_1)\,\chi_a(\mathbf{r}_2) + \chi_b(\mathbf{r}_1)\,\chi_b(\mathbf{r}_2)$$

and as "covalent".

$$\dot{H}_a\dot{H}_b + \dot{H}_b\dot{H}_a \quad (II.28)$$

$$\Phi^{cov} = \chi_a(\mathbf{r}_1)\,\chi_b(\mathbf{r}_2) + \chi_b(\mathbf{r}_1)\,\chi_a(\mathbf{r}_2)$$

While this appears to be a fair representation of a chemical bond close to its equilibrium distance, it qualitatively fails for two hydrogen atoms at large distance, I, which are described by Φ^{cov} alone:

$$\dot{H}_a\cdots\dot{H}_b$$
$$I$$

Since, with infinite separation, the energy of (II.27) is higher than that of (II.28) (by the sum of the ionization potential and the electron affinity), the HF one-determinant ansatz greatly overestimates the dissociation energy and the potential curve ends at an incorrect state. The HF problem (II.7) has another solution also given by symmetry:

$$\psi_2(\mathbf{r}) = c_2(\chi_a(\mathbf{r}) - \chi_b(\mathbf{r})) \quad (II.29)$$

This "antibonding" orbital may be used to construct a determinant

$$\Psi_2(\mathbf{r}_1, \mathbf{r}_2) = |\psi_2(\mathbf{r}_1)\alpha(\sigma_1)\,\psi_2(\mathbf{r}_2)\beta(\sigma_2)| \quad (II.30)$$

that is "doubly substituted" with respect to ψ_1. Substituting (II.29) in (II.30) shows

$$\Psi_2 = \Phi^{ion} - \Phi^{cov} \quad (II.31)$$

At large distances, ψ_2 becomes energetically degenerate with ψ_1 and the proper ground state, Φ^{cov}, is obtained as

$$\Phi^{cov} = \Psi_1 - \Psi_2 \quad (II.32)$$

At arbitrary distances, the optimum mixture of covalent and ionic contributions can be found from the two-configuration ansatz.

$$\Psi = C_1\Psi_1 + C_2\Psi_2 = C^{cov}\Phi^{cov} + C^{ion}\Phi^{ion} \quad (II.33)$$

Instead of solving for the optimum coefficients C_1 and C_2 in (II.30), it is also possible to make the equivalent two-configuration ansatz

$$\Psi^{GVB}(\mathbf{r}_1, \mathbf{r}_2) =$$
$$|\phi_1(\mathbf{r}_1)\,\alpha(\sigma_1)\,\phi_2(\mathbf{r}_2)\,\beta(\sigma_2)| + |\phi_2(\mathbf{r}_1)\,\alpha(\sigma_1)\,\phi_1(\mathbf{r}_2)\,\beta(\sigma_2)|$$
$$(II.34)$$

and to solve for the optimum orbitals

$$\phi_1(\mathbf{r}) = c_{1a}\chi_a(\mathbf{r}) + c_{1b}\chi_b(\mathbf{r}) \quad (II.35a)$$

$$\phi_2(\mathbf{r}) = c_{2a}\chi_a(\mathbf{r}) + c_{2b}\chi_b(\mathbf{r}) \quad (II.35b)$$

Ψ^{GVB} includes both Φ^{cov} and ψ_1 as special cases. At infinite distance the optimum orbitals are just $\phi_1 = \chi_a$ and $\phi_2 = \chi_b$ and $\Psi^{GVB} \to \Phi^{cov}$. Forcing ϕ_1 and ϕ_2 to be equal yields $\Psi^{GVB} = \Psi_1$. Applications of the variational principle to (II.34) and (II.35) leads to HF-like equations, and the computational problems are similar as described in section II.A. The method is known as the two-configuration SCF or generalized valence-bond (GVB) method.[72] It can be found in recent versions of standard ab initio programs like GAUSSIAN86[44] and HONDO 6.5.[48]

As the H_2 example shows, HF calculations are not capable of providing potential surfaces for processes involving breaking and/or formation of chemical bonds. For such purposes, the GVB and other multiconfiguration SCF (MC-SCF) methods are the proper choice.[73] As long as one is interested in a *qualitatively* correct description only, small polarized basis sets, e.g., DZP, or even nonpolarized split-valence basis sets, e.g., 3-21G, may be employed. Combined with gradient techniques and methods for localizing stationary points on hypersurfaces, small basis set MCSCF calculations proved very powerful tools for qualitative studies of potential surfaces.[74] An example for the use of a multideterminant wave function to describe surface reactions is provided by the ab initio study[75] of the symmetric path for the dissociative chemisorption of H_2 on a defect of the MgO surface (cf. Table 16). A DZ basis set was employed.

A similar failure of the one-determinant HF method has been observed in the description of the Si(111) and Si(100) electronic surface states (cf. section VI).[76-79] Let us consider[76] two atoms of the Si(111) surface, IIa,
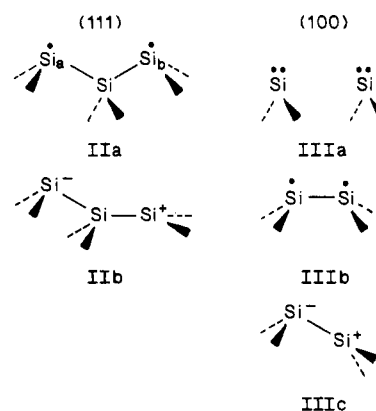
and of the Si(100) surface, IIIa, the latter, however, after formation of a surface bond between pairs of surface atoms, IIIb. In both cases we have two weakly overlapping orbitals each occupied with one electron, just the biradicaloid situation of almost dissociated H_2, I. For both structures the one-configuration HF method will yield a too high energy due to contamination of the wave function with an energetically unfavorable ionic contribution. Moving one surface atom up and the other down creates structures IIb and IIIc, whose optimum wave functions are more ionic. (A planar geometry about Si favors the cation, while stronger pyramidalization favors the anion.) Hence, when within

a one-determinant HF calculation the surface atoms are allowed to relax, the fixed ionic component of the wave function favors structures like IIb and IIIc. The point is that such a finding may be an artefact of the one-determinant ansatz and need not persist when nondynamical correlation is included by a GVB treatment. Indeed, calculations on Si(111)[78,79] and Si(100)[77] surface models have shown that the electronic ground state of these surfaces has singly occupied orbitals on each surface atom spin-paired to an overall singlet state.

A third example of the same Hartree–Fock pathology (two or more orbital configurations become energetically degenerate) is the mixing of $3d^{n+1}4s^1$ and $3d^n4s^2$ configurations of transition-metal atoms when forming a bond with hydrogen atoms[80,81] or with ligands.[81,82] In spite of some promising developments (e.g., the CASSCF-CCI method by Siegbahn et al.;[83-85] cf. ref 81), transition-metal systems are still a "challenge"[86] for quantum chemistry and routine methods are not available.

(2) Dynamical Correlation Effects. The HF determinant is a good zero-order approximation. This type of correlation makes minor corrections to the HF results of molecular geometries, force constants, molecular properties, or ionization and excitation energies. A typical dynamical correlation effect is the dispersion energy, a contribution to intermolecular bonding not obtained at the HF level. Although the dispersion energy is very small compared with the total energy of interacting subsystems, it is responsible for the van der Waals bond between rare-gas atoms and nonpolar molecules and contributes also significantly to other types of intermolecular bonding, e.g. hydrogen bonds. Hence, HF calculations should not be expected to yield reliable stabilization energies for rare-gas, ionic or molecular crystals (cf. section V). There are indications[87-89] that dispersion energy is also involved in the binding of molecules onto metal surfaces.

Economic methods are available for coping with dynamical correlation effects[8,9] that focus on the dominant contribution coming from doubly substituted determinants: configuration interaction including (single and) double substitutions, CI-(S)D; coupled pair functional,[90] CPF; coupled electron pair approximation,[90] CEPA and Møller–Plesset perturbation theory.[91] The latter includes only double substitutions up to second or third order (MP2, MP3) while in the fourth order also singles, triples, and quadruples may be included (SDTQ-MP4). More advanced methods start from a multideterminant wave function built from MCSCF orbitals (vide supra) and consider all determinants that are singly or doubly substituted with respect to *all* determinants in the multideterminant wave function. This leads to the general MCSCF-MRCI (multireference configuration interaction) scheme, which accounts for both nondynamical and dynamical correlation and is almost equivalent to full CI. The MCSCF part is also comparably expensive. There are, however, some approximate schemes that have gained practical importance: GVB-CI (Goddard et al.[76]) has been used in model studies on semiconductors;[77,78] CASSCF-CCI (Siegbahn et al.[83-85]) has been employed to study the bonding of transition-metal atoms to various ligands;[81,82] MRD-CI of Buenker and Peyerimhoff[92,93] (which avoids the MCSCF step and works with the one-configuration

HF orbitals) has met considerable success in calculating electronic excitation energies. It is important to note that the description of dynamical correlation effects requires much larger basis sets than SCF solutions do. Polarization functions are absolutely mandatory. In contrast to multiconfiguration calculations for qualitative purpose (vide supra), calculations that aim at dynamical correlation effects but employ nonpolarized basis sets as occasionally found in literature are simply meaningless.

In spite of the fact that going beyond the HF approximation and taking electron correlation into account, even in an approximate way, is computationally very demanding, for molecules, calculations at the correlated level are going to become routine now. The simplest approximation to the (dynamical) correlation energy, $E_{corr}^{(2)}$, is provided by the Møller–Plesset perturbation theory up to the second order (MP2):[91]

$$E_{corr}^{(2)} = \sum_{\substack{ij \\ ab}} \frac{\langle ia|jb\rangle[2\langle ia|jb\rangle - \langle ib|ja\rangle]}{E_i + E_j - E_a - E_b} \quad \text{(II.36)}$$

The expression refers to a closed-shell ground state, i and j being doubly occupied orbitals. The most time-consuming step is the transformation from integrals over basis functions, $\langle \mu\nu|\lambda\sigma\rangle$ (eq II.14), to the integrals over molecular orbitals, $\langle ia|jb\rangle$:

$$\langle ia|jb\rangle = \sum_{\substack{\mu\nu \\ \lambda\sigma}} c_{i\mu}c_{a\nu}c_{j\lambda}c_{b\sigma}\langle \mu\nu|\lambda\sigma\rangle \quad \text{(II.37)}$$

Efficient computer codes are available (GAUSSIAN82,[43] GAUSSIAN86,[44] HONDO/MP,[94,95] HONDO6.5,[48] CADPAC[47]) that yield the MP2 correlation energy in about the same time as the SCF energy and in an even shorter time if explicit use is made of point symmetry in the integral transformation step.[95] Analytical gradients[44,47] (and even analytical second derivatives[47,96]) of the MP2 energy with respect to molecular coordinates are also available in standard programs and facilitate greatly the search for equilibrium structures and the evaluation of vibrational frequencies. It seems that already at the MP2 level rather accurate geometries and harmonic vibrational frequencies can be obtained (cf. Tables 1 and 3), in particular if sufficiently extended basis sets are used.[96] There is also a substantial improvement of electric multipole moments and intermolecular interaction energies. Moreover, substantial portions of the dispersion energy can already be obtained by the simple MP2 method (see, e.g., ref 97–102 and references therein).

In molecular calculations, MP2 is taking over now the position of "the" standard method of computational quantum chemistry held by the SCF method since the late 1960s. To this role belongs that one knows exactly how to improve the MP2 result in case it fails: taking the double substitutions to higher orders, including higher substitutions (triples, quadruples, and also singles in SDTQ-MP4) or switching to a multireference treatment.

D. Density Functional Approach

The computational problems of conventional "Hartree–Fock plus correlation energy" methods of electronic structure calculations, in particular the frustratingly steep increase in computer requirements

TABLE 2. Examples of ab Initio and Local Density Approximation Studies Employing Basis Sets of Gaussian-Type Functions (Units: Bond Distances (R), pm; Bond Angles, deg; Harmonic Vibrational Frequencies ($\tilde{\nu}$), cm^{-1}; Energies (D_e and ΔE), kJ/mol)

local density approximation			ab initio method		
system; basis set[a]	parameter	result[b]	system; basis set[a]	parameter	result: HF/beyond HF
$H_3SiOSiH_3$[128]	R(Si–O)	164.2 (163.4)[b]	$H_3SiOSiH_3$[129–131]	R(Si–O)	163.2/165.5[d]
GTO (25)[c]	∠Si–O–Si	142.5 (144.1)[b]	6-31G*	∠Si–O–Si	143.7/135.0[d]
			$H_3SiOSiH_3$[130,131]	R(Si–O)	.../163.7[d]
			6-31G** (2d, 2p)[e]	∠Si–O–Si	.../144.7[d]
H_2O–Cu[133]	R(Cu–O)	200	H_2O–Ni[89]	R(Ni–O)	227/217[h]
(14,10,6,1),[f] DZP	D_e[g]	73	[7,6,4,3/6,5,4,2/4,3]	D_e[g]	12/20[h]
Ni(CO)$_4$[134]	R(Ni–C)	180.5 (182.5)[b]	Ni(CO)$_4$[135]	R(Ni–C)	181.4
[11,8,3/6,4,1]	R(C–O)	113.7 (112.2)[b]	[5,3,3/3,2]	R(C–O)	113.5
	$\tilde{\nu}_{NiC}$	418 (371)[b]		$\tilde{\nu}_{NiC}$	277
	$\tilde{\nu}_{CO}$	2150 (2132)[b]		$\tilde{\nu}_{CO}$	2351
Al_4(3-1)–O[i,124,125]	R[j]	53	Al_{10}(7-3)–O[i,136]	R[j]	76
numerical atomic orbitals	ΔE[k]	8.1	[4,3/4,3]	ΔE[k]	116

^{a} See text for an explanation of the symbols and abbreviations. Basis sets are specified by giving the number of s, p, d, ..., functions in brackets. Square brackets refer to contracted GTFs while parentheses refer to uncontracted (primitive) basis functions. A slanted stroke separates entries for atoms from different periods in descending order. ^{b} Observed values in parentheses. ^{c} 25 GTFs localized on nuclei and bond midpoints; cores replaced by pseudopotentials. ^{d} MP2 results. ^{e} Two sets of polarization functions on all atoms. The McLean/Chandler basis set was used on Si.[132] ^{f} Uncontracted GTF set on Cu. ^{g} Binding energy. ^{h} CI-SD corrected for missing quadrupole substitutions (Davidson). ^{i} Al$_z$(x–y) denotes a cluster of z atoms having x atoms in the first and y atoms in the second layer. ^{j} Distance of the O atom above the Al surface. ^{k} Surface penetration barrier.

TABLE 3. Comparison of Results of the Local Density Approximation (LDA) with ab Initio HF and MP2 Results for Water (Units: Distances, pm; Angles, deg; Dipole Moments (μ), e·a_o; Wavenumbers ($\tilde{\nu}$), cm^{-1})

local density approximation						ab initio					
basis set	functional	R(OH)	∠HOH	μ	ref	basis set	method	R(OH)	∠HOH	μ	ref
4-31G	GL[a]	97.9	111		115	4-31G	HF	94.2	111	0.98	115
4-31G	Xα	97.7	105		113		MP2	97.5	109		44
DZP'[b]	Xα[c]	96.8	105.3	0.80	133	DZP	HF	94.4	106.6	0.86	99, 137
						DZP	MP2	96.2	104.5	0.85	99, 137
TZPP[d]	Xα[e]	97.7	104.7		120	[5,4,2/3,2]	SCF	94.1	106.3	0.80	137
GTF (13)[f]	CA[g]	97.4	105.5	0.74	119	[5,4,2/3,2]	MP2	95.8	104.5	0.78	137
LMTO[h]	VWN[i]	97.1	106.0	0.73	112						
obsd[j]		95.7	104.5	0.73		obsd[j]		95.7	104.5	0.73	

local density approximation					ab initio				
basis set	functional	$\tilde{\nu}_{OH}$[k]	$\tilde{\nu}_{HOH}$[l]	ref	basis set	method	$\tilde{\nu}_{OH}$[k]	$\tilde{\nu}_{HOH}$[l]	ref
DZP'[b]	Xα[c]	3734	1839	133	DZP	SCF	4152	1750	96
					DZP	MP2	3913	1665	96
GTF (13)[f]	CA[g]	3712	1618	119	STO[5,4,2/31]	SCF	4132	1772	138
LMTO[h]	VWN[i]	3680	1590	112	[5,4,2/3,2]	MP2	3859	1641	96
obsd (harmonic)[j,m]		3832	1649		obsd (harmonic)[j,m]		3832	1649	

^{a} Gunnarson-Lundqvist.[107] ^{b} P' denotes flat polarization functions (small exponents). ^{c} α = 0.708 96. ^{d} Triple-ζ Slater-type orbital (STO) basis set augmented by two sets of polarization functions (two p functions for hydrogen, two d functions for all other atoms). ^{e} α = 0.7.[111] ^{f} 13 GTO localized on nuclei and bond midpoints; cores replaced by pseudopotentials. ^{g} Ceperly-Alder.[110] ^{h} Localized muffin tin orbitals. ^{i} Vosko-Wilk-Nusair.[108] ^{j} For reference to observed values, see the quoted theoretical papers. ^{k} Symmetric OH stretch. ^{l} Deformation. ^{m} Harmonic wavenumbers.

with the length of the basis set, is a permanent challenge. Hohenberg and Kohn[103] have shown that the energy of a many-electron system is a unique functional of electron density, $\rho(\mathbf{r})$. Hence, to get the energy one needs not know the many-particle wave function $\Psi(\mathbf{r}_1, \mathbf{r}_2, ..., \mathbf{r}_n)$, but the one-particle density, $\rho(\mathbf{r})$, only. Kohn and Sham[104] have further shown that the density that yields the minimum energy of a given system can be found by solving a single-particle equation with an effective "exchange-correlation" potential, $v_{xc}[\rho(\mathbf{r})]$

$$\{h(\mathbf{r}_1) + j(\mathbf{r}_1) + v_{xc}[\rho(\mathbf{r}_1)]\} \psi_i(\mathbf{r}_1) = E_i \psi_i(\mathbf{r}_1) \qquad (II.38)$$

with

$$\rho(\mathbf{r}) = \sum_i \psi_i(\mathbf{r}) \psi_i^*(\mathbf{r}) \qquad (II.39)$$

Formally, this equation resembles closely the HF equation (II.3) with the Coulomb potential $j(\mathbf{r}_1)$ given

by eq II.5b, but having the HF exchange potential (II.5c) replaced by v_{xc}. The point is, however, that the exact form of the functional of the exchange correlation energy and, hence, also of the exchange-correlation potential, v_{xc}, are *unknown* in general. The local density approximation[103] (LDA) assumes that the exchange plus correlation energy can be expressed as

$$\int \rho(\mathbf{r}) \, \epsilon_{xc}[\rho(\mathbf{r})] \, d\mathbf{r} \qquad (II.40)$$

and a local approximation to the exchange-correlation potential is formally obtained as

$$v_{xc} = \frac{d\rho(\mathbf{r}) \, \epsilon_{xc}[\rho(\mathbf{r})]}{d\rho(\mathbf{r})} \qquad (II.41)$$

Only for simple model systems, however, can an explicit expression be derived for v_{xc}. For the homogeneous electron gas one obtains

$$\mathbf{v_{xc}}(\mathbf{r}) = -\tfrac{3}{2}\alpha \left[\frac{3}{\pi}\rho(\mathbf{r})\right]^{1/3} \qquad (\text{II.42})$$

with $\alpha = {}^{2}/_{3}$. The parameter α was introduced to connect (II.42) with a very similar result, $\alpha = 1$, derived by Slater[105] as a statistical approximation to the exchange potential only. The parameter α is frequently used as adjustable parameter.

Potentials similar to those in (II.38) but allowing different densities for electrons with α and β spins are known as local spin density (LSD) approximation.[106] Various potentials have been proposed over the years, e.g. the potential of Gunnarson and Lundqvist (GL).[107] The most advanced ones are the parametrization of Vosko, Wilk, and Nusair[108] (VWN) and Perdew and Zunger[109] (PZ) of accurate Monte Carlo simulations of the electron gas.[110]

The appealing feature of the LDA approach is that it treats both exchange and correlation effects on an equal footing and requires only to solve one-particle equations with a *local* effective potential. Its limitation is that *the exact potential is not available* and one is forced to work with expressions transferred from simple model systems. This brings an empirical element in such calculations, although they avoid adjustable parameters. Therefore, a clear distinction in terminology seems desirable between the exact-exchange "HF plus electron correlation" approach on the one hand and the LDA or LSD-based approaches on the other hand. The former are known as "ab initio" methods, while for the latter the terminus "first principle" method is widely accepted. Perhaps it is better to be more specific and refer directly to the "density functional" (DF) or to the "local (spin) density approximation" (LDA, LSD).

As far as the computational aspects are concerned we will consider only the most recent developments that have led to methods that allow us to evaluate accurately total energies and geometries of molecular systems. They all expand the one-electron functions $\psi_i(\mathbf{r})$ into a basis set (cf. eq II.6). Besides Slater-type orbitals (STO)[111] and the very peculiar localized muffin tin orbitals (LMTO),[16,112] Gaussian-type functions (GTF, eq II.13) have the largest use.[113-118] It is the use of the latter that now brings density functional methods close to the mainstream of computational quantum chemistry and allows a direct comparison between ab initio and LDA-type calculations. As pointed out in previous paragraphs of this section, the major obstacle in conventional "HF plus correlation energy" calculations is the huge number of four-center two-electron integrals (eq II.14). In the LDA-type methods four-center integrals can be completely avoided by least-squares fitting the one-electron density to auxiliary basis sets of GTF (e.g., ref 113, 117, and 119):

$$\tilde{\rho}(\mathbf{r}) = \sum_{\lambda} a_\lambda \chi_\lambda{}^{(J)}(\mathbf{r}) \qquad (\text{II.43})$$

$$-\tfrac{3}{2}\alpha \left[\frac{3}{\pi}\tilde{\rho}(\mathbf{r})\right]^{1/3} = \sum_{\sigma} b_\sigma \chi_\sigma{}^{(\text{xc})}(\mathbf{r}) \qquad (\text{II.44})$$

This yields for the matrix elements of the Coulomb and exchange-correlation potential

$$J_{\mu\nu} = \langle\mu|\tilde{j}|\nu\rangle = \sum_{\lambda} a_\lambda \langle\mu\nu|\lambda{}^{(J)}\rangle \qquad (\text{II.45})$$

and

$$(V_{\text{xc}})_{\mu\nu} = \langle\mu|v_{\text{xc}}|\nu\rangle = \sum_{\sigma} b_\sigma \langle\mu\nu|\sigma{}^{(\text{xc})}\rangle \qquad (\text{II.46})$$

respectively. Hence, the matrix elements of the LDA one-particle operator (cf. eq II.11 and II.12 for the corresponding HF expressions)

$$F_{\mu\nu}{}^{\text{LDA}} = \langle\mu|h|\nu\rangle + J_{\mu\nu} + (V_{\text{xc}})_{\mu\nu} \qquad (\text{II.47})$$

are built up from three-center integrals

$$\langle\mu\nu|\lambda{}^{(J)}\rangle = \int \chi_\mu{}^*(\mathbf{r}_1)\,\chi_\nu(\mathbf{r}_1)\,\frac{1}{r_{12}}\,\chi_\lambda{}^{(J)}(\mathbf{r}_2)\,d\mathbf{r}_1\,d\mathbf{r}_2$$
$$(\text{II.48})$$

only. Note that it is the nonlocal character of the HF exchange potential (eq II.5c) that prevents a similar expansion in HF calculations.

Having no own experience with LDA/GTF-type calculations, it is difficult to assess the computer requirements in comparison with HF (or MP2) calculations for the same basis set. It may well be that there is no significant difference for small- and medium-sized molecules.[120] It is claimed,[120] however, that LDA methods get the advantage as the size of the system studied increases. The limitation to three-center integrals results in computational work that (formally) grows for LDA methods like m^3 instead of m^4 for HF calculations (m is the number of basis functions). Moreover, it seems that LDA results are less basis set dependent and effects of higher polarization functions (beyond d for first row atoms, beyond p for hydrogen) are negligible.[117,121,122]

Until recently the use of LDA methods for molecular structure determination was limited (i) by difficulties to ensure that the numerical error of the density fits (eq II.43 and II.44) is equally small for different points of the potential surface (see, e.g., ref 123) and (ii) by the lack of expressions for an analytical evaluation of energy gradients that proved exceedingly effective in ab initio molecular structure calculations (cf. section II.A).[39-42] Gradient expressions for LDA total energies have been derived for both STO[120] and GTF[124,125] basis sets. Due to these and other technical developments such as effective core potentials[126] or optimized basis sets,[127] the number of high-quality LDA calculations on molecules employing GTF (or STO) basis sets will rapidly grow and their limits and merits in comparison with conventional ab initio methods will emerge.

Table 2 shows examples of applications of both types of approach (HF and LDA) to the same or a similar problem. Table 3 provides a more specific comparison for the equilibrium structure, the harmonic vibrational frequencies, and the dipole moment of the water molecule. From this table the sensitivity of the results toward details of the calculations (the basis set employed or the specific form of the density functional adopted) can be assessed. It is customary to compare LDA results with HF results. Since, within the conventional ab initio approach, correlation can also be included by the MP2 approximation (cf. section II.C) at little extra expense (about the same as for the HF calculation itself), a fair comparison should consider MP2 results as well.

The equilibrium geometries of 40 molecules have been very recently determined by LDA calculations making use of analytical energy gradients.[120] STO basis sets of triple-ζ quality augmented by two sets of po-

larization functions (two p functions on H, two d functions on all other atoms) were employed. The mean absolute error of bond angles (1–2°) was slightly larger than that observed for HF/6-31G* calculations on the same set of molecules. The mean absolute error in the bond lengths was below 1 pm, which is smaller than the mean absolute error of the HF model. However, as Table 3 indicates, the MP2 model is likely to perform better than LDA for this type of basis set (see also Table 1). When the 4-31G basis set was employed for calculations of the harmonic vibrational frequencies of eight diatomic molecules,[115] the mean error of the HF results was 11% (as typical of SV basis sets; cf. the 3-21G results in Table 1), but it was only 5% for the LDA results. While the HF model tends to yield too short bond distances (cf. Table 1), LDA results show the opposite trend. The MP2 model, however, seems to yield highly accurate geometries provided that only sufficiently extended basis sets are used.[96] Since the accuracy of the harmonic vibrational frequencies is largely due to the accuracy of the equilibrium geometry at which the force constants are evaluated, these trends explain that frequencies are overestimated by the HF model, underestimated by the LDA model, and quite satisfactorily reproduced by extended basis set MP2 calculations. (Comparison should be made with observed *harmonic* frequencies; otherwise, anharmonicity effects may cause an apparent agreement between observed and LDA results.) These trends on bond distances and vibrational frequencies are also illustrated by results for the water molecule (Table 3) and for some diatomic molecules.[139]

The most tempting performance of the LDA model is its ability to provide reasonably accurate bond dissociation energies while the one-configuration HF method fails. In the previous paragraph it was pointed out why. It is also clear from section II.C that MP2 cannot repair this defect. One should be aware, however, that this nice feature of the LDA model depends upon sizable error cancellations between the separate atom and molecular energies. Within the LDA, total energies typically lie above the HF limit and even above the HF result obtained with the same basis set, although it accounts for part of the correlation energy. The largely overestimated energy of the van der Waals bond in the Be_2 dimer[16,116] is a clear indication that such an error compensation need not always work. It would be interesting to see applications of LDA-type methods to van der Waals complexes, e.g. the water dimer. Such a calculation has been recently mentioned, but no energies have been reported.[140] Large-scale HF plus CI-SD calculations predict a weak van der Waals bond for the H_2O–Ni complex[89] (Table 2). In contrast, LDA calculations[133] predict a much stronger bond for the H_2O–Cu complex. It is presently not clear to what extent basis set problems contribute to this difference. The latter calculation uses an uncontracted set of GTF on the Cu atom, which is likely to produce a significant basis set superposition error (cf. section V.C). It has been already mentioned that the success of LDA-type methods relies on subtle error cancellations between exchange and correlation energies. Thus, attempts to evaluate these contributions separately within density functional theory have met with little success. On the one hand, the LDA functional (II.42) (with $\alpha = 1$) was

originally derived by Slater as a statistical approximation to the HF exchange energy.[105] In practice, however, results obtained by this or more advanced exchange functionals (e.g., ref 139) do not converge to the HF limit but effectively account for correlation effects. On the other hand, attempts have been made to find a "correlation-only" functional for a posteriori calculation of the correlation energy, e.g. by eliminating the exchange part from the LSD functional[141,142] (Lie and Clementi;[143] Colle and Salvetti (CS);[144] Stoll, Pavlidou, and Preuss (SPP)[141,142]). The SPP functional has been tested in calculations of diamond[145] and silicon crystals.[146] For diatomic molecules,[147] the SPP correlation approximation leads to a contraction of bond lengths while the experimental values are larger than the SCF prediction (vide supra). The utility of the CS functional[144] has been tested in both molecular (e.g., for generating interaction potentials between water molecules[148]) and solid-state applications[149] (cf. section III.D).

The two recent volumes on ab initio methods in quantum chemistry[8,9] contain three review articles that discuss the theoretical background and molecular applications of LDA-type methods in great detail.[16–18] For additional information, we refer to recent review volumes.[14,15]

In summary, substantial progress is being made with predicting molecular structures and total energies from DF theory. However, it is also obvious that there are significant practical and theoretical problems not mentioned in this paragraph (e.g., the "term and multiplet" problem[17,18]) and justify to make a clear distinction between LDA-type methods and exact-exchange "HF plus electron correlation" ab initio methods. The most serious difficulty is certainly that there is presently no straightforward way to improve the density functional when necessary.

III. "Physical" Approach: Crystal Orbitals

A. Basic Idea

The difficulty in dealing with solids is that in this case the Roothaan equations (II.7) attain infinite dimension, reflecting (on the molecular scale) the infinite extension of crystallites. The expansion of the "molecular" orbitals (eq II.6) extends not only over functions centered on atoms within one elementary cell (index μ) but also over all elementary cells labeled by a triple of integers that count the lattice translations with respect to the reference cell, $\mathbf{l} = (l_1, l_2, l_3)$:

$$\psi_i(\mathbf{r}) = \sum_{\mathbf{l}}^{3N} \sum_{\mu}^{m} c_{\mu i}^{\mathbf{l}} \chi_\mu^{\mathbf{l}}(\mathbf{r}) \qquad (III.1)$$

As N approaches infinity, the direct solution of the equations

$$\sum_{\mathbf{m}}^{3N} \sum_\nu^m (F_{\mu\nu}^{\mathbf{lm}} - E_i S_{\mu\nu}^{\mathbf{lm}}) c_{\nu i}^{\mathbf{m}} = 0 \qquad (III.2)$$

whose dimension is $3N \times m$ is practically impossible. Bloch[150] showed how translation symmetry can be exploited to make the problem tractable. For an ideally periodic solid, at the same point $\mathbf{r}$ in different repeating units, the orbitals differ only by a complex phase factor $e^{i\mathbf{k}\mathbf{l}}$:

$$\varphi_i(\mathbf{r} + \mathbf{1}) = e^{i\mathbf{k}\mathbf{1}}\varphi_i(\mathbf{r}) \qquad \text{(III.3)}$$

Note that

$$\mathbf{1} = l_1\mathbf{a}_1 + l_2\mathbf{a}_2 + l_3\mathbf{a}_3 \qquad \text{(III.4)}$$

is now a lattice vector describing translations in real space. This implies that the wave vector

$$\mathbf{k} = k_1\mathbf{b}_1 + k_2\mathbf{b}_2 + k_3\mathbf{b}_3 \qquad \text{(III.5)}$$

is defined in the reciprocal space (but is not necessarily a vector of the reciprocal lattice). Equation III.3 says that the electron density at the same point of different repeating units is identical:

$$|\varphi_i(\mathbf{r} + \mathbf{1})|^2 = e^0|\varphi_i(\mathbf{r})|^2 \qquad \text{(III.6)}$$

Of course, any proper solution of eq III.2 would show the properties demanded by eq III.3 and III.6. However, to take advantage of translation symmetry, from the very beginning one makes use of "symmetry-adapted" functions as basis functions,[151] i.e., functions belonging to certain irreducible representations of the translation symmetry group. This implies that matrix elements between basis functions belonging to different irreducible representations vanish, a well-known fact for point symmetries of molecules and, e.g., the origin of selection rules in spectroscopy. In the case of crystals, the following combinations represent translation symmetry

$$\chi_\mu^\mathbf{k} = \sum_\mathbf{1} e^{i\mathbf{k}\mathbf{1}}\chi_\mu^\mathbf{1} \qquad \chi_\mu^\mathbf{1} = \chi_\mu(\mathbf{r} - \mathbf{1}) \qquad \text{(III.7)}$$

where the wave vector $\mathbf{k}$ is indicative of different irreducible representations. They are called "Bloch functions". The solutions $\psi_i(\mathbf{r})$ we seek, the "crystal orbitals", are now expanded in $\mathbf{k}$-dependent Bloch functions instead of atomic orbitals in real space. What we have gained is that matrix elements between Bloch functions belonging to different $\mathbf{k}$ vectors vanish, e.g.

$$F_{\mu\nu}^{\mathbf{k}\mathbf{k}'} = \int \chi_\mu^\mathbf{k}(\mathbf{r})\, F(\mathbf{r})\, \chi_\nu^{\mathbf{k}'}(\mathbf{r})\, d\mathbf{r} = \delta_{\mathbf{k}\mathbf{k}'}F_{\mu\nu}^{\mathbf{k}\mathbf{k}} = \delta_{\mathbf{k}\mathbf{k}'}F_{\mu\nu}^{(\mathbf{k})} \qquad \text{(III.8)}$$

As result, the infinitely dimensioned matrix blocks and the secular problem reduces to secular problems, one for each $\mathbf{k}$ vector, resembling that of molecules:

$$\sum_\nu^m (F_{\mu\nu}^{(\mathbf{k})} - E_i(\mathbf{k})\, S_{\mu\nu}^{(\mathbf{k})})c_{\nu i}^\mathbf{k} = 0 \qquad \text{(III.9)}$$

Their dimension is m, the number of CGTF within an elementary cell. If there were only one orbital in the cell, the HF solutions would be entirely given by translation invariance and would be identical with the "symmetry-adapted" orbitals $\chi_\mu^\mathbf{k}$ themselves (eq III.7). In the general case however, there is mixing between different Bloch functions belonging to the same $\mathbf{k}$ vector:

$$\psi_i^\mathbf{k}(\mathbf{r}) = \sum_\mu c_{\mu i}^\mathbf{k}\chi_\mu^\mathbf{k}(\mathbf{r}) \qquad \text{(III.10)}$$

The coefficients $c_{\mu i}^\mathbf{k}$, which determine the crystal orbitals $\psi_i^\mathbf{k}(\mathbf{r})$, are obtained when solving (III.9) for a particular $\mathbf{k}$ vector. Note that we use the $\mathbf{k}$ vector also to label the HF solutions. Hence, i extends over m only. Formally, the HF solutions of the crystal could be expanded like

$$\psi_i^{\mathbf{k}'}(\mathbf{r}) = \sum_\mathbf{k}\sum_\mu c_{i\mu}^{\mathbf{k}'\mathbf{k}}\chi_\mu^\mathbf{k}(\mathbf{r}) \qquad \text{(III.11a)}$$

However, due to symmetry blocking

$$c_{i\mu}^{\mathbf{k}'\mathbf{k}} = \delta_{\mathbf{k}\mathbf{k}'}c_{i\mu}^\mathbf{k} \qquad \text{(III.11b)}$$

Evaluation of electron density requires summation over all the occupied orbitals of each $\mathbf{k}$ subspace.

$$R_{\rho\sigma}^{\mathbf{rs}} = \sum_\mathbf{k}\sum_{i(\mathbf{k})}^{occ} e^{i\mathbf{k}(\mathbf{r}-\mathbf{s})}c_{i\rho}^\mathbf{k}(c_{i\sigma}^\mathbf{k}) \qquad \text{(III.12)}$$

These matrix elements enter the two-electron part $G(\mathbf{R})$ of the Fock matrix (cf. eq II.12), which involves a double sum over all cells in direct space:

$$G(\mathbf{R})_{\mu\nu}^{\mathbf{o}\mathbf{l}} = \sum_\mathbf{r}\sum_\mathbf{s}\sum_\rho\sum_\sigma R_{\rho\sigma}^{\mathbf{rs}}[\langle \mathbf{o}\mu\mathbf{l}\nu|\mathbf{r}\rho\mathbf{s}\sigma\rangle - \langle \mathbf{o}\mu\mathbf{r}\rho|\mathbf{l}\nu\mathbf{s}\sigma\rangle] \qquad \text{(III.13)}$$

$$F_{\mu\nu}^{\mathbf{o}\mathbf{l}} = h_{\mu\nu}^{\mathbf{o}\mathbf{l}} + G(\mathbf{R})_{\mu\nu}^{\mathbf{o}\mathbf{l}} \qquad \text{(III.14)}$$

The Fock matrix elements of a particular $\mathbf{k}$ vector are given as a Bloch sum or over all cells:

$$F_{\mu\nu}^{(\mathbf{k})} = \sum_\mathbf{1} e^{i\mathbf{k}\mathbf{1}}F_{\mu\nu}^{\mathbf{o}\mathbf{l}} \qquad \text{(III.15)}$$

Methods that solve Roothaan equations of type III.9 for solids to get the "crystal orbitals" (eq III.10) that are translation symmetry adapted are called *crystal orbital* (CO) methods or, more explicitly, LCAO-CO methods. For details and references to original papers we refer to the reviews in ref 12 and 152.

B. Difficulties of a Nonempirical Treatment

Compared with the molecular problem, the solution of the Roothaan equations for the solid (eq III.9) is complicated by two facts. The minor problem is that we have to solve them for an infinite number of different wave vectors and that we have to sum over all the solutions (cf. eq III.12) to get the electron interaction potential that enters the Fock operator for any $\mathbf{k}$ vector. In practice, we need only a relatively small finite number.

First, only wave vectors within the first Brillouin zone (BZ) of the reciprocal space yield nonidentical contributions to Bloch sums: If $\mathbf{g}$ is a reciprocal lattice vector defined by $\mathbf{1}\cdot\mathbf{g} = 2\pi n$ where n is an integer, each wave vector may be written as $\mathbf{k} = \mathbf{k}' + n\mathbf{g}$ where $\mathbf{k}'$ is within the first BZ. Hence, $\mathbf{1}\mathbf{k} = \mathbf{1}\mathbf{k}'$.

Second, the number of wave vectors is large but finite. Namely, we can safely assume that a crystallite, in molecular scale, is large, but *finite and periodic* (Born-von Kármán periodic boundary conditions). Finally, the summation over $\mathbf{k}$ vectors is replaced by three-dimensional integration, and the number of k points within the first BZ really needed is determined by practical considerations of the numerical integrations. It turns out that 5-10 points for each dimension will do unless one aims at special features, e.g., very accurate density of states.

The major difficulty, however, of a nonempirical CO calculation is the summation over all interactions in direct space. If the calculation and handling of two-electron integrals $\langle\mu\nu|\rho\sigma\rangle$ is already the bottleneck in molecular calculations, it is even more critical when interactions with the electrons in neighboring cells have to be included up to distances where the electrostatic

TABLE 4. Examples of ab Initio Crystal Orbital Studies

system	dim	basis set	aim of the study	ref
$(H_2)_\infty$, $(LiH_3)_\infty$, $(LiH_5)_\infty$, $(LiH_7)_\infty$	1	STO-3G	effect of doping on structure and energy levels of a chain of H atoms	183
$(H_4C_4N^+\cdots BF_4^-)$	1	MB	influence of dopants on polypyrrole films	187
$(C_{12}H_8N_2)$, $(C_{12}H_8N_2\cdot HCl)$	1	MB	band structure of polyaniline	188
$(H_2O)_\infty$	1	TZP, DZ	structure, force constants, cooperative effects in hydrogen	173
$(CH_3OH)_\infty$	1	DZ	bonding	173
$(HCOOH)_\infty$	1	DZ, STO-3G		170
$(H_2NCOOH)_\infty$	1	DZ		189
$(HCN)_\infty$	1	DZP, DZ, STO-3G		172
$(HF)_\infty$	1	(10,6,2/6,1), DZP, DZ		190
$[(HF)_2]_\infty$	1	DZ	stabilization energy	191
graphite, BN	2	STO-3G	structure, force constants, band structure	192
$(C_6\cdots H)_\infty$	2	STO-3G	chemisorption site and binding energy for H on graphite	185
$(Be_n)_\infty$	2	[3,2]	electronic structure of films, surface states	193
$(H-Be_n-H)_\infty$ (n = 3, 4), $(H-Be_3)_\infty$	2	[3,2/1]	chemisorption site and binding energy, band structure	184
$(H-Be_3)_\infty$, $(H-Be-H)_\infty$	2	[3,2/1,1]		
Be	3	[4,2]	structure, force constants, Fermi surface shape, band structure charge distribution, compton profile	164
diamond	3	[4,3]	lattice constant, force constant	194, 195
diamond, Si, cubic BN	3	STO-3G	structure, force constants, band structure	145, 146, 196
LiH	3	[1/1], (STO-4G), [2,1/3,1]	structure, force constants, band structure, compton profiles	197
Li_3N, Li_2O	3	[4,3/2,1]		198, 199
H (fcc)	3	MB	lattice constant, bulk modulus	156
Li, Na (fcc)	3	EC-[2]		
MgO	3	[3,2/3,2]	geometry, energy and equation-of-state parameters for three different crystal structures	200
MgO(001) surface (slab of 3 planes)	2	[3,2/3,2]	surface relaxation and "rumpling", charge distribution,	201
MgO(110) surface (slab of 2–4 planes)	2	[3,2/3,2]	surface energy, projected density of states	202
CO on Mg(001) (MgO monolayer)	2	MgO: [3,2/3,2]	adsorbate geometry, energy of adsorption, charge distribution	203
CO on MgO(110) (slab of 2 planes)	2	CO: 3-21G		204
α-Al_2O_3 (corundum)	3	STO-3G	cohesive energy, density of states, electron charge distribution	166
SiO_2 (α-quartz)	3	STO-3G	bond distance, bond angles, atomic charges	165

interactions are fading. If N is the number of neighboring cells and m the size of the CGTF expansion within an elementary cell, the number of integrals increases as $N^3 \times m^4$ in the worst case, in practice less, e.g. as $N \times m^2$ for more distant cells. Moreover, better basis sets (larger m) usually also require larger N values since the GTFs become more diffuse and fall off slowly with the distance.

The problems are formidable and to cope with them is a major challenge to theoreticians working in this field. Different techniques have been developed and have been implemented in different ways in the crystal orbital computer programs used by different groups:[152] different cutoff procedures to truncate lattice summations,[152] separation of short- and long-range interactions and efficient multipole expansions for the long-range (Coulomb) contributions,[153–155] use of pseudopotentials for the core electrons,[156–158] use of helical symmetry for complex polymers,[159,160] and use of point symmetry within the elementary cell.[161]

Moreover, expression III.13 can be rewritten ($\mathbf{m} = \mathbf{s} - \mathbf{r}$)[162,163]

$$G(\mathbf{R})^{ol} = \sum_{\mathbf{m}} \sum_\rho \sum_\sigma R_{\rho\sigma}^{om} \, G\begin{pmatrix} o\,l & | & \ddagger\,\ddagger & +m \\ \mu\,\nu & | & \rho & \sigma \end{pmatrix} \quad \text{(III.16)}$$

showing that only one of the direct space summations (over $\mathbf{m}$) must be repeated in each of the iterations. The summation over $\mathbf{r}$ is carried out only once

$$G\begin{pmatrix} o\,l & | & \ddagger\,\ddagger & +m \\ \mu\,\nu & | & \rho & \sigma \end{pmatrix} = \sum_{\mathbf{r}} \left(\left\langle \begin{matrix} o\,l & | & r\,r & +m \\ \mu\,\nu & | & \rho & \sigma \end{matrix} \right\rangle - \left\langle \begin{matrix} o\,r & | & 1\,r & +m \\ \mu\,\rho & | & \nu & \sigma \end{matrix} \right\rangle \right) \quad \text{(III.17)}$$

and the number of two-electron matrix elements $G\begin{pmatrix} o\,l & | & \ddagger\,\ddagger & +m \\ \mu\,\nu & | & \rho & \sigma \end{pmatrix}$ that have to be stored and processed is considerably smaller than the number of all two-electron integrals $\left\langle \begin{matrix} o\,l & | & r\,s \\ \mu\,\nu & | & \rho\,\sigma \end{matrix} \right\rangle$.

In spite of all efforts, 17 million integrals had to be handled in the crystal orbital calculation of such a simple system as beryllium metal.[164] Making use of the D_3^4 space group of quartz, the number of integrals that have to be computed in a STO-3G calculation has been estimated to be 10 million and the number of two-electron matrix elements to be stored and processed at each iteration to 1.5 million. This applies to truncation criteria that will yield an accuracy of about $0.001E_h$/unit cell (about 2.6 kJ/mol). Hence, due to important program development recently made,[161] calculations on systems with more than three to four atoms per elementary cell are within reach now.[165,166] For systems with very few atoms per cell this means that one will be able to pass to better basis sets. In doing so another problem appears. Because of the high density of atoms, the basis set composed of the overlapping atomic sets shows linear dependencies.[157,164]

The limited accuracy of the CO methods (in the order of magnitude of 10 kJ/mol), in particular the discontinuities in the energy curves for variations of geometry parameters connected with the approximations in the two-electron integral part, prevents at present the optimization of geometry parameters with slowly varying energy curves.[165] Such difficulties could be avoided by analytical gradients that have been formulated also for CO Hartree–Fock methods[167] but are implemented in one of the LCAO-CO programs only.[168]

C. Survey of Present Achievements

Table 4 shows representative crystal orbital studies with emphasis on two- and three-dimensional systems. In spite of technical progress and impressive computer code developments, applications to one-dimensional periodic structures (polymers)[12,169] prevail among the nonempirical crystal orbital calculations reported in literature. For such systems it has been possible to employ DZ basis sets even when calculating force constants for an asymmetric unit as large as $HCOOH$[170] (calculations on infinite chains of HF, HCN, and H_2O used polarization functions[171-173]) or to perform complete gradient optimizations on special conformations of polyacetylene with a unit cell as large as C_4H_4 (4-31G basis set).[168]

Attempts to include electron correlation effects in ab initio CO studies have been also limited to polymers.[12,174-177] Referring to the infinite extension of solids, most authors opt for size-consistent methods, e.g. Møller–Plesset perturbation theory up to second[174-176] or third order[177] (MP2, MP3; cf. section II.C, eq II.36). The aim of these studies was to improve the optical excitation energies (band gaps) that come out too large in CO Hartree–Fock calculations. Both for semiconducting polymers[174-176] and for a bent chain of HF molecules,[177] reduced band gaps were obtained as the correlation corrections yielded quasi-particle valence and conduction bands that were shifted upward and downward, respectively. A similar study was made on solid CH_4.[178]

In addition to correlation effects that were already mentioned (section II.C), in periodic studies on *metallic* systems a specific failure of the HF approximation is observed, namely the density of states at the Fermi energy vanishes.[179] A recent analysis has shown that this feature is connected with the particular form of the HF exchange operator.[180-182]

Due to their very nature, crystal orbital methods have difficulties when treating systems with "broken" translatory symmetry. Defect sites, e.g., would be treated as quasi-periodic. To avoid artificial interactions between neighboring defects, the effective cell size necessary would exceed present computational possibilities. Attempts in this direction are confined to very simple models like chains of hydrogen atoms when doped with lithium[183] (Table 4). In crystal orbital studies of surface problems slab models are adopted; i.e., periodicity is exploited only parallel to the surface while the vertical extension is treated like a cluster with two surfaces. Again, computational limitations prevent us from making the slab thick enough so that unwanted interactions between both surfaces vanish. In a pioneering chemisorption study[184] a beryllium slab three or four atoms thick has been used and covered on both sides with hydrogen. (When only one surface is covered, the surface states of the free surface interfere with the chemisorptive bond.) A STO-3G study of hydrogen on graphite (a single graphite layer only)[185] revealed serious deficiencies of previous semiempirical CNDO/2 calculations. A theoretical description of impurities, vacancies, or surfaces with chemisorbed particles that properly takes into account the infinitely extended nature of the system is possible by Green's function technique.[186] It starts from the crystal orbital solution of the unperturbed periodic system and determines the per-turbation by a self-consistent solution of the so-called Dyson equation.[186] The latter computations, however, are even more complex than a CO solution of the periodic system. The only nonempirical calculation reported so far (to the authors' knowledge) was made for an infinite chain of Li atoms doped with a hydrogen atom and used an STO-3G basis set.[186]

D. Alternatives and Prospects

The computer demands of ab initio CO calculations may lend an appealing appearance to semiempirical methods in the field of solid-state problems, though they are almost completely abandoned now in structure determinations and total energy calculations for molecules. Indeed, CO variants were developed for most semiempirical methods popular in quantum chemistry,[28] e.g. EHT,[13,205,206] CNDO/2,[207] and MINDO/3.[208,209] They are certainly of some use for qualitative purpose, particularly in the hands of scientists with good intuition (the exciting EHT studies[13,210] from Hoffmann's group are a prominent example). But it is also not surprising that semiempirical methods that rely on the neglect of differential overlap approximation such as CNDO, INDO, NDDO, and their modified variants MINDO/3 and MNDO cannot make reliable structure predictions for solids, which frequently contain heavier elements or exhibit unusual bonding situations. Anderson's ASED method,[211] an EHT-type approach upgraded by an atom–atom repulsion potential, might be more successful in this respect. It proved capable of making interesting structure predictions in large cluster studies of surface complexes,[212] and it should be interesting to see its performance in CO studies.

The vast number of periodic calculations on bulk and surface properties of solids indicates that the methods of solid-state physics may offer a possibility to bypass the computational bottleneck of ab initio techniques. All these methods rely on the local density approximation (LDA; cf. section II.E).[14,15] In the past, a broad variety of semiempirical methods was available for the calculation of band structures.[29,30] It was sufficient to get the one-electron energy levels with an accuracy of a few tenths of an electronvolt. This means, however, that the error of the total energy was several times larger.

In recent years the accuracy of density functional methods has been pushed up to a level that is sufficient for total energy, structure, and force constant calculations.[21,22] These methods replace the core electrons by nonempirical pseudopotentials and expand the one-electron functions for the valence electrons into a basis set of plane waves instead of atomic like functions with great computational advantages (by their very nature, however, plane waves are of no use for molecules). The LDA one-particle equations (II.38) can be effectively solved in momentum space, and when the derivatives of the energy are evaluated analytically with respect to the nuclear coordinates, only the so-called Hellman–Feynman term appears, but not terms connected with the derivatives of the basis functions as in LCAO-type methods.[22] The latter form is the most time-consuming part of the gradient evaluation in molecular ab initio calculations.[41] Holzschuh[213] compares the results of different pseudopotential calculations for silicon and studies the dependence on the particular density

TABLE 5. Periodic Hartree–Fock (HF) and Local Density Approximation (LDA) Results (Units: Lattice Parameters (a, c) pm; Cohesive Energy (E_{coh}), kJ/mol; Bulk Modulus (B), Mbar)

crystal	parameter	Hartree–Fock method GTF[a]		obsd[b]	local density approximation LCAO[c]	GTF[d]	PW[e]
Be	a	323[f]		229			225[g]
	c	364[f]		358			357[g]
				1.14–1.27			1.37[g]
C	a	359[h]	355[i]	357	358[j]	356[k]	360[l]
	E_{coh}	549[h]	485[i]	709–735	753[j]	756[k]	730[l]
	B	5.90[h]	4.38[i]	4.43		4.37[k]	4.41[l]
Si	a	558[m]	542[n]	543		535[o]	545[l]
	E_{coh}	247[m]	241[n]	447		496[o]	450[l]
	B	1.25[m]	1.20[n]	0.99		1.13[o]	0.98[l]
BN	a	359[p]		362[q]	365[r]		
	E_{coh}	950[p]	805[q]	1255	1235[r]		

[a] Crystal orbital method employing a basis set of contracted Gauss-type functions. [b] For references to experimental work, see quoted theoretical papers. [c] Numerical basis set (discrete variational method). [d] Calculations within the LDA employing a GTF basis set. [e] Pseudopotential calculations within the LDA employing a basis set of plane waves. [f] Reference 164. [g] Reference 219. [h] Reference 145. [i] References 194 and 195. [j] Reference 220. [k] Reference 217; not fully self-consistent. [l] Reference 221. [m] Reference 146; STO-3G basis set. [n] Reference 146; STO-3G for 1s and 2sp orbitals and STO-4G for 3sp orbitals. [o] Reference 219. [p] Reference 196. [q] Reference 222. [r] Reference 223.

functional adopted (cf. section II.E) and on the number of plane waves in the basis set. He shows that up to about 300 basis functions may be necessary to obtain converged results, even for a crystal as simple as Si. This is a great disadvantage of the method. Another one is that the localized core electrons cannot at all be described by plane waves. Therefore, also in solid-state physics, methods have been developed that solve the one-particle LDA equations in real space for a basis set of GTF or STO (LCAO-CO-LDA methods). There are a number of review articles[19–22,214] and a recent conference volume[11] (see, in particular, the contributions by Martin,[215] Kunc,[216] Nielsen and Martin,[218] and Louie[217]) providing details of modern solid-state LDA calculations employing basis sets of both plane waves and atomic like functions (GTF, STO), for total energies, energy derivatives, force constants, and structures. Table 5 contains a small selection of applications and makes comparison with ab initio calculations (Results of both approaches for ionic materials are presented in Table 15.).

Table 5 marks the point where the lines of significant technical developments in solid-state physics (LCAO-CO-LDA methods) and in quantum chemistry (ab initio LCAO-CO methods) come very close to each other as Scheme 1 illustrates. The scheme shows also that molecular applications of LDA methods have their origin in LCAO-type solid-state approaches or their predecessors, LCAO-type band structure calculations.

When results of ab initio HF calculations are compared with those of LDA methods and with observed values (Table 5), a picture emerges for these periodic treatments that we know from studies on molecules (section II). Both approaches make reliable structure predictions. Cohesive energies are poor for the HF model and much better for the LDA methods. As far as electron excitation energies are concerned ("band gap"), HF theory yields typically too large values (by about 20%) while LDA methods yield values that are reduced by as much as 50%.[22] This is not only a practical problem, but, more seriously, there is no theoretical justification for getting excitation energies within the LDA.[22] The recent review of Srivastava and Weaire[22] mentions some further, presently unsolved problems of the LDA methods. But it also points to promising developments toward a unified approach to

SCHEME 1. Total Energy Calculations

```
   molecules              periodic solids
(domain of chemists)    (domain of physicists)

      LCAO                LCAO-CO methods
  HF plus correlation     HF (plus correlation)
        ↕                        ↕
  (Tables 2 and 3)           (Table 5)
        ↕                        ↕
    LCAO-LDA     ◄────── LCAO-CO-LDA
                              ↓
                      plane waves-LDA
                      (pseudopotential)
```
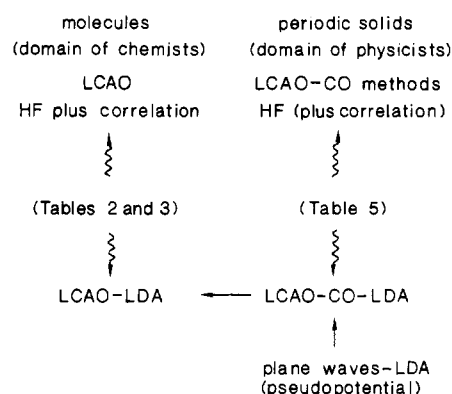
self-consistent solutions of the one-particle equations, structure determination, and molecular dynamics within the LDA. In summary, as with molecules, the LDA is without doubt a very useful and, for some types of solids, a particularly well-adapted approximation. But also with solids the exact form of the density functional is unknown; therefore, LDA methods will face limits beyond which they cannot be improved. It is clear that both solid-state LDA and ab initio CO methods are only at the beginning of producing results on more complex solids, but it is also clear that we cannot do without the ab initio CO methods.

In ab initio calculations on solid-state problems there is also no alternative to pushing forward the CO techniques since this is the only way to exactly take into account the infinite extension of the system. Moreover, CO results are of paramount importance as benchmarks to assess the approximations connected with the cluster approach.

The situation is paradoxical in so far as in ab initio crystal orbital calculations very sophisticated techniques seem to be unavoidable to achieve balanced approximations, while molecular models or clusters making implicitly very drastic cutoffs of the interactions with the surroundings are apparently rather successful. While it is only today that minimal basis set crystal orbital calculations for quartz are being completed,[165] molecules as small as orthosilicic acid or disilicic acid, $Si(OH)_4$ and $(HO)_3SiOSi(OH)_3$, tell us much about structure and properties of silica (sections IV and VII)
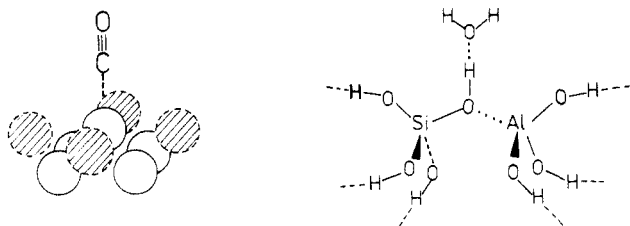
Figure 2. Clusters and molecules as models.

and allow one not only to use reliable basis sets but also to take electron correlation into account at least at a simple level (MP2).[130,131]

But, just this paradoxon gives reasonable hope that finally quantum chemists will learn how to make efficient and balanced approximations for two-electron integrals between a reference cell and its surroundings in solids. There is no doubt that in coming years the list of systems treated by ab initio crystal orbital methods will extend and the theoretical level will improve (larger basis sets, inclusion of electron correlation).

IV. "Chemical" Approach: Molecular Methods

A. Introduction

The physical approach to the electronic structure problems of solids contrasts sharply with the chemist's feeling that local interactions dominate structure and properties of molecular systems. Such feeling is expressed in terms like functional group and homologous series. Hence, it is very appealing to replace the infinite solid, which is difficult if not impossible to treat quantum chemically, by finite models of the sites of interest. Intuitively, cutouts from the bulk or the surface are made and treated like molecules. In the case of metals, these cutouts are clusters of metal atoms and are called cluster models. When cutouts are made from solids with directed bonds, the "dangling" bonds that would connect the cutout with the bulk are intuitively saturated by hydrogen atoms to yield hypothetical or real molecules as models. In this case we prefer the name molecular models (Figure 2). The concept of cluster or molecular models proved very fruitful. It reduces the problem of electronic structure and local geometry of the solid to the common problem of determining the geometry and electronic structure of molecules, it reduces the problem of the bonding of molecules or atoms on to surface sites to the problems of molecular reactivity and intermolecular interactions, and it reduces the problem of surface reactions to the problem of potential surfaces for reactions between molecules.

The molecular approach to solid-state and surface problems has met undisputed success, and the reader may expect this review to just give an account of its achievements and to consider its limitations for different types of materials. This is done in sections V–VII. However, having in mind the difficulties of a nonempirical crystal orbital calculation, one may wonder why the molecular approach work so well and when this is the case. The heart of molecular models is a localized description of the electronic structure of solids. Therefore, we start (section IV.B) with analyzing the conditions under which and the extent to which local-

ization of the orbitals of a crystal in a limited region can be achieved. The answer is different for different types of solids and depends also on the particular way the model is chosen, i.e. the way the cutout is made. It goes without saying that a model is the more realistic the larger it is. What we are interested in in this section are rules that allow one to find the best possible model of a given size, or better to say of a given amount of computational work. This section does not provide a complete list of the numerous suggestions made in literature, but rather attempts to present them in a systematic way and to rationalize them from common principles. In paragraphs IV.C–E different aspects of molecular modeling are discussed (embedding techniques, Madelung potentials, saturator pseudoatoms). Though in each paragraph for illustration reference is made to those types of solids for which the respective model aspects are dominant (i.e., metals, ionic and molecular crystals, and crystals with covalent bonds), the rules emerging from all of these paragraphs should be considered when designing an optimal model for a specific problem. Section IV.F deals with possible improvements of a model by proper handling of its geometry.

When the results of a specific calculation on a molecular model or a cluster model are compared with experimental results for the infinite solid, any deviation observed can be due to shortcomings of the model or approximations made in the method applied. This problem is addressed in the final section.

B. Conditions of a Localized Description

Rules for the best possible choice of a model for a given site of a solid become obvious when an analysis is made for approximations involved in the process of modeling the infinite solid by finite systems. What we would like to do is to solve HF-type equations—possibly slightly modified ones—for a finite model only. What we would like to achieve is that the orbitals localized in this limited cutout are also *approximate* solutions of the HF equations for the infinite solid. This problem of localization is well-known in quantum chemistry. The solutions of the HF equations of a given system are determined only up to a unitary transformation among the occupied orbitals. Use can be made of this freedom to pass from the delocalized molecular orbitals obtained as canonical solution of the HF equations to localized orbitals corresponding to a chemist's idea of atomic cores, lone pairs, bonding electron pairs, etc. Note that these orbitals are still orthogonal and, therefore, not stictly localized, but they show small coefficients (tails) on atoms outside the localization region. The total energy, the one-electron density function ρ, and all properties calculated from the n-electron determinantal wave function are not affected by this transformation.

Let us consider the conditions under which and the extent to which localization in a limited region of a solid can be achieved. The solid is divided into a cutout (index C) and its surrounding (index S). Solving the HF equations for the solid

$$F\psi = \psi E \qquad (IV.1)$$

an infinite set ψ of k-dependent crystal orbitals $\psi_i(\mathbf{r}_1)$ is obtained, which extend over the whole solid. In section III the wave vector $\mathbf{k}$ is used to label the orbitals,

but here it is convenient to absorb $\mathbf{k}$ into the index i running now over all the orbitals of the solid. Moreover, a special matrix notation proves convenient,[224] which considers $\psi_i(\mathbf{r}_1)$ as element of a matrix with continuous (the electron coordinate $\mathbf{r}_1$) and discrete (the orbital index i) variables, $\psi(\mathbf{r}_1, i)$. Correspondingly, F and E are matrices of type $F(\mathbf{r}_1, \mathbf{r}_1)$ and $E(i, j)$. The unitary transformation into a set φ of localized orbitals is given by the matrix T:

$$\varphi = \psi \cdot \mathbf{T} \tag{IV.2}$$

We are interested in a transformation that yields orbitals φ, a subset of which, φ_C, is localized in the given cutout (and, approximately, satisfies HF-type equations of this model):

$$\varphi = (\varphi_C, \varphi_S) = \psi(\mathbf{T}_C, \mathbf{T}_S) \tag{IV.3}$$

Already at this point we have made an important assumption in our model, namely that a definite number of orbitals with a definite number of electrons can be attributed to it (assumption 1). Localization, in general, can be achieved by adding a localization potential to the Fock operator. The orbital set φ_C, which we are seeking, can be obtained by solving the Adams–Gilbert equation[224,225]

$$(F^{C,lr} + V^{S,sr} - \rho V^{S,sr}\rho)\varphi_C = \varphi_C E^{C,lr} \tag{IV.4}$$

with

$$E^{C,lr} = \varphi_C{}^+ F^{C,lr}\varphi_C \tag{IV.5}$$

and

$$\rho = \psi\psi^+ \tag{IV.6}$$

These equations describe a model system consisting of the electrons and nuclei of the cutout that feel the long-range (lr) potential of the surroundings, $v^{S,lr}$:

$$F^{C,lr}(\mathbf{r}) = F^C(\mathbf{r}) + v^{S,lr}(\mathbf{r}) \tag{IV.7}$$

The short-range (sr) potential of the surroundings, $v^{S,sr}$, is screened by the localization operator $\rho(r) \, v^{S,sr}(r) \, \rho(r)$, which acts within the subspace of occupied orbitals of the total system. Use was made of a division of the potential suggested by Kunz and Klein:[226]

$$F(\mathbf{r}) = F^{C,lr}(\mathbf{r}) + v^{S,sr}(\mathbf{r}) \tag{IV.8}$$

It is based on the partitioning

$$F(\mathbf{r}) = F^C(\mathbf{r}) + v^S(\mathbf{r}) \tag{IV.9}$$

where $F^C(\mathbf{r})$ includes, besides the kinetic energy operator, interactions inside the cutout only, while $v^S(\mathbf{r})$ describes the potential due to the nuclei, $v^{n,S}$, and the electrons, $j^S(\mathbf{r}) - k^S(\mathbf{r})$, of the surroundings:

$$v^S(\mathbf{r}) = v^{n,S}(\mathbf{r}) + j^S(\mathbf{r}) - k^S(\mathbf{r}) \tag{IV.10}$$

This "external" potential is further divided into short-range contributions, decaying exponentially with the distance, $v^{S,sr}(\mathbf{r})$, and long-range contributions, $v^{S,lr}(\mathbf{r})$:

$$v^S(\mathbf{r}) = v^{S,lr}(\mathbf{r}) + v^{S,sr}(\mathbf{r}) \tag{IV.11}$$

Separation of both terms is achieved by expanding the Coulomb potential, $j^S(\mathbf{r})$, in a multipole series. The multipole contribution, together with the potential of the nuclei, forms the long-range potential, while that part of the Coulomb potential due to the overlap of the

charge clouds (charge penetration contribution) is combined with the exchange potential to give the short-range part.

The localization potential, $\rho(\mathbf{r}) \, v^{S,sr}(\mathbf{r}) \, \rho(\mathbf{r})$, acts in the following way on orbitals within the occupied subspace of the total system: Electrons in orbitals that are not localized in the cutout are not stabilized (because the potential $v^{S,sr}(\mathbf{r})$ that would do this is canceled by the localization potential) and are shifted to higher energies, while the electrons in orbitals localized in the cutout are affected only slightly (because $v^{S,sr}$ and, consequently, its screening effect is weak for them).

Passing to the algebraic approximation (section II), all the orbitals are expanded in terms of the full basis set χ of the infinite system

$$(\varphi_C, \varphi_S) = \chi(\mathbf{C}_C, \mathbf{C}_S) \tag{IV.12}$$

and the matrix form of the Adams–Gilbert equations (IV.4)

$$(\mathbf{F}^{C,lr} + \mathbf{V}^{S,sr} - \mathbf{SRV}^{S,sr}\mathbf{RS})\mathbf{C}_C = \mathbf{SC}_C\mathbf{E}^{C,lr} \tag{IV.13}$$

has infinite dimensions ($\mathbf{SR}$ is the algebraic representation of the projection operator ρ).

Although eq IV.4 and IV.13 would yield orbitals for the infinite solid that are localized in a limited cutout of it, no real progress has been made in deriving these equations. They still involve all the interactions with the surroundings (which in section III were shown to be very difficult to treat). Yet we need the complete solution for the total system to set up the one-electron density ρ

$$\rho(\mathbf{r}) = \varphi_C\varphi_C{}^+ + \varphi_S\varphi_S{}^+ \tag{IV.14}$$

and the orbitals φ_C, albeit localized, have tails in the surroundings that express the orthogonality with the orbitals localized thereon. That we have to know the exact solution for the perfect solid is the major obstacle with all "embedding" procedures (see, e.g., ref 186). Nevertheless, equations of type (IV.4) or (IV.13) can be a basis of efficient embedding techniques provided the surrounding is described by a simpler wave function than the cluster (vide infra, section IV.C).

What we are ultimately interested in when trying to find rules for an optimal choice of a model are the approximations involved in passing to equations of type

$$\mathbf{F}_{CC}^{C,lr}\tilde{\mathbf{C}}_{CC} = \mathbf{S}_{CC}\tilde{\mathbf{C}}_{CC}\mathbf{E}_{CC}^{C,lr} \tag{IV.15}$$

In these equations the expansion of the orbitals of the cutout C extends over a subset χ_C of CGTF assigned to this model system only, and the short-range potential of the neighboring cells giving rise to the huge number of two-electron integrals is suppressed. $\mathbf{F}_{CC}^{C,lr}$ and $\mathbf{S}_{CC}$ are submatrices of $\mathbf{F}^{C,lr}$ and $\mathbf{S}$ appearing in eq IV.13; e.g.

$$\mathbf{F}^{C,lr} = \begin{pmatrix} \mathbf{F}_{CC}^{C,lr} & \mathbf{F}_{CS}^{C,lr} \\ \mathbf{F}_{SC}^{C,lr} & \mathbf{F}_{SS}^{C,lr} \end{pmatrix} \tag{IV.16}$$

with

$$\mathbf{F}_{CC}^{C,lr} = \langle \chi_C | F^{C,lr} \chi_C \rangle \tag{IV.17}$$

and

$$\tilde{\varphi}_C = \chi_C \tilde{\mathbf{C}}_{CC} \tag{IV.18}$$

The matrix equations (IV.13) reduce to block diagonal

form and, consequently, to eq IV.15 when the nondiagonal blocks $\mathbf{F}_{CS}$ and $\mathbf{S}_{CS}$ disappear. This happens when the differential overlap, $\chi_\mu(\mathbf{r}_1) \chi_\nu(\mathbf{r}_1) \, d\mathbf{r}_1$, and the resonance integrals, $\langle \mu | h | \nu \rangle$, are negligible ($\mu$ and ν label CGTFs on atoms of the cutout and of the surroundings, respectively). At this level of approximation also the term $V_{CC}^{S,sr}$ vanishes as the short-range potential depends on overlap. These are the conditions for which eq IV.15 is an approximation to eq IV.13. That means the solutions $\mathbf{C}_{CC}$ of eq IV.15 defined for a limited model of the solid are as well approximate solutions of the HF equations of the infinite solid (eq IV.13) if the cutout is made as follows: (1) A fixed number of electrons can uniquely be assigned to it. (2) A subset of CGTF can be attributed to it. (3) Differential overlap and resonance integrals between its orbitals and those of the surroundings are negligible. It is obvious that these requirements can be met only approximately. Their significance is that they may guide us to make a cut that yields the best possible model of a given size for a given solid. Roughly speaking, the model is to be chosen such that a definite number of electrons can be assigned to a subset of atomic orbitals of the solid in a way they interact as little as possible with the electrons of its surroundings. How this is achieved for different types of solids will be discussed in the following paragraphs. For each type of bonding a particular aspects of the embedding problem will be stressed. Although metals are not the main interest of this review, we start with a short account of embedding techniques designed for them because they are generally applicable. After a few comments on peculiarities of ionic solids and molecular solids, we pass to solids with significant covalent bond contributions, the materials of main interest here.

C. Metals: Embedded Clusters

The above approximations are not justified for metals. For them, delocalized electronic states are characteristic, originating from the strong overlap between the valence orbitals of closely packed atoms. Hence, the tails on atoms of the surrounding that belong to the orbitals of the cluster region, φ_C, must not be neglected, and passing from eq IV.13 to eq IV.15 is a heavy approximation. Large clusters of metal atoms will be necessary to successfully model bulk or surface sites of metals. For example, to study the interaction of H atoms with bcc iron,[227] clusters of up to 66 Fe atoms were used, but cluster edge effects were still sensible. To be able to use sufficiently flexible wave functions for the site of interest (or, for a given quality of wave function, to be able to study models that are large enough), the model is divided into two parts: the interior region constituted by the atoms at the site considered, and the exterior part, which isolates the interior from the physically incorrect boundary. The idea is to treat the exterior part in a more approximate way. However, we cannot simply employ basis sets of different quality on the atoms of the interior and exterior parts of the model (as, e.g., done in ref 227) since in any variational calculation this will lead to undesirable superposition effects. To avoid artifacts, one of the following measures of "embedding" can be taken (listed in order of decreasing demands): (1) explicit localization as described by eq IV.3;[228-239] (2) frozen orbital approximation for the exterior region; (3) use of effec-

tive core potentials for exterior atoms;[240,241] (4) replacement of all the electrons of exterior atoms by pseudopotentials.

Localization of "cluster" orbitals φ_C (analogous to eq IV.1-14, but including a separate transformation step) is the essence of Whitten's technique.[228,229] Let us consider the consecutive steps of his procedure for the specific case of H_2 adsorption on titanium.[230,231]

(1) As a model of the "infinite" solid surface, a rather large cluster is used, denoted $Ti_{38}(19\text{-}12\text{-}7)$, which consists of 19 atoms in the surface layer, 12 atoms in the second, and 7 atoms in the third layer. The SCF equations (eq IV.1) for this model plus adsorbed H_2 are solved employing a minimal basis set of 4s and 1s orbitals on Ti and H, respectively.

(2) An interior region of the model is chosen: the seven central metal atoms of the surface layer next to the adsorption sites plus the adsorbed H atoms. The remaining 31 Ti atoms represent the surrounding. To single out from the 20 occupied orbitals those that are localized in the adsorption region (index C in IV.B) we have to find a unitary transformation T. We know from section IV.B that a short-range potential is needed that acts either on the interior part or on the surrounding. Whitten makes use of the exchange potential $k^{(i)}$ defined by the $m^{(i)}$ atomic basis functions φ_μ of the interior part:

$$k^{(i)}(\mathbf{r}_1) \, \varphi_k(\mathbf{r}_1) = \sum_{\mu=1}^{m^{(i)}} \chi_\mu(\mathbf{r}_1) \int \frac{\chi_\mu^*(\mathbf{r}_2)}{r_{12}} \, \varphi_k(\mathbf{r}_2) \, d\mathbf{r}_2 \tag{IV.19}$$

Transformed orbitals (cf. eq IV.2)

$$\varphi_k = \sum_l \chi_l T_{lk} \tag{IV.20}$$

are obtained that maximize the exchange energy γ_k with the orbitals of the interior atoms:

$$\gamma_k = \sum_\mu \langle k\mu | \mu k \rangle \tag{IV.21}$$

In the present example, the nine occupied orbitals with the largest γ values are assigned to the "cluster" set φ_C (cf. section IV.B), while the remaining 11 orbitals define the fixed electron distribution of the environment (set φ_S). It is important to keep in mind that the orbitals φ_C have tails on atoms of the exterior region while those of the environments set φ_S have tails on the interior region. These tails reflect significant properties of a metal and cannot be neglected. I.e., for metals the division of the electronic space into subspaces of the "cluster" electrons and of the "surrounding" electrons does not coincide with the "geometric" division of the whole assembly of atoms into an interior and an exterior region.

(3) The "cluster" basis set can now be improved by adding to the nine localized orbitals assigned above to the site of interest further basis functions centered on the atoms of the interior region. A second s-type CGTF is added to the valence basis sets on Ti and H atoms; moreover, p polarization functions are added to the latter. It is also at this stage that the 3d constraint is removed and 3d orbitals are included (localization of d orbitals is not necessary since they overlap only weakly). For this extended basis set another SCF and a CI calculation are made. To enhance convergence of the CI expansion, a second localization is performed in

TABLE 6. Small-Cluster and Embedding-Cluster Results for Hydrogen Chemisorption[231,232,234,236] (SCF Interaction Energies, kJ/mol; Negative Values Denote Exothermic Processes)

system	small cluster[a]		embedded cluster[a]
H$_2$ on Ti(0001)[b,231]	Ti$_7$(7)–H$_2$	Ti$_{10}$(7-3)–H$_2$	{Ti$_7$–H$_2$}/Ti$_{38}$(19-12-7)–H$_2$
site 1-2[c]	–30		+40
site 1-3[c]	–175	–220	–50
site 1-4[c]	–200	–260	–40
H on a Ti ad-atom on a 3-fold site on Ti(0001)[95,236]	Ti–H	Ti$_4$(1-3)–H	{Ti$_4$(1-3)H}/Ti$_{20}$(1-12-7)H
top	–100	–185	–350
interstitial		–90	–450
H on Cu(100)[232]		Cu$_9$(4-5)–H	{Cu$_9$–H}/Cu$_{25}$(12-9-4)–H
4-fold hollow site		–320	–190

[a] The following notation is used: {interior part}/total model (number of first-layer–second-layer–third-layer atoms). [b] Energies with respect to undissociated H$_2$. [c] Cf. Figure 3.
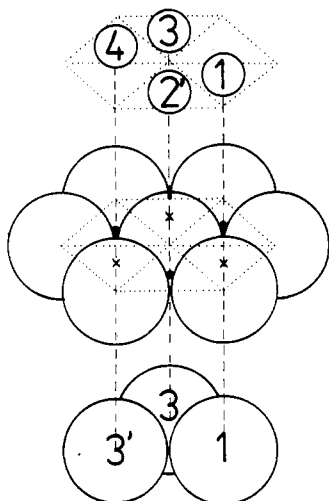
Figure 3. Models used to study the dissociative H$_2$ adsorption in different pairs (1-2, 1-3, 1-4) of 3-fold hollow sites on the Ti (0001) surface.[230,231] The H atoms (top) are 132 pm above the surface plane, and the H–H distances for the 1-2, 1-3, and 1-4 sites are 170, 295, and 341 pm. The figure shows the Ti$_{10}$(7-3) cluster with seven Ti atoms in the surface layer and three Ti atoms in the second layer.

TABLE 7. Effect of Second-Layer Atoms on Binding of CO on Metal Atoms[240] (Units: Equilibrium Distances (R_e), pm; Interaction Energies (ΔE), kJ/mol; Negative Values Indicate Stabilization)

model	M = Cu (x = 4)		M = Ni (x = 4)		M = Al (x = 3)	
	R_e	ΔE	R_e	ΔE	R_e	ΔE
M–CO	(205)[a]	43	(202)[a]	43	(198)[a]	20
M$_x$M–CO[b]	206	–46	204	–49	199	–22
M$_x$M–CO	205	–43	202	–54	198	–23

[a] The potential curves are repulsive. Energies are given for the equilibrium distance of the two-layer cluster. [b] Effective core potentials on the x second-layer atoms M.

the same way as described above. Only in this third step is a computational advantage taken as the "cluster" orbitals expanded into a good basis set are obtained in the potential of the fixed "surrounding" orbitals described by a rather primitive basis set. The reduction of basis set size achieved this way is substantial. The calculation of the (embedded) Ti$_{38}$(19-12-7)–H$_2$ cluster involves altogether 60 orbitals (40 s, 9 s', 2 p, 9 d). With the full double ζ basis set on all Ti atoms, this number would increase up to 91 (40 (s + s'), 2 p$_\perp$, 9 d).

The purpose of the localization may be summarized as follows: (1) It introduces the delocalized character of the valence band electrons into a subspace involving the electrons of the site of interest. (2) It insulates the interior part of the model from the crudely described exterior part and the physically incorrect boundary. Table 6 shows the significant effect the embedding procedure has on computed adsorption energies for hydrogen. In the larger (embedded) clusters they are strongly reduced. This can be naively explained as follows: In the small (one- or two-layer clusters) bonds connecting the surface atoms with the bulk are cut, and this makes these atoms more free to bond with hydrogen. On interstitial positions, however, stronger bonding of hydrogen is predicted for embedded clusters[236] than for the free Ti$_4$ cluster.[234] The embedding technique described above has been employed in studies of

the adsorption and dissociation of H$_2$ on titanium,[230,231,236] copper,[232,233] and titanium–copper alloy[238] surfaces. In addition, hydrogen bonding on interstitial bulk[239] and below-surface positions[236] has been investigated. There is also some work on CO bonding on the Ti(0001) surface[237] and on adsorption of atomic hydrogen on the Li(100) bcc surface.[235]

While Whitten's technique has been rarely used (certainly because it requires some investment in programs), the third of the above-mentioned possibilities to deal with exterior atoms, use of effective core potentials, requires only a program feature that becomes more and more standard in programs of molecular calculations.[242] Computer time savings are substantial, and effective core potentials have become very popular in metal cluster studies.[240,241,243-246] In a study of CO adsorption on metal surfaces (cf. Table 7) the calculation on the Cu$_5$(1-4)–CO model involves 221 basis functions. Although only 96 of them remain when effective core potentials (replacing also d electrons) are introduced on the four second-layer metal atoms,[240] the results are hardly affected. In contrast, complete neglect of second layer atoms in the minimal Cu–CO model fails to yield any binding at all while only a further 20 basis functions are saved. The use of effective core potentials for the environment metal atoms made it possible to study even larger models involving as many as 34 Cu atoms.[241] The central Cu atom was described by an all-electron basis set while for all other atoms of the cluster only the 4 sp electrons were included. The resulting interaction energies for on-top adsorption of CO (R(Cu–C) = 196 pm) show a strong oscillation with increasing cluster size (kilojoules per mole, negative values indicate stabilization): Cu$_1$(1)–CO, +48; Cu$_5$-(1-4)–CO, –43; Cu$_{10}$(5-4-1)–CO, +39; Cu$_{14}$(5-4-5)–CO, –27; Cu$_{34}$(9-16-9)–CO, +53. A careful analysis[241] revealed that the oscillation is due to electrostatic and substrate polarization contributions while others such

as charge transfer and CO polarization are nearly constant. Most importantly, relations between the electronic structure of the bare Cu_n cluster and its interaction with CO have been established making it possible to predict whether this interaction will be attractive or repulsive. It is believed that these conclusions apply to adsorbate–metal systems other than Co–Cu(100) as well.

These findings, although being a sign of warning, do not contradict studies on chemisorption that employ small clusters, but rather point to the urgency of a careful selection of the model and a thorough analysis of the results.

In spite of all difficulties in getting converged results from cluster studies one should remember (1) that different properties have different demands on cluster size and (2) that minimal models of surface complexes, even those involving a single metal atom, may yield useful results on the nature of bonds involved[87,135,247-249] or on the ability of some methods to describe certain types of surface bonds properly.[82,250-252] Theoretical results for metal atom clusters and their relations to bulk metal and surface properties have been recently reviewed in this journal.[38]

D. Molecular and Ionic Crystals: Madelung Potentials

For molecular crystals or ionic crystals it is as easy to choose models that conform to eq IV.15 as it is difficult for metals. In clusters of ions or molecules electrons are well localized on the individual species. Overlap between orbitals on different species is weak, and the interactions between the species fall into the category of intermolecular forces. The only point deserving attention is the way the potential of the surrounding species that appears in the Fock operator of the model is approximated. Equation IV.11 implies that the long-range part of the electrostatic potential is used. The simplest approximation replaces $v^{S,lr}$ by its leading contribution, the Madelung term, which describes the interactions with point charges located at the atoms or ions of the environment:

$$v^{S,lr}(\mathbf{r}) \approx v^M(\mathbf{r}) = \sum_i^{(S)} q_i/(\mathbf{r} - \mathbf{r}_i) \qquad (IV.22)$$

Implementation of this embedding procedure is computationally cheap (it requires calculation of additional one-electron integrals, only) and straightforward. The only questions to be answered are as follows: (1) How large should be the point charge array? (2) What are the optimum values for the point charges?

(1) The finite array of charges should reproduce the exact Madelung potential that can be calculated by the Ewald method[253] on all atoms on the explicitly treated cluster.[254,255] This is reached when the chosen array reflects properly the symmetry of the crystal and when appropriate fractions of charges are put on its surface and corner positions ("Evjen" model,[256] see also ref 258). This also helps to keep the model neutral. However, there is no guaranty that the Evjen model yields better agreement with the exact Madelung potential than the simple unit charge model.[256,257] A recommended method is to adjust the charges of the point ions of the outermost shells of the array in order to reproduce the Madelung potential for the infinite crystal.[254-256]

TABLE 8. Polarizabilities of Ions (a_0^3) in Different Environments[265-268]

model[a]	SCF	correlation	total
Na^+, free	0.944	0.058[b]	1.002
$\{Na^+\}^P$ (NaF)	0.945	0.058[b]	1.003
Ag^+, free	8.26	0.36[c]	8.62
$\{Ag^+\}^P$ (AgF)	8.73		(9.66)[d]
F^-, free	10.65	5.52[b]	16.18
$\{F^-\}^P$ (LiF)	7.30	1.78[b]	9.08
$\{F^-(Li^+)_6\}^P$ (LiF)	5.39	0.79[b]	6.18
	(4.45)[e]		(5.24)[e]
$\{O^{2-}\}^P$ (MgO)	21.2	5.3	26.5
$\{O^{2-}(Mg^{2+})_6\}^P$ (MgO)	10.9	1.4	12.3

[a] $\{\}^P$ denotes embedding by a point ion array. [b] MP2. [c] CI-SD. [d] Estimate obtained by adding effects of correlation, point ion field, and relativistic corrections.[267] [e] Full Boys–Bernardi correction.

(2) Only for purely ionic crystals like alkali halides, MgO, NiO, etc. is the use of full ion charges justified. For crystals containing polyatomic ions, e.g., NaOH,[259] for molecular crystals, e.g., solid HCOOH, NH_3, and ice, or for partially covalent solids, e.g., SiO_2 or Al_2O_3, fractional charges on the atoms are needed. Frequently, they are determined from a Mulliken population analysis. This, however, is not the best choice. Since we are interested in a set of charges that reproduces as closely as possible the long-range potential (eq IV.22), so-called "potential-derived" (PD) charges[260-264] are superior. They are determined such that they give the best fit to the electric multipole moments and/or the molecular electrostatic potential of the polyatomic ion or molecule considered. This definition depends neither on the basis set size nor on whether the basis functions are centered on atoms or elsewhere in space. On the contrary, the Mulliken partitioning becomes more and more arbitrary as the basis set is extended beyond minimum. E.g., diffuse functions may have their radial density maximum closer to a neighboring atom than to the atom on which they are centered. In the study of solid NaOH, the charges in the group were chosen to reproduce its dipole moment. A hydrogen effective charge of +0.443e was obtained as opposed to a value of +0.259e from population analysis.[259] Further examples are given in section V. In any case, the process of charge determination should be repeated until the charges used for embedding and the charges derived from the wave function of the embedding cluster are self-consistent.

The effect of embedding by a point charge array can be summarized as follows: (1) It has a negligible effect on cations unless they have d electrons. (2) It greatly stabilizes anions and compresses their charge clouds. (3) It enhances ionicities of bonds. Table 8 illustrates the first two points by recently calculated "in-crystal" polarizabilities of ions.[265-268] Further results will be reported in section V. The calculations on clusters that explicitly include first neighbor ions show that for anions overlap compression of the charge clouds through its interaction with the charge clouds of its neighbors (i.e., the effect of the short-range potential) is important. Moreover, it follows from the study of Gutowski et al.[269] on deformation of the orbitals of fluoride ions in LiF and NaF crystals that it is the exchange potential that brings about the improvement. Replacing the point charge term (eq IV.22) by the full Coulomb potential while neglecting exchange even deteriorates the

results. Obviously, the attractive penetration part of the electrostatic potential is partly counterbalanced by the repulsive exchange part.

For some purposes, e.g., the calculation of the nearest-neighbor distances[256,257] or the description of defect electrons in ionic crystals,[254,255,270,271] it proved necessary to include second[256,257] or even third and fourth neighbors[254,255,270,271] in the part of the model that is explicitly treated. Since the computational demands are very rapidly growing with the number of ions, simplifications are inevitable. An obvious possibility is to employ minimal basis sets for the outer ions hoping that this will produce only minor changes on the short-range potential felt by the inner ions. The danger of such an approach, namely that badly balanced basis sets may lead to intolerably large superposition errors, can be avoided, and the same goal reached when the electrons on the outer ions are described by frozen orbitals or even replaced by effective potentials ("total ion potentials"[256,257]). It has been also suggested to replace the short-range potential of a shell of neighboring ions by a spherical pseudopotential[272] or to simulate it by additional point charges.[267]

As far as molecular crystals are concerned, in a pioneering study Noell and Morokuma have found only marginal effects of point ion arrays on the bonding of $H_3N \cdot BH_3$.[273] Generally, bond polarities increase on embedding a molecule in its crystalline environment. Examples are crystal water[274,275] and NH_3 in solid ammonia.[276] In a study of the structure of the ammonia crystal[277] the $(NH_3)_7$ complex was used as a model. While the SCF calculation yields orbitals extending over all seven molecules in the cluster, after applying a localization procedure "in-crystal" orbitals for the central NH_3 molecule are obtained. The five orbitals belonging to this molecule are selected and their delocalization tails on the surrounding six molecules neglected. Finally, all NH_3 molecules in the crystal are made equivalent by transfer of these quasi-orthogonal orbitals. In this way, a set of quasi-Wannier functions for the infinite crystal is produced. (Note the similarity of this procedure with Fink's approach;[278] cf. section VI.)

E. Covalent Bonds: Saturator Atoms

Throughout this section models of different forms of SiO_2, of alumosilicates and related oxides, as well as models of silicon will serve as examples. Their main purpose is to demonstrate ideas. Numerous other model calculations will be referred to only in the tables of sections V–VII.

1. Fractional Atom Scheme

In crystals with covalent or essentially covalent bonds the valence electrons cannot be assigned to specific atoms, but rather to bonds. To get a meaningful model, the cut has to be made such that bonding electron pairs are not affected. This rule is easily understood when applied to a basis set of hybrid orbitals. Let us consider the Si–O bond in silica (Chart 1). A bond orbital is formed by the overlap of a Si sp^3 hybrid orbital and an O sp hybrid orbital, which should not be taken to literally, however. What is important is that it is one of two equivalent orbitals available for bonding. The Fock matrix element between the two hybrid orbitals forming

CHART 1. Fock Matrix Elements in Hybrid Orbital Basis for SiO_4 Tetrahedra in SiO_2
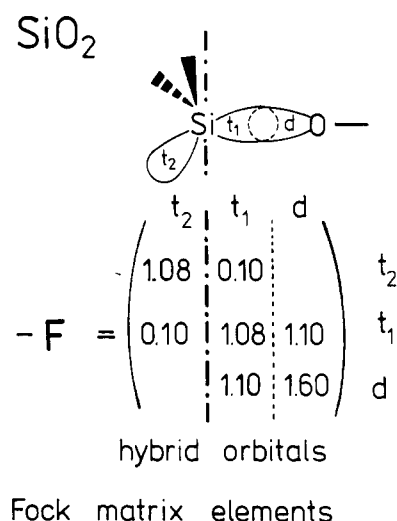
the bond is substantial and should not be neglected. A qualitatively wrong picture of electronic states is obtained when bonds are cut. Owing to neglect of Fock matrix elements that bring about stabilization, artificial surface states of unpaired electrons are created ("dangling bond states") that will be found within the gap between valence and conduction band. In contrast, overlap between different hybrid orbitals on the same atom is zero, and the coupling through Fock matrix elements is significantly smaller. Neglect of these intraatomic interactions results in too narrow bands of one-electron levels. But this effect is not serious if one only makes sure that the model involves some complete atoms.
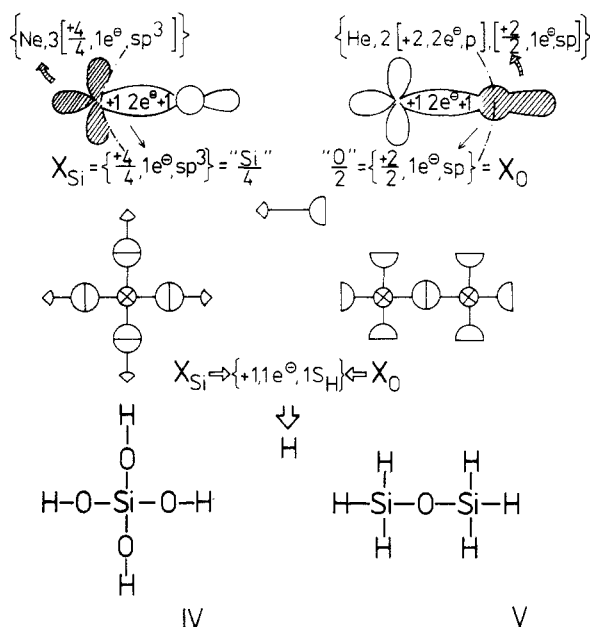
Hence, a procedure is recommended that assigns bonding and lone electron pairs (and core electrons as well) either to the cluster or to the surrounding. A corresponding share of the nuclear charge of the atoms involved in a bond must also be ascribed to the cluster to minimize the electrostatic interactions, expressed by $v^{S,lr}$ in eq IV.11 and IV.15, with the surrounding. Such a cut divides atoms into two pseudoatoms, one bordering the cluster and the other one belonging to the surrounding (Chart 2). Cutting a Si atom will leave a pseudoatom at the cluster's border with one electron (effective nuclear charge 1+) in a sp^3 hybrid orbital. One may even speak in terms of "a quarter of a Si atom" and, cutting correspondingly an O atom, of "a half of an O atom".

Such a "fractional atom" scheme has the advantage that the model preserves the stoichiometry of the solid. For example, model IV (Chart 2) has the composition $Si_4\{Si/4\}_4 = SiO_2$ and model V (Chart 2) the composition $Si_2O\{O/2\}_6 = SiO_2$. Namely, nonstoichiometric models even may possess a different number of electrons than the same building unit within the infinite crystal if it is polar as, e.g., SiO_2. The reason is that charge separation occurs within bonds. Let us assume that for SiO_2 0.25e is transferred within a Si–O bond from the Si atom to the O atom. In the infinite solid having the brutto formula $Si^+(O^{0.5-})_2$ this gives $3 + (4 \times 6.5) = 29$ valence electrons on a single $Si^+(O^{0.5-})_4$ tetrahedron, and this is also true for models IV and V above. In an isolated SiO_4 tetrahedron (a nonstoichiometric model) the total number of electrons is fixed by the number

TABLE 9. Comparison of Atomic Charges[a] for Different Types of Molecular Models of SiO$_2$ ($\Sigma q = q$(Si) $+ 2q$(O))

geometry	model	ref	Σq	q(Si)	$2q$(O$_{br}$)	$2q$(O$_{nbr}$)	$4q$(H)
optimized	H$_3$SiOSiH$_3$	284	−0.39	0.82	−1.21		−0.68
	Si(OH)$_4$	284	+0.33	*1.31*		−0.98	+0.66
	(HO)$_3$SiOSi(OH)$_3$	284	−0.06	1.36	*−1.42*	−1.00	+0.66
optimized (transf[b])	Si(OSiH$_3$)$_4$	285	+0.07	*1.47*	−1.40		
obsd (α-quartz)[c]	crystal orbital	165	0.0	1.40	−1.40		
	H$_3$SiOSiH$_3$	284	−0.47	0.88	−1.35		−0.73
	Si(OH)$_4$	286	+0.38	*1.54*		−1.17	+0.78
	(HO)$_3$SiOSi(OH)$_3$	286	+0.11	1.52	*−1.41*	−1.17	+0.78
	O$_3$Si-*O*-SiO$_3$$^{6-}$	284	−0.98	*0.74*	*−1.72*	−1.92	
	Si(O$\bar{\text{H}}$)$_4$ ($\zeta = 0.62$)[d]	286	0.00	1.45		−1.45	+1.44
	($\bar{\text{H}}$O)$_3$SiOSi(O$\bar{\text{H}}$)$_3$ ($\zeta = 0.62$)[d]	286	0.05	1.45	−1.40	−1.45	+1.43
	Si(O$\bar{\text{H}}$)$_4$ ($\zeta = 1.65$)[d]	286	0.01	1.45		−1.44	+1.44
	($\bar{\text{H}}$O)$_3$SiOSi(O$\bar{\text{H}}$)$_3$ ($\zeta = 1.65$)[d]	286	0.02	1.44	−1.46	−1.44	+1.44
obsd (ferrierit, T2[e])	*Si*[O Si(OH)$_3$]$_4$	287		*1.47*	−1.40	−1.05	
obsd (ZSM-5, T12[e])	*Si*[O Si(OH)$_3$]$_4$	288		*1.45*	−1.45	−1.32	

[a] Mulliken population analysis, SCF/STO-3G calculations. [b] Bond lengths and angles transferred from optimized structures of H$_3$SiOSiH$_3$ and (HO)$_3$SiOSi(OH)$_3$, respectively; cf. ref 285. [c] Levien, L.; Prewitt, C. T.; Weidner, D. J. *Am. Mineral.* **1980**, *65*, 920. [d] Slater exponent of 1s functions for bordering siligens; see the text. [e] Crystallographic position of central Si atom; cf. ref 287 and 288.

CHART 2. Rationalization of Molecular Models[a]

[a] Cutting atoms rather than bonds yields "a quarter of Si" and "a half of O" pseudoatoms, which may be substituted by H atoms.

each atom contributes, $4 + (4 \times 6) = 28$, and the charge distribution is Si$^+$(0$^{0.25-}$)$_4$.

The idea of stoichiometric models has been even further advanced in the so-called "orbital stoichiometric" models of SiO$_2$ and γ-Al$_2$O$_3$.[279] Care is taken that in the cluster the same relations hold between number and type of orbitals as in the perfect crystal.

2. Hydrogens and Other Real Atoms

There are several possibilities to implement the fractional atom idea into computational schemes. A very simple but powerful one is to replace the one-electron pseudoatoms by real atoms, i.e., to terminate the cluster by hydrogen atoms. We arrive at (real or hypothetical) molecules as models. This idea has gained such great popularity not only because of the readiness of computer programs for molecular calculations but also because it is in line with chemists' intuition. Although resting on some additional approximations compared with the pseudoatom concept, molecular

models have the virtue of stressing connections between structures and properties of molecules in the gas phase and of bulk[280-282] or surface sites of solids (see also sections VI and VII). For example, although disiloxan (V), orthosilicic acid (IV), and disilicic acid (VI) are models for building units of silica frameworks, ortho-silicic acid can also serve as a model of surface hydroxyls on silica (section VII).

VI

To what degree hydrogen atoms are suited to replace bordering pseudoatoms depends on the solid considered and is a matter of experience. An assessment of the quality of a model by comparison with experimental data is complicated by systematic errors connected with any quantum chemical approach (cf. section IV.G). For an ideal model, certain relations between the charges on different atoms hold. They provide "internal" criteria for the quality of a model. For models of SiO$_2$, stoichiometry implies that

$$|q(\text{Si})| = 2|q(\text{O})| \qquad \text{(IV.23)}$$

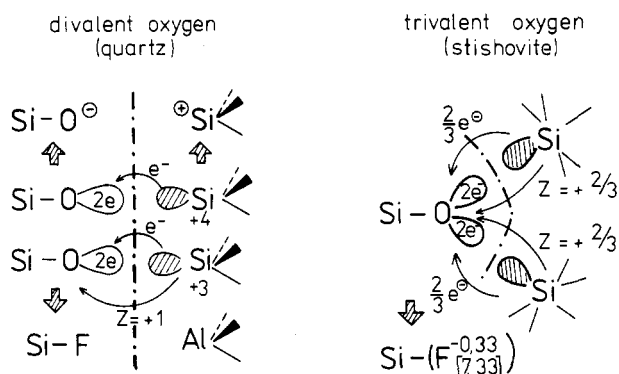Moreover, if hydrogen atoms would play their role as "a quarter" of a Si atom perfectly

$$4q(\text{H}) = q(\text{Si}) \qquad \text{(IV.24)}$$

should hold and, in the disilicic acid model (VI) there should be no difference between "bridging" (br) oxygen atoms (having two Si neighbors as in the perfect lattice) and "nonbridging" (nbr) oxygen atoms (having one Si and one H atom as neighbors):

$$q(\text{O}_{\text{nbr}}) = q(\text{O}_{\text{br}}) \qquad \text{(IV.25)}$$

Table 9 shows the atomic charges for different models of SiO$_2$ in a way that all entries in one row would be equal in absolute magnitude if the model were perfect. It is seen that hydrogen can substitute both Si and O atoms in Si-O bonds as it is able to accept electrons in Si-H bonds and to release electrons in O-H bonds. But quantitatively, hydrogen is not efficient enough in doing so. This shows that the electronegativities of Si sp^3 and

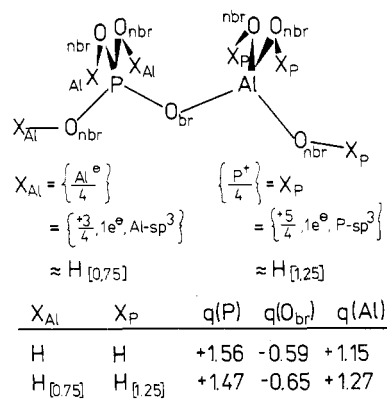**CHART 3. Termination of Molecular Models by >SiO⁻ and >SiF Groups**

divalent oxygen (quartz)   trivalent oxygen (stishovite)

$Si-O^{\ominus}$ $^{\oplus}Si$

$Si-O$ Si

$Si-O$ Si
$+4$

$+3$

$Si-F$ Al
$Z=+1$

$Si-O$

$Z=+^{2}/_{3}$

$Z=+^{2}/_{3}$

$Si-(F^{-0.33}_{[7.33]})$

CHART 4. Molecular Models of Aluminum Phosphate Frameworks

$X_{Al} = \left\{\dfrac{Al^{\ominus}}{4}\right\}$ $\left\{\dfrac{P^{+}}{4}\right\} = X_P$

$= \left\{\dfrac{+3}{4},1e^{\ominus}, Al\text{-}sp^3\right\}$ $= \left\{\dfrac{+5}{4},1e^{\ominus}, P\text{-}sp^3\right\}$

$\approx H_{[0.75]}$ $\approx H_{[1.25]}$

X_{Al}	X_P	$q(P)$	$q(O_{br})$	$q(Al)$
H	H	+1.56	−0.59	+1.15
$H_{[0.75]}$	$H_{[1.25]}$	+1.47	−0.65	+1.27

O sp orbitals are different from that of the H 1s orbital (cf. paragraph E.4).

Table 9 shows also results for the $[O_3SiOSiO_3]^{6-}$ anion. This model[283] is obtained by a heterolytic fission of Si–O bonds that connect cluster and environment (Chart 3). The bonding electron pairs are preserved, but they are accommodated in oxygen orbitals instead of in Si–O bond orbitals. Although the oxygen orbitals are less stabilized, they are still within the valence band since nonbonding oxygen orbitals form the top edge of the valence band in SiO_2. Such anionic models are not stoichiometric. Their main disadvantage is their large charge and, consequently, their large electrostatic interaction with the surrounding. Embedding in a point ion array becomes mandatory. The model can be made neutral by transferring, in addition to an electron, also the corresponding share of nuclear charge (1+) from Si to O. Formally, this creates an F atom as bordering atom while leaving an Al atom in the surrounding (Chart 3). We obtain hexafluorodisiloxane, $F_3SiOSiF_3$, as a neutral model.[282] In calculations one may also consider the use of, together with the $Z = 9$ nucleus (fluorine), basis functions optimized for oxygen. Anyhow, disilicic acid appears as the better founded model, and it is also more sound from the chemical point of view.

3. Pseudoatoms: Effective Nuclear Charges

In what follows we will discuss modifications on bordering hydrogen atoms that are still compatible with standard programs but make them more realistic. A very simple one is to change the effective nuclear charge on terminating hydrogen atoms. As an example we consider aluminum phosphate frameworks (composition $AlPO_4$), which are isoelectronic with SiO_2 frameworks and consist of alternating joined AlO_4^- and PO_4^+ tetrahedra. Chart 4 shows a model that is the analogue of disilicic acid (VI) for SiO_2.[289] The pseudoatoms X_P and X_{Al} represent "a quater of P^+ and Al^- atoms", respectively. For them hydrogen atoms may be substituted, but their effective charge should be modified to $5/4 = 1.25+$ and $3/4 = 0.75+$, respectively. The resulting model, $(H_{[0.75]}O)_3POAl(OH_{[1.25]})_3$, is neutral and has the proper stoichiometry. The charges on the central P–O–Al atoms calculated for this model are notably different from those calculated for the naive $(HO)_3POAl(OH)_3$ model (cf. Chart 4). For the perfect lattice, neutrality and stoichiometry require
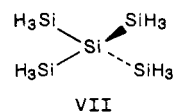
$$q(Al) + q(P) + 4q(O_{br}) = 0$$

The model terminated by hydrogens yields 0.35+ for this sum. When the above modifications on effective nuclear charges are made, this improves to 0.16+.[289]

The pseudoatom concept in general and the modifications made on effective nuclear charges for terminating hydrogen atoms in particular are also compatible with the *electrostatic valence rule*.[290] It defines the electrostatic bond strength of a cation as the quotient of its (formal) electric charge and its coordination number. Hence, the bond strength is +1 for Si in SiO_2 and $+^3/_4$ and $+^5/_4$ for Al and P, respectively, in $AlPO_4$. The rule says that an ionic lattice is stable if the formal electric charge of an anion (with reversed sign) is equal to the sum of the bond strnegths to all cations surrounding it. This sum is 2 in SiO_2 and also in $AlPO_4$ ($+^3/_4 + ^5/_4 = 2$). It is retained for all oxygens of the models introduced above for SiO_2. However, when the above $AlPO_4$ model is naively terminated by hydrogen atoms (bond strength +1), the bond strength sums for nonbridging oxygen atoms are +1.75 and +2.25 in the AlO_4^- and PO_4^+ tetrahedra, respectively. Only for the modified $H_{[0.75]}$ and $H_{[1.25]}$ atoms is the sum +2 for all oxygen atoms of the model.

4. Pseudoatoms: Variation of Orbital Exponents

The fractional pseudoatoms at the border of a cutout are defined by the following parameters: effective nuclear charge, number of electrons, and type and exponent of the valence orbital. In previous paragraphs we have dealt with the first two of them; now we turn to the orbitals itself. In the beginning we will stick to the assumption that the valence orbitals can be approximated by a 1s-type Slater orbital. (In practice, it is a 1s-type CGTF; see section II.) The atomic charges given in Table 9 show that the O–H bonds that terminate the SiO_2 models do not have the same polarity as the O–Si bonds inside the models. Similar observations can be made for $AlPO_4$ (Chart 4) and other solids, even if the nuclear charges on the terminating atoms are properly chosen. The obvious reason is that the electronegativity of the hydrogen 1s orbital is different from that of the sp^3 hybrid orbital of the Si atom in the perfect crystal that it replaces. Let us consider models of solid Si.[291] Since H is more electronegative than Si, the Si–H bonds in the

H_3Si SiH_3
      Si
H_3Si SiH_3

VII

TABLE 10. Effect of Replacing Bordering Hydrogen Atoms by "Siligen" Pseudoatoms[291,293]

model		X = H	X = $\bar{\text{H}}$
$X_3Si^{\bullet}$	IP,[a] eV	8.6	6.1
$(X_3Si)_3Si^{\bullet}$	IP,[a] eV	7.9	5.95
$X_3Si\!-\!O\diagdown_{O^{\bullet}}$	r(Si–O), pm	163	168
	r(O–O), pm	137	132
	∠SiOO, deg	126	116

[a] Ionization potential; experimental value 5.6–5.9 eV.

model are polar and cause a nonzero residual charge also on the central Si atom. This prompted Redondo et al.[291] to scale the Slater 1s orbital on the hydrogen atoms such that a neutral central Si atom is obtained. The orbital exponent ζ found this way was 0.2944, significantly different from the standard value of about 1.2. Hence, hydrogen atoms with $\zeta = 0.2944$ have effectively the same electronegativity as Si atoms in the bulk. Since they mimic bulk Si atoms, they are referred to as *siligens*[291] and denoted by $\bar{\text{H}}$. Siligens were found to have a significant effect on structure and properties of a model (cf. Table 10)[291] and have been used in subsequent studies.[77–79,292] For example, the $(\bar{\text{H}}_3Si)_3Si^{\bullet}$ model yields a value for the ionization potential (surface dangling bond) that is in excellent agreement with experiment (Table 10), and even the $\bar{\text{H}}_3Si^{\bullet}$ model is off by only 0.2 eV.

The optimum value of the Slater exponent depends on several factors. For a given model, it depends on the basis set used. For the STO-3G basis set the charge on the central Si atom is zero for $\zeta = 0.25$ and $\zeta = 1.5$.[286] Moreover, the optimum value of the exponent depends on the choice of the distance between the terminating hydrogen-like pseudoatom and its neighbor. Redondo et al.[291] put the siligens at exactly the positions of the Si atoms they replace; i.e., r(Si–$\bar{\text{H}}$) = r(Si–Si). The other possibility is to retain in the model only the bond direction of the crystal and to adopt for the bond distance a typical value of the corresponding X–H bond; i.e., R(Si–$\bar{\text{H}}$) = r(Si–H) = 148 pm (taken from SiH$_4$). The optimum ζ values become significantly smaller (ζ < 0.2 and $\zeta = 1.36$). Finally, the *siligens* turn out to be different for different solids. When the ideas of Redondo et al.[291] are adopted for the Si(O$\bar{\text{H}}$)$_4$ model of SiO$_2$,[286] the optimum ζ values (STO-3G basis set) are 1.65 and 0.62. (To fix the ζ values, use was made of the same criterion as considered above for judging the quality of the model [q(Si) = $-2q$(O)] and, hence, $4q(\bar{\text{H}})$ = q(Si).) Table 9 shows that the optimum values derived for Si(O$\bar{\text{H}}$)$_4$ yield a very satisfactory description of the charge distribution in the (HO)$_3$SiOSi(OH)$_3$ model.

It is worth mentioning that two different ζ values yield the same bond polarity. This can already be anticipated from the connection between orbital exponent and electronegativity, χ. From the ionization potential
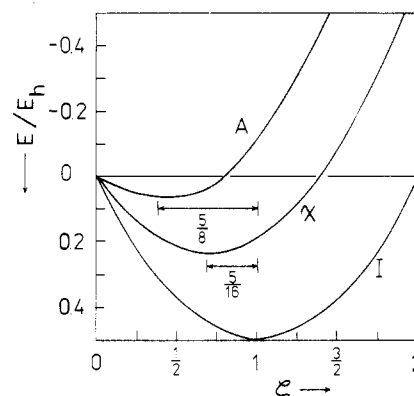
$$I = E_{X^+} - E_X \qquad \text{(IV.26)}$$

and the electron affinity

$$A = E_X - E_{X^-} \qquad \text{(IV.27)}$$

one finds for a hydrogen-like 1s orbital ($E_{H^+} = 0$):[291]

$$\chi = \tfrac{1}{2}(I + A) = -\tfrac{1}{2}E_{H^-} = -\tfrac{1}{2}\zeta^2 + \tfrac{11}{16}\zeta \qquad \text{(IV.28)}$$

Figure 4. Dependence of ionization potential, I, electron affinity, A, and electronegativity, χ, of a hydrogen atom on the Slater orbital exponent, ζ (energies in hartrees, E_h; $E_h = 2625.47$ kJ/mol).

When atoms with nuclear charges, Z, different from Z = 1 are considered, eq IV.28 should be replaced by

$$\chi = -\tfrac{1}{2}\zeta^2 + (Z - \tfrac{5}{16})\zeta \qquad \text{(IV.29)}$$

Equations IV.28 and IV.29 reflect the parabolic dependence of the energy of H$^-$ on ζ (cf. Figure 4). They give an idea how electronegativity responds to changes of the orbital exponent. The suggestion[291] to make use of eq IV.28 to estimate ζ directly from experimental χ values without any optimization, however, does not work for other systems, e.g. SiO$_2$ (vide supra), as it does for Si. There are so many assumptions underlying the pseudoatom concept that ζ should be taken merely as a system, basis set, and geometry dependent parameter that ensures proper "electronic" boundary conditions. It may be adjusted to mimic the influence of the (neglected) potential created by the surrounding. Different values may be used to introduce changes into the model that occur in the "embedding medium" of a given site.

5. Pseudoatoms: Stishovite Example

In the high-pressure modification of SiO$_2$, stishovite, each Si atom is coordinated by six oxygen atoms in octahedral configuration and each oxygen atom is bonded to three silicon atoms. There is considerable interest in the question on how the electronic structure and bonding patterns of SiO$_2$ change when passing from four-coordinated to six-coordinated polymorphs, e.g., from α-quartz to stishovite. Previous density functional band structure calculations[294] reached the conclusion that the higher coordination (and higher density) in stishovite favors a more covalent bonding (reduced net charges) while the opposite trend is observed in X-ray studies.[295] The net atomic charge on Si increases with coordination number.[295] Ab initio calculations[295,296] on molecular models seem to support the latter result. We are well aware of the fact that atomic charges have meaning only within the model defining them and that the underlying models are quite different for charges derived from X-ray experiments and those obtained from a Mulliken population analysis. The point of interest here is that the answer one gets from ab initio calculations sensibly depends on the choice of the model (Table 11).
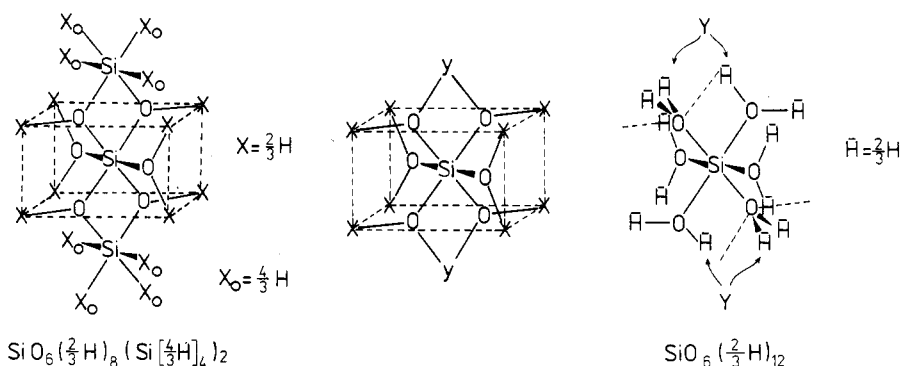
To find an appropriate molecular model of the octahedrally coordinated Si atom in stishovite is not as easy as it is for the polymorphs containing the SiO$_4$ tetrahedra. For the latter the obvious choice was ortho-

TABLE 11. Comparison of Atomic Charges for Different Models of Four-Coordinated and Six-Coordinated Silica Modifications[286,295,296]

basis set	four-coordinated (α-quartz)		six-coordinated (stishovite)	
	model	charge	charge	model[c]
STO-3G	Si(OH)$_4$, std[a]	1.36[a]	1.51[b]	SiO$_6$($^2/_3$H)$_{12}$
	Si(OH)$_4$	1.54[d]		
	Si(OH̄)$_4$[e]	1.36[d]	1.32[d]	SiO$_6$H$_8$(SiH$_4$)$_2$
	(H̄O)$_3$SiOSi(OH̄)$_3$[e]	1.39[d]	1.26[d]	SiO$_6$($^2/_3$H̄)$_8$(Si[$^4/_3$H̄]$_4$)$_2$[f]
STO-3G[(*)]	Si(OH̄)$_4$, std[a]	0.81[a]	0.87[b]	SiO$_6$($^2/_3$H)$_{12}$
	Si(OH)$_4$[a]	0.81[d]		
	Si(OH̄)$_4$[g]	0.77[d]		
	(H̄O)$_3$SiOSi(OH̄)$_3$[g]	0.80[d]	0.72[d]	SiO$_6$($^2/_3$H̄)$_8$(Si[$^4/_3$H̄]$_4$)$_2$[h]
6-31G[(*)]	Si(OH)$_4$, std[a]	1.1[a]	1.78[b]	SiO$_6$($^2/_3$H$_{12}$)
6-31G*	Si(OH)$_4$, opt	1.5[i]		
X-ray[b] expt		1.0	1.7	

[a] Reference 296; a standard (std) geometry was adopted (D_{2d}) with STO-3G values for the SiOH bond angle and the OH bond distance. [b] Reference 295. [c] Cf. Figure 5. [d] Reference 286. [e] ζ(H̄) = 1.58. [f] ζ($^2/_3$H̄) = 1.30, ζ($^4/_3$H̄) = 1.43. [g] ζ(H̄) = 1.32. [h] ζ($^2/_3$H̄) = 1.00, ζ($^4/_3$H̄) = 1.43. [i] Reference 69.

Figure 5. Molecular models for stishovite (Si centered).[286,295]

silicic acid (IV). The analogue of this model for stishovite is much larger and more complex (Figure 5). It is bordered by two types of pseudoatoms, "one-sixth" (X$_{Si}$) and "one-third of a Si atom" (Y$_{Si}$), respectively:

$$\{Si/6\} = X_{Si} \equiv \{^1/_6+, \, ^1/_6e, \text{ one hybrid orbital}\}$$

$$\{Si/3\} = Y_{Si} \equiv \{^1/_3+, \, ^1/_3e, \text{ two hybrid orbitals}\}$$

The model has the composition SiO$_6$(Si/6)$_8$(Si/3)$_2$ = Si$_3$O$_6$ and, hence, preserves the SiO$_2$ stoichiometry. The X$_{Si}$ atom can be replaced by a hydrogen atom if an effective charge of $^2/_3+$ is specified and, in addition, only two-thirds of an electron is added to the model for each of these atoms.[295] Such a modified H atom (described by an hydrogen 1s orbital) will be symbolized as $^2/_3$H. Of course, all modified terminating atoms together must contribute an integer number of electrons. The difficulty with Y$_{Si}$ is that it has two orbitals and an atom with two, but only two equivalent orbitals, and does not exist. A projection technique is necessary to handle such pseudoatoms. In a recent quantum chemical study on stishovite this difficulty has been bypassed by substituting for each Y$_{Si}$ two modified hydrogen atoms, $^2/_3$H.[295] This cannot be done without changing the local geometry, and structures of T_h and D_{2h} symmetry have been adopted[295] for the SiO$_6$($^2/_3$H)$_{12}$ model to minimize repulsion between the $^2/_3$H atoms within the pairs representing Y$_{Si}$ (see Figure 5).

The SiO$_6$($^2/_3$H)$_{12}$ model yields a Si net charge of 1.51+, and this was compared with a calculation on Si(OH)$_4$ yielding 1.36+ (Table 11).[295] However, the result depends sensibly on the SiOH bond angle. If, instead of 109.5°,[295] the value observed for the SiOSi

angle in α-quartz (144°) is adopted, the difference between the two polymorphs disappears (Table 11). However, the sum q(Si) + 2q(O), which should be zero for a perfect model, attains values of 0.38+[286] and 0.32+[296] for the α-quartz and stishovite models, respectively, indicating that both have defects. Therefore, calculations were made on models of both α-quartz and stishovite that used the observed atomic coordinates, even for the bordering pseudoatoms. When the exponent of the H 1s orbital is varied to make q(Si) + 2q(O) zero, the Si charge for the Si(OH̄)$_4$ model is significantly reduced. The Si charge calculated with this exponent for the disilicic acid model is very close to the result of the crystal orbital calculation (1.40+).[165] For stishovite no improvement was made on the SiO$_6$($^2/_3$H)$_{12}$ model, but rather the model was extended to avoid the above "Y$_{Si}$ problem". The Y$_{Si}$ = {Si/3} pseudoatoms (Figure 5) were replaced by Si{O/3}$_4$ groups, and the role of the "one-third of an oxygen" pseudoatoms

$$\{O/3\} = X_O \equiv \{^1/_3+, \, ^1/_3e, \text{ one hybrid orbital}\}$$

is readily played by $^4/_3$H atoms. In stishovite, O is assumed to have three equivalent valence orbitals and the two electrons in the fourth orbital we put into the core. This SiO$_6$($^2/_3$H̄)$_8$ (Si[$^4/_3$H]$_4$)$_2$ model yields for stishovite q(Si) = 1.26, slightly less than predicted for quartz. It is not claimed that this is the *correct* trend; it is only claimed that another choice of the model can *reverse* the trend. Nevertheless, it should be very conclusive to see the results of crystal orbital calculations on stishovite. One could argue that d orbitals play a more important role in SiO$_6$ than in SiO$_4$ structures.

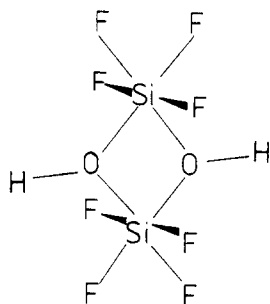**Figure 6.** Molecular model of the Si_2O_2 four-ring in stishovite.[295]

Charges calculated by the STO-3G$^{(*)}$ basis set (Table 11), though smaller in absolute value, show the same pattern, however. (The 6-31G$^{(*)}$ basis set does not seem to be well-balanced as the Si charge in $Si(OH)_4$ changes greatly when d orbitals are added on O atoms as well.)

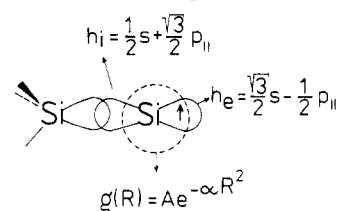Several other molecules have been suggested as models of stishovite,[280,295,297] all of which violate pseudoatom principles. STO-3G calculations on the $Si(OH)_4(OH_2)_2$ model[297] yielded $q(Si) = 1.39$. This model puts Si in its proper octahedral coordination and keeps neutrality, but it yields improper electrostatic bond strength sums for the oxygen atoms ($^5/_3$ and $^8/_3$ instead of 2). This defect is removed in the octahedral molecule with the same brutto formula (H_8SiO_6) but with the eight H atoms symmetrically arranged on the 3-fold axes of the SiO_6 octahedral group (O_h point symmetry).[280] Since each of these hydrogens has three nearest neighbors, its bond strength is $+^1/_3$ and the bond strength sum to each oxygen atom is exactly 2.

To model the Si_2O_2 four-ring present in stishovite, the $[Si_2(OH)_2F_8]^{2-}$ anion has been suggested (Figure 6) and used to investigate shared edge distortions of the SiO_6 octahedra in this mineral.[295] An analysis of this model in terms of pseudoatoms shows that the effective charge of the bordering atoms is 7.33+ and that they contribute 7.33 electrons each (cf. Chart 3). Hence, the bordering fluorine atoms should be modified accordingly, $F^{0.033-}_{[7.33]}$, and the $Si_2(O^2/_3H)_2(F^{0.33-}_{[7.33]})_8$ model should be adopted. Its total number of electrons is 80, the same as the $[Si_2(OH)_2F_8]^{2-}$ model has, but owing to appropriate effective nuclear charges (0.66+ on H and 7.33+ on F), it has the advantages of being electrically neutral and of satisfying the electrostatic valence rule.

6. Hybrid Orbitals and Pseudopotentials

In the last three paragraphs we have considered all the modifications that can be applied to made a hydrogen (or another) atom better suited as bordering atom in a molecular model. When they still do not serve our needs, we have to look for a less intuitive but more systematic way to implement the "fractional atom" idea (paragraph E.1). For the bordering atoms a complete set of valence hybrid orbitals is defined, but only those are included in the model basis set that form bonds with atoms inside the cluster. The electrons in the excluded hybrid orbitals are replaced by a pseudopotential that, however, has to be angle dependent. In their minimal basis set study on SiO_2, Litinski and Zyubin[279] terminate the $(\overline{Si}O)_3SiOSi(O\overline{Si})_3$ cluster by pseudoatoms $\overline{Si}$ that possess only one sp^3 hybrid orbital in bond direction. The remaining electrons are replaced by an angle-dependent pseudopotential. This proce-

dure makes the difference between electron populations on comparable orbitals of inner and bordering atoms of the cluster smaller than 0.01e.[279] Angle-dependent pseudopotentials would also solve the problem of the pseudoatom Y_{Si} with two hybrid orbitals in models of stishovite (see paragraph IV.E.5 and Figure 5).

Malvido and Whitten[298] avoid the need of a non-spherical pseudopotential by retaining a back-bond hybrid orbital, h_e, which is assigned to the frozen core and occupied with one electron (cf. Chart 5). A spherical density, $\rho(R)$, that integrates to two electrons replaces the other two valence electrons in the remaining orbitals (two p orbitals perpendicular to the bond axis). These pseudoatoms, $\overline{Si}$, were used to saturate the $Si(Si\overline{Si}_3)_4$ and $(·Si\overline{Si}_3)_4$ models, the latter designed to describe neutral vacancy defects in silicon. The calculations show good agreement with previous results[299] obtained for the "classical" hydrogen-bonded $(·SiH_3)_4$ model.

7. Concluding Remarks

There are presently not yet enough demonstrations that pseudoatoms involving fractional charges and modified orbital exponents actually yield improved agreement with experimental results. In particular, there is very limited experience with geometry optimizations. It is also true that any chemist (including the author) feels better when he deals with a real (or hypothetical) molecule that, at least in principle, can be observed than with an artifact. However, the indisputable advantages of the pseudoatom concept are as follows: (i) It helps to understand why a particular atom is well-suited to terminate the dangling bonds of one type of solid and why this is not the case for other types of solids. (ii) Comparison of results obtained with real atoms and pseudoatoms as bond saturators indicates how *sensitive* the results are to reasonable changes of the model. A striking example of the latter are the calculations on stishovite (section IV.E.5).

Implementation of the pseudoatom concept appears more difficult when the basis sets are extended. There are not enough internal criteria to fix the increasing number of orbital exponents. The recommended solution is passing to a hybrid orbital basis set on the terminating atoms. This requires a projection technique in combination with the frozen orbital approximation. Steps in this direction were described in section IV.E.6. Since impressive improvements of the results are not yet visible, so far there has been little incentive for adopting this more elaborate, though conceptually appealing, approach.
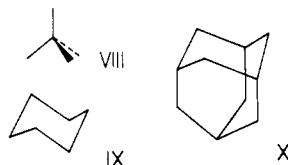
F. Geometric Boundary Conditions

To determine theoretically the optimum geometry for a cluster or a molecular model the powerful methods

TABLE 12. Effect of "Geometric" Boundary Conditions on Bond Distances (pm) and Angles (STO-3G Basis Set)

model	type of optimizn[a]	T^1–O–T^2, deg	$r(T^1$–$O_{br})$	$r(T^1$–$O_{nbr})$	$r(T^2$–$O_{br})$	$r(T^2$–$O_{nbr})$	O–T^1–O	O–T^2–O	ref
(HO)₃SiOSi(OH)₃	free	141[b]	161.7[b]	(162.2)[b,c]			not reported		302
	free	143	159.4	(165.8)[c]			108.2		282
	free	144	159.1	165.8			(109.5)[c]		282
	bc	154	158.1	(158.4)[d]			(109.5)[c]		286
	periodic	133	160.5				(109.5)[c]		165
[(HO)₃SiOAl(OH)₃]⁻	free	139	156.9	(167.1)[c]	169.5	(171.9)[c]	112.8	108.0	282
	free	139	157.5	167.1	168.9	171.9	(109.5)[c]	(109.5)[c]	282
	bc	142	157.0	(158.0)[d]	168.1	(168.8)[d]	(109.5)[c]	(109.5)[c]	286
(HO)₃POAl(OH)₃	free	125	158.1	165.2	177.4	170.8	(109.5)[c]	(109.5)[c]	289
	bc	126	157.2	(157.2)[d]	176.1	(175.3)[d]	(109.5)[c]	(109.5)[c]	289

[a] Key: bc, "geometric" boundary conditions; free, "free-space" optimization. Note that the latter may also be constrained to reduce the number of optimization parameters. [b] The 6-31G basis set augmented with d functions on the Si and O_{br} atoms was employed. [c] Parameter fixed in optimization. [d] Parameter constrained by geometric boundary conditions.

available for molecules[39,40] (cf. section II.A) can be adopted. A recent theoretical study[300] of small silicon clusters (Si$_n$, n = 2–7, 10) illustrated how difficult it is to get results of some relevance for the crystal if neither electronic nor geometric boundary conditions are imposed. The optimum structures for a given number of silicon atoms possess a topology that is completely different from that of the corresponding small crystal fragments. For n = 5 it is not the tetrahedral structure VIII, for n = 6 it is not a six-membered ring IX, and for n = 10, it is not the adamantane-type structure X

that are the most stable ones. It became obvious that much larger clusters would be required before the microcrystal structures with many dangling bonds become competitive with the more compact clusters in which the Si atoms are better coordinated. The conclusion is that searches on hyperfaces should be limited to structures with the same topology as fragments of the crystal one is going to model. Moreover, electronic boundary conditions should be imposed as described in preceding paragraphs.

Numerous calculations of such a type have been made to estimate bond distances and angles for solids (cf. sections V–VII). Again, we take silica and related framework structures as example (see, e.g., ref 282, 301, and 302). Table 12 shows bond lengths and angles for optimum structures of (HO)₃T⁽¹⁾–O–T⁽²⁾(OH)₃ models (T = Si, Al⁻, P⁺). Their structure deviates significantly from that of the corresponding building units of the infinite solid. Due to termination by hydrogen atoms the model exhibits two different types of oxygen atoms: bridging atoms, O_{br}, which are bonded with two silicon neighbors and nonbridging atoms, O_{nbr}, which are bonded with one silicon and one hydrogen neighbor.

Correspondingly, two types of T–O bonds exist, T–O_{br} and T–O_{nbr}, which have different lengths, and the optimum T–O_{nbr}–H angles are different from the optimum T–O_{br}–T angles. In contrast, in the bulk of the

framework structures considered, only one type of oxygen atom (bridging) occurs and all T–O bonds have the same length. Of course, as many studies have shown, the results for the central T⁽¹⁾–O_{br}–T⁽²⁾ groups are representative for the situation in the bulk and not very much affected by the improper geometry of the bordering Si–O_{nbr}–H groups.

Nevertheless, we can make a model more realistic by employing knowledge on periodicity of the structure and impose "geometric" boundary conditions in addition to the "topologic" ones mentioned above. I.e., we require

$$r(T–O_{nbr}) = r(T–O_{br}) \qquad (IV.30)$$

and

$$\angle T–O_{nbr}–H = \angle T–O_{br}–T \qquad (IV.31)$$

The same bond angle on O_{br} and O_{nbr} will enforce the same hybridization on both types of oxygen atoms and, consequently, will reduce the charge difference between O_{nbr} and O_{br} atoms. To obey eq IV.30 and IV.31 is trivial if we can work with the known positions of the atoms of the site of interest in the crystal and would like to calculate the energy and wave function for this geometry. The terminating hydrogen-like atoms either are put directly on positions of real atoms (as described above for the Si(SiH₃)₄ model[291]) or are put on the line connecting this atom with its neighbor X inside the model at a distance typical of X–H bonds. This way the bond angles of the bulk are preserved.

However, if we are going to determine bulk values of bond distances and angles theoretically, we have to ensure that eq IV.30 and IV.31 are valid in each step of the optimization procedure. The difference to a normal optimization run is that increments for changing the geometry parameters are calculated for the T–O_{br} bonds and T–O_{br}–T angles only, but using these increments identical steps are made for the T–O_{nbr} distance and T–O_{nbr}–H angle as well:[286,289]

$$\Delta r(T–O_{nbr}) = \Delta r(T–O_{br}) \qquad (IV.32)$$

$$\Delta\angle T–O_{nbr}–H = \Delta\angle T–O_{br}–T \qquad (IV.33)$$

Such optimizations under "geometric" boundary conditions are conveniently carried out by geometry optimization programs that transform the calculated energy gradients into internal coordinates to make a step toward the energy minimum. Examples are Pulay's force relaxation method[39] as implemented into HONDO5 by Čársky et al.[303] or Schlegel's method[40] as imple-

mented into the GAUSSIAN programs.[43,44] Note, one cannot obtain the same result in a standard optimization run by simply constraining $r(T-O_{br})$ and $r(T-O_{nbr})$ or $\angle T-O_{br}-T$ and $\angle T-O_{nbr}-H$ to change by the same amount at the same time. This would yield average bond distances and angles affected (in the present case even dominated) by the values that are optimal for the artificially introduced $T-O_{nbr}-H$ groups. For example, for $T = Si$ the optimal $T-O_{br}-T$ angle is about 145°, while the optimum $T-O_{nbr}-H$ angle is about 108°. Table 12 compares for three models the results of nonconstraint with those of constraint optimizations. The effect of geometric boundary conditions is not dramatic, but a properly constrained optimization certainly helps to separate errors connected with the model from those connected with the quantum chemical method and basis set. Table 9 shows that the charge difference between bridging and nonbridging O atoms of the $(HO)_3SiOSi(OH)_3$ model is halved for geometries compatible with geometric boundary conditions (e.g., for observed geometries). In calculations on relaxation of the (111) surface of silicon[79] and formation of bonded pairs on (100) surfaces,[77] the "siligens" belonging to the surface layer of the model were also moved according to geometric boundary conditions (cf. section VI).

G. Reliable Predictions from Approximate Calculations on Limited Models?

Ab initio calculations on molecular models of solids are affected by two types of errors: errors due to approximations connected with the quantum chemical method (section II) and errors due to replacing the solid by a finite model (this section).

When dealing with models of solids, we are in the domain of medium-sized or large molecules (systems starting from five up to dozens of atoms) frequently containing elements from higher periods and involving unusual bonding types. Although the situation is expected to improve rather dramatically soon, for the time being the majority of applications presented in sections V–VII neglect electron correlation and employ small basis sets that do not always contain polarization functions. From the discussion in section II it is evident that such results can be fraught with sizable uncertainties. It is a further complication that the error due to replacing the solid by a finite model is also unknown. How is it possible, in spite of this, to make reliable predictions?

First, one should try to empirically find increments to correct for errors introduced by the method/the basis set used: (1) Select a set of molecules with electronic structures comparable with your model for which you know the accurate result (either from experiment or from a accurate calculation). (2) Perform calculations on these molecules with the method/basis set you intend to use for your model (or find results in literature). (3) Compare your results with the accurate ones. (4) In case you find considerable regularity in the deviations, derive increments or scale factors to correct your results. (5) Get corrected results for the models investigated.

Examples of this type of approach are the "empirically corrected theoretical geometries"[304] recommended by Pulay[305] and the "scaled force fields" suggested by Blom and Altona,[304] Pulay,[306] and others.
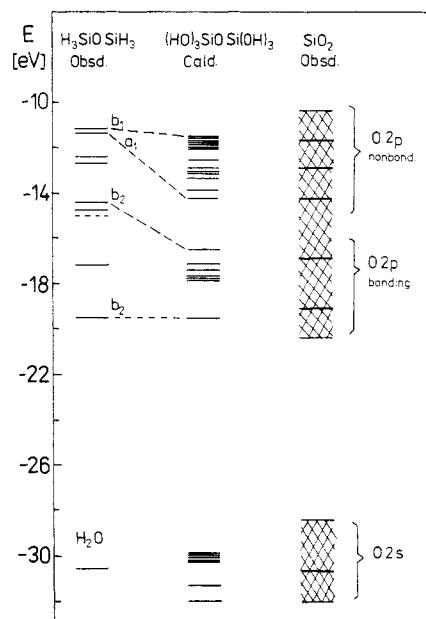
Figure 7. Valence electron levels of SiO_2. Observed values[308] compared with predictions based on STO-3G calculations for the disilicic acid model and both observed and calculated data for the disiloxane and water molecules (see text).

Another example is the calculation of the valence electron levels of SiO_2 that used the STO-3G basis set and adopted the disilicic acid molecule (VI) as model. The systematic error connected with the STO-3G basis set was evaluated by making calculations[307] on the $H_3SiOSiH_3$ and H_2O molecules for which photoelectron spectra were observed. Hence, from the calculations it was inferred how the O 2p and O 2s levels shift when passing from the disiloxane and water molecules, respectively, to the disilicic acid molecule. Figure 7 shows that after such an "empirical correction" the valence electron levels of disilicic acid satisfactorily reproduce the levels observed for SiO_2.[308]

Second, one should try to apply what is called the "hierarchic" approach: (1) Design a series of models of increasing complexity. (2) Select a series of methods/basis sets of increasing reliability. (3) Study the smallest model by all the methods and study all the models by the simplest method. As an example we consider the binding of a molecule (say H_2O) onto the surface of transition metals. An adequate model must certainly include many metal atoms (from different layers). However, we will not understand the binding in such an advanced model if we do not understand the nature of the binding between a single transition-metal atom and a H_2O molecule. Investigating this "minimal" model by methods including electron correlation showed that binding is largely due to dispersion energy.[87,89] Previously predicted stability at the SCF level was shown to be due to an artifact, namely basis set superposition error (cf. section V.C). This shows that it is useless to study complexes of H_2O with several transition-metal atoms at the SCF level.

The combination of both of the above ideas is exemplified by the predictions made for the local structures of terminal ($\equiv SiOH$) and bridged ($\equiv SiOH \cdot Al \equiv$) hydroxyl groups in zeolites (Figure 8).[69] These geometries are difficult to deduce from experiments, but to know them is important for understanding their catalytic (Brönsted) activity (cf. section VII). The predictions

TABLE 13. Calculations on Perfect Lattices of Ice and Other Molecular Crystals (Units: Energies, kJ/mol; Distances, pm)

(type) method; model	ref	crystal			dimer [(H₂O)₂]			monomer (H₂O):
		$-\Delta E$	R_{OO}	$r_{OH}{}^a$	$-\Delta E$	R_{OO}	$r_{OH}{}^a$	r_{OH}
				Ice I				
experiment[b]	310[b]	59.0	275	100,[b] 99.5[c]	22.6 ± 2.9	296 ± 1		95.72
(A) SCF/4-31G; cyclic hexamer	314		272	97.4	33.8	286	95.7	95.2
(A) SCF/VDZ; cyclic hexamer	315	45.4	263–272					95.1
(A) SCF/[5,3,1/3,1]; infinite chain	173	29.3	284	95.4	21.8	298	94.6	94.2
(B) MP2/6-31G*; dimers, trimers	310	51.5	287	(95)	21.8	298	(95)	95
(C) MCY; hexamer	315	30.0	280–288	(95.7)				
(C) MCY + 3-body + 4-body; hexamer	315	35.6	265–274	(95.7)	24.6	287	(95.7)	95.7
(C) MCY, 3-dim lattice	316	49.6	296	(95.7)				
(C) modified MCY, 3-dim lattice	317	54.3	290	(95.7)	25.3	298	(95.7)	95.7
(C) modified MCY + 3-body + OH stretch; 3-dim lattice	317	66.1[d]	279[d]	97.7[d]	25.3	298	(95.7)	95.7
		59.8[e]	285[e]	97.2[e]	25.3	298	(95.7)	95.7
				Formic Acid				
experiment[b]	318[b]	61.9	263	104[f]	66.9, 61.9[f]	270	103.6[f]	97.2
(A) SCF/[4,2/2]; infinite chain	170	66.5	261	99.3	101.3	264	88.7	96.0
(C) potential; 3-dim lattice	318	52.3–56.5[g]	263–269[g]		46.9	267		
				Acetic Acid				
experiment[b]	318[b]	68.2	263		62.8	268		
(C) potential, 3-dim lattice	318	51.9–52.3[g]	266–264[g]		50.2	265		

[a] Values in parentheses not optimized (fixed at the monomer value). [b] For references to experimental work, see quoted theoretical papers. [c] Reference 319 [d] Pma2₁ structure. [e] Cmc2₁ structure. [f] Reference 170. [g] Two different procedures were used to optimize the lattice geometry.[318]
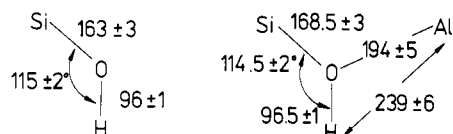

Figure 8. Recommended estimates for the local geometry of terminal and bridged hydroxyls in zeolites.[69]

are based on SCF calculations on the H_3SiOH and $H_3SiOH \cdot AlH_3$ models that used the 6-31G* basis set. Increments to correct for systematic errors of geometry parameters and error limits were inferred from the results compiled in ref 51 and the data of Table 1. The sensitivity of the results on extension of the models up to $Si(OH)_4$ and $(HO)_3SiOH \cdot Al(OH)_3$ was estimated by calculations employing the minimal STO-3G and MINI-1 basis sets.[69]

The point in adopting models of different sizes and employing basis sets of different qualities is that one does not get just one number, but one gets a feeling of how uncertain this number may be and this should be indicated explicitly by specifying error limits for the results.

V. Molecular and Ionic Crystals

A. Molecular Crystals

The geometry and the properties of a molecule in crystalline state are different from the respective gas-phase values. Moreover, the interaction between pairs of molecules is also affected by the crystalline environment.

As crystal orbital (CO) methods to cover all interactions are not yet feasible (note, however, an early minimal basis set study of the band structure of solid methan[309]), three different types of approaches are currently employed:

(A) Large Finite Clusters. It is hoped that most significant interactions are included. Infinite chains are a special case; they adopt the cluster approach in two dimensions but employ the crystal orbital technique in the third dimension. Hydrogen-bonded chains of HF, H_2O, CH_3OH, HCOOH, H_2NCOOH, and HCN were extensively studied by Karpfen et al.[170–173,189,190] The cluster approach is also most suited to study defects and other local phenomena (vide infra).

(B) Superposition of All Different Dimer and Trimer (and Possibly Tetramer) Interaction Energies. This approach expands the total stabilization energy of the crystal into two-body, three-body, and higher many-body contributions and, thereby, replaces the calculation on a huge cluster by a number of calculations on the respective n-membered clusters. Computational savings arise from the possibility (1) to neglect n-body interactions when the distance of the species involved is beyond a given cutoff limit and (2) to treat the dominant two-body terms by better methods than the many-body terms. Both the "supermolecule" approach, e.g. ref 191 and 310, and intermolecular perturbation theory, e.g. ref 269, 311, and 312, may be employed.

(C) Analytical Potential Functions. These are used to evaluate the two-body (and possibly many-body) contributions to the energy of the crystal. Empirical atom–atom potentials are described in ref 313. We consider only nonempirical potential functions. Their parameters are obtained by a fit to results of type B.

One of the most studied crystals is ice (Table 13). From experiments we know that its cohesive energy is about 2.5 times the stabilization energy of the gas-phase dimer. The crystal potential compresses the O⋯O distance by about 21 pm and, at the same time, stretches the OH bond by about 4 pm compared with the gas-phase dimer.

Cyclic hexamers are typical building units of ice and, hence, suitable cluster models. But they contain only one hydrogen bond per molecule while ice contains about two. It is therefore not surprising that calculations[314,315] on hexamers (Table 13) predict a stability increase by only a factor 1.3 compared with the dimer, while an increase of 2.6 is observed for ice. The same

increase (factor 1.3) is found for the infinite chain,[173] which is also stabilized by one hydrogen bond per molecule. Neither of the model calculations yields the full compression of the O···O distance. Note that these results are affected by both imperfections of the model and shortcomings of the basis set such as superposition error and overestimation of the water dipole. While the former will result in a too large an O···O distance, the latter will make it too short. When all dimer and trimer interactions are properly computed, making corrections for the basis set superposition error (BSSE) and including correlation effects at a simple level (MP2), the calculated cohesive energy comes close (up to a few kilojoules/mole) to the experimental value.[310] The importance of three-body effects is underlined by the results obtained with nonempirical potential functions. Both for the cyclic hexamer[315] and the three-dimensional lattice[317] the O···O distance shrinks by about 13-19 pm on inclusion of many-body contributions. The stretching of the O-H bond is found to be nearly independent on the shrinkage of the O···O bond. The effect of the O-H stretch is just to increase the binding energy. The use of the famous "Matsuoka–Clementi–Yoshimine" (MCY) pair potential[320] for calculations on ice revealed that it is not only too attractive in the bonding region (see the result for the dimer) but also too repulsive at short distances (as consequence the calculated O···O distance of ice becomes even longer than that for the gas-phase dimer). On the basis of additional calculations, a new fit of the MCY potential has been suggested[317] that improves the description of ice.

Nonempirical pair potentials were also employed to predict structures and energies of carboxylic acids.[318] While reasonable accuracy was reached for the structures of dimers and crystals, the calculated energies are in error by about 30% (Table 13). A compilation of calculations on models of defects and local sites in ice and crystalline NH_3 is given in Table 14.

In summary, promising attempts have been made along different lines to treat molecular crystals theoretically, which are not yet converged to definite results. Future successful studies are expected to show the following features: (1) Three-body and possibly higher many-body contributions must be included. (2) Two-body potentials must be very accurately evaluated, paying attention to all that is known today on how to properly calculate intermolecular interactions.[321,322] The hardest problem to overcome if quantitative results are attempted is to get converged results for the dispersion energy (see, e.g., ref 321). So far only crude estimates (by the MP2 approximation) have been made for ice[310] and hydrogen fluoride.[191] (3) The convergence of the cluster approach could be improved (with little extra cost) when the cluster is embedded in properly fixed point ion arrays. This way, "in-crystal" pair interactions would be obtained that might be particularly useful for procedure B above. (4) Frozen molecule geometries will do as long we are interested in lattice parameters and cohesive energies. When aiming at "in-crystal" vibrational frequencies and, e.g., O-H distances, accurate (anharmonic) potentials are indispensable.[317] Full optimizations of geometry parameters are limited to type A approaches. Results have been reported for infinite chains[170,171,173] of HF, H_2O, HCN, HCOOH, and CH_3OH

as well as for oligomers of H_2O[314,315] and HCN.[323] Force constant calculations do not yet go beyond harmonic terms, and quantitative agreement of observed O-H frequencies is not yet reached.

Finally, we should mention two special techniques for nonempirical calculations on molecular crystals. The first method[324] starts from the isolated molecule model and approximates the SCF solution for the crystal by perturbation theory. When taken to sufficiently high order, it becomes ultimately equilvent to the CO method. Compared with the latter, it does not save anything on the integral side but it avoids integration over **k** space (cf. section III) as the solution is obtained directly in terms of density matrix elements. Hence, the method is computationally advantageous only when the expansion converges rapidly, i.e. when the (free space) molecular orbitals provide a good approximation to density matrix elements of the crystal. To the authors knowledge the only application up to now is a study on the "in-crystal" dipole and quadrupole moments of HCl and HF employing the 3-21G basis set.[325] Contrary to the above-mentioned results of CO calculations on the one-dimensional chains[173,190] (cf. section III), it predicts lower dipole moments in the crystal than in the gas phase.

The second method[326,327] also starts from molecular orbitals localized on individual molecules that, however, are relaxed "in-crystal" orbitals. As orbitals belonging to different molecules are nonorthogonal, the energy expression for the total energy of the crystal depends explicitly on the inverse overlap matrix, S^{-1}. This resembles the treatment of the cohesive properties of ionic solids in the pioneering work of Löwdin[328] and in subsequent studies (ref 311 and 312 and references therein). For ionic crystals the smallness of the off-diagonal elements of the overlap matrix **S** justifies a power series expansion of S^{-1} that is truncated after terms in S^2. The present method, however, is particularly designed to treat molecular crystals under pressure, where the off-diagonal elements of **S** are relatively large. A set of simple linear equations is suggested[326] to solve for the elements of S^{-1}. The method evolves its computational advantages only when combined with a term by term treatment of first-neighbor, second-neighbor, and so on interactions and with additional approximations. The only application to date deals with solid H_2 under high pressure.[327]

B. Ionic Crystals and Surfaces

With the exception of CO studies (which have been only recently completed for MgO[200] and LiH[197]), since the pioneering work of Löwdin[328] theoretical concepts for ionic crystals rely on the assumption that ions retain their individuality in the crystal and are described by well-localized orbitals. Table 15 shows what has been achieved in describing perfect crystals. The same classification, types A–C, can be applied as introduced above for molecular crystals. Löwdin's approach has been substantially advanced and extended by Andzelm and Piela.[311,312] Their studies on LiF[311] and NaF[312] point to the important role of second order, e.g., dispersion effects and of many-body contributions. A more recent extension[269] of this work takes account of exchange effects in the deformation of the interacting ions.

TABLE 14. Calculations on Models of Local Sites in Molecular and Ionic Crystals

subject	model[a]	method/basis set[b]	aim	ref
ice, Bjerrum and ionic defects	$(H_2O)_5$, $(H_2O)_6$	SCF/STO-3G SCF/4-31G	"in-crystal" dipole moment of a water molecule in ice	319
ice, Bjerrum L defect	$(H_2O)_5$ $(H_2O)_4$	SCF/4-31G SCF/6-31G*	activation energy for L defect migration via rotation of the central H_2O	310
ice Ih, orientational defects	$(H_2O)_4$, $(H_2O)_5$	SCF/3-21G	local geometry and relative energy of L and D defects	329
ice	$(H_2O)_n$ $(n = 1, ..., 5)$	SCF/[4,3/2], SCF/[5,4/3], SCF/[4,3,1/2,1]	^{17}O and ^{2}H nuclear quadrupole coupling constants	275
ice Ih and VIII	$(H_2O)_5$, $\{H_2O\}^P$ $\{(H_2O)_5\}^P$	SCF[d]	electric field gradients at nuclei	330
NH_3 crystal	$(NH_3)_4$ $\{NH_3\}^P$	SCF/DZ SCF/[4,3,1/2,1]	electric field gradients at nuclei	331
bonding in $B_6H_6^{2-}$ within the $[(CH_3)_4N^+]_2(B_6H_6^{2-})$ crystal	$\{B_6H_6^{2-}\}^P$	SCF/6-31G*	orbital energy levels, influence of point ion field	332
interionic potentials of LiF	$\{Li^+\}^P$, $\{F^-\}$,^{P}, $\{Li^+F^-\}^P$ $\{(Li^+)_2\}^P$, $\{(F^-)_2\}^P$, $\{(Li^+)_2F^-\}^P$ $\{Li^+(F^-)_2\}^P$, $\{(Li^+)_2(F^-)_2\}^P$	SCF/[2,1/1] SCF/(8,4/6,4) SCF/(8,4,1/6,4)	total energies; two-, three-, and four-body contribution to binding energies; difference between free and embedded clusters	255
interionic potentials of NaCl	$Na^+\cdots Cl^-$ $Na^+\cdots Na^+$, $Cl^-\cdots Cl^-$	MR-CI/[10,6,1/8,3,1]	rigid-ion pair potential parameters	333 334
interionic potentials in solid NaOH	$\{H-O^-\}^P$	CI/DZP+dif p,d	structure including O-H bond length	259
	$\{Na^+\cdots OH^-\}^P$ $\{OH^-\cdots OH^-\}^P$	SCF/DZP+dif p,d	rigid-ion pair potential parameter	
interionic potential in MgO	$\{O^{2-}\cdots O^{2-}\}^P$	SCF/(7,4,3)	shell model potential parameter	335
electronic structure of NiO	$\{Ni^{2+}(O^{2-})_6\}^P$	RHF,UHF/[431/31]	one-electron levels (IP)	336
core level shifts in LiF, BeO, and MgO	$A^\pm$: $\{A^+\}^P$, $\{AB_6^{5\pm}\}^P$, $\{AB_6A_{12}^{7\pm}\}^P$, (A, B = Li, F)	RHF/[4,3/4,2]	core- and valence-electron levels, relaxation energies, effective	337
	O^{2-}, $\{O^{2-}\}^P$, $\{OBe_6^{10-}\}^P$, $\{OBe_4^{6-}\}^P$, $\{OBe_4O_{12}^{18-}\}^P$, $\{OMg_6^{10-}\}^P$, $\{OMg_6O_{12}^{14-}\}^P$	RHF/[6,4/4,3/4,2]	orbital sizes, shake-up probabilities	338
Na^+ hole states in NaF	$\{NaF_6^{5-}\}^P$	RHF/(17,8)/[3,2,1] RHF/[10,7/3,3,1]	wave functions for evaluation of Auger rates	339
F center in LiF and other halides	$\{e^-(Li^+)_6\}^P$ $\{e^-(Li^+)_6(F^-)_{12}\}^P$ $\{e^-(Li^+)_6(F^-)_{12}(Li^+)_8\}^P$	RHF/DZ(F$^-$DZ+dif)^c RHF/MB(F$^-$DZ+dif)^c	^{2}S → ^{2}P excitation energy	270 254
F and F_A centers in alkali halides	$\{e^-(Li^+)_6\}^P$ $\{e^-(K^+)_6\}^P$	UHF/[4] (4s)^c UHF/[4,3] (4s)^c	optical absorption energies, hyperfine splitting constants	258
F^+ center in MgO	$\{e^-(Mg^{2+})_6\}^P$ $\{e^-(Mg^{2+})_6(O^{2-})_{12}\}^P$	UHF/DZP (5s)^c UHF/MB (3s)^c	optical properties, lattice distortion, polarization	271
Cu^+ ion impurity in NaF and NaCl	$\{NaX_6Na_{18}^{13-}\}^{P,e}$ $\{CuX_6Na_{18}^{13-}\}^{P,e}$ X=F, Cl	SCF/[10,9,3/6,4,1] F, Cl: EC-[2,3]	Cu-B equilibrium distance, optical spectra ($^1A_{1g}$, $^{1,3}E_g$, $^{1,3}T_{2g}$ energy levels)	256 257
optical spectrum and Jahn-Teller splitting of Cu^{2+} sites in K_2CuF_4	$\{(CuF_6)^{4-}\}^P$	MR-SD-CI/SV	energies of d-d excitation, harmonic force constants, JT coupling constants, adiabatic (anharmonic) potentials	340
excitations in cuprous halides	$\{[CuX_4]^{3-}\}^P$, X=Cl, Br $\{[Cu_4Cl]^{3+}\}^P$ $\{[CuClCu]^+\}^P$	SCF, first-order CI^d	photoionization spectrum	341 342
$CoCl_4^{2-}$ ion in Cs_3CoCl_5	$\{CoCl_4^{2-}\}^P$	CAS-SCF/[8,5,3/6,4]	spin density, optical spectrum	343

$^a\{\}^P$ denotes embedding by a point ion array. ^{b}See sections II.A and C for explanations of symbols and abbreviations. Basis sets may be specified by giving the number of s, p, d, ..., functions in brackets. Square brackets refer to contracted GTFs while parentheses refer to uncontracted (primitive) basis functions. A slanted stroke separates entries for atoms from different periods in descending order. ^{c}Basis set for the defect electron at the anion site. ^{d}Basis set not specified. ^{e}All 10 electrons of the 18 second nearest-neighbor Na^+ ion are replaced by an effective core potential (total ion potential).

From these results as well as from the significant differences between "in-crystal" and gas-phase properties of anions (cf. section IV.D, Table 8), it follows that any attempt to derive ion-pair potentials should be made for an ion pair embedded in a point ion array (as done in some cases,[255,311,312] listed in Table 14) or, even better, for a cluster including first neighbors as well.[269,344] Hence, the intention of Laaksonen and Clementi[333,334] to derive nonempirical pair potentials that can be applied to (1) diatomic and dimeric species in the gas phase, (2) perfect and defect crystals, and (3) the molten salt seems not very promising. Their potential has been derived from gas-phase calculations. And indeed, the error it produces on the energy of co-

hesion of NaCl (10%, cf. Table 5) by far exceeds the error for LiF, NaF, and MgO for which embedded clusters were used. Another successful ab initio structure prediction via pair potentials has been reported for solid NaOH (cf. Table 4).

For simulation of perfect and defect ionic lattices as well as for impurity centers, theoretical methods have been developed that rely on ion-pair potentials.[345] Although the use of empirical potentials has met some success, serious parameterization problems have arisen that call for ab initio pair potentials. It will also be typical to combine ab initio potentials for some type of interaction ($O^{2-}\cdots O^{2-}$) with an empirical potential ($Mg^{2+}\cdots O^{2-}$) as recently done in a study[355] on bulk and

TABLE 15. Cohesive Energy (E_{coh}, kJ/mol), Lattice Constant ($2a_0$, pm), and Compressibility (β, 10^{-11} m²/N) for Perfect Ionic Crystals

	type of calculation	ref	E_{coh}	$2a_o$	β
LiF					
calcd	CO[a]	346	1077	397	
calcd	LDA/CO[b]	223	945	409	
calcd	B[c]	311	1024.7	404	1.44
calcd	B[c]	269	1028.4	403	1.36
obsd[d]			1032.6 ± 8.8	403	1.43
			1021	401	
NaF					
calcd	B[c]	312	932.5	458	2.24
calcd	B[c]	269	934.3	458	2.31
calcd	A[c]	256		462.5	
obsd[d]			932.2	460.5	1.93
			911.7 ± 8.8	463.4	1.94
NaCl					
calcd	C[c]	334	850.2	576	4.85
calcd	A[c]	257		566	
calcd	LDA/PW[e]	21		556	3.52
obsd[d]			775.3	564	3.65–3.76
LiH					
calcd	CO[a]	197	888	410	2.93
obsd			908	408	2.88–4.39
MgO					
calcd		347	1004		
calcd	CO[a]	200	961	420	0.54
calcd	LDA/PW[e]	348	961	419	0.68
obsd[d]			1008	421	0.56–0.65

[a] Crystal orbital calculations; cf. section III.C. [b] Crystal orbital calculations within the LDA (cf. sections II.D and III.D). [c] Type of approach (A–C) as described in section VI.A. [d] For references see quoted theoretical papers. [e] Pseudopotential calculations within the LDA (cf. section II.D) employing a basis set of plane waves (cf. section III.D).

defect properties of MgO. The ab initio potential performs as well as the empirical potential although the $O^{2-}\cdots O^{2-}$ short-range interactions *have different signs* in both schemes. This finding underlines the ambiguity of empirical potentials. Table 14 provides a key to further calculations on defects and local phenomena.

Table 16 lists studies of chemisorption and physisorption on ionic surfaces. The first question asked in chemisorption studies is for the mechanism, e.g., whether H_2 is split heterolytically or homolytically. To decide, accurate relative energies for different bonding situations are needed. These, however, are not provided by the SCF method that most studies use but require beyond Hartree–Fock techniques (see. e.g., ref 75; cf. section II.C). Hence, the answers are no more than qualitative (section VI). It seems characteristic that chemisorption occurs on defective surfaces only, while physisorption (binding of intact molecules) can occur on planar (nondefective) surfaces. In the most advanced physisorption studies, pair potentials between the ad-atom (He) and the ions of the solid (Li^+F^-) are derived from SCF calculations on next-neighbor models (NNM), $F^-(Li^+)_5$, embedded in point charge arrays.[344] Repulsion potentials between He atoms and "in-crystal" ions are found to be significantly weaker than those involving free ions (compare similar findings for interionic potentials mentioned above), and surface anions are much less polarizable than free anions (but only slightly more than bulk anions).

Simpler "supermolecule" approaches to physisorption rely on the assumption that the major binding effect is due to electrostatic interactions and polarization of the ad-molecule by the ionic lattice. The quantum

chemical problem is solved for a model consisting of the ad-molecule and a single surface ion (or very few ones), while the remainder of the crystal is included as point charge array on the Hamiltonian of the model.[349,350,359,362] Adsorption of CO on the MgO(001) surface has been studied by both embedded ion cluster models[359] and periodic crystal orbital techniques (cf. section III.C)[203] within the HF approximation. The stabilization energy with finite models (38 kJ/mol) is about twice as large as the result of the periodic calculation (about 18 kJ/mol). Both nonphysical and physical factors may account for the difference. First, the calculations use different basis sets. Second, the periodic calculation uses a single layer of the MgO crystal only, which may be a poor approximation of the electric field due to the semiinfinite crystal. Third, the periodic calculation includes lateral repulsion between neighbored CO molecules, which, however, has been estimated to be not larger than about 2 kJ/mol.[203] When comparison is made with observed heats of adsorption, one should be aware that there are also attractive lateral interactions in an ad-layer of CO molecules due to dispersion forces[365] and, hence, obtained only when electron correlation is included (cf. section II.C). Electron correlation is also necessary to reproduce the correct sign of the dipole moment of CO.

In some physisorption studies, the ionic surface is merely represented by its electrostatic properties. I.e., the quantum chemical equations are solved for the ad-molecule only and the electrostatic properties of the ionic surface are included in the Hamiltonian either as point charge array[361] or (connected with a multipole expansion) by characteristic values of the potential, the electric field, the field gradient, etc.[367,368] In such cases, since no repulsive terms are present, an assumption has to be made for the equilibrium distance of the ad-molecule above the surface[361,367,368] or an empirical atom–atom potential has to be added to account for repulsion (and possibly dispersion).[361]

In conclusion, for ionic solids there is no problem with modeling as long as the clusters are properly embedded in point charge arrays. Frequently, in particular in adsorption studies, single-ion models will do. However, the quantum chemical method deserves more attention. Some problems will be mentioned in the next paragraph.

C. Basis Set Superposition Error and Other Computational Problems

When dealing with complexes or clusters consisting of ions and/or molecules, there is the danger of basis set superposition effects (see, e.g., ref 321 and 322). The basis sets commonly used to describe the ions or molecules are far from being saturated and, hence, in a complex or cluster each subsystem will tend to use the basis functions of all the other subsystems to lower its energy. This makes nonphysical contributions to the stabilization energy of the cluster and leads to artificial charge transfer (from the subsystem considered onto the subsystem from which the orbitals are "borrowed"). The stability of results with respect to the superposition of orbitals of the other subsystems can be checked by the Boys–Bernardi method.[369] To the basis functions of a subsystem, e.g., A, all the basis functions of the other subsystems (we consider only one, e.g., B) without

TABLE 16. Models for Chemisorption and Physisorption Studies on Ionic Crystals

subject	model[a]	method/basis set[b]	aim	ref
Chemisorption				
H₂ chemisorption on MgO(001) surfaces (nondefective surface; surface defects, self-trapped hole, anion vacancy, V_s⁻ center; low coordination edge sites)	HO^{n-}}^{P,c} HMg^{n+}}^{P,c} HO_s^{-}}^{P,c} H}^{P,c} H(Mg²⁺)_5}^{P,a} HMg^{n+}(O²⁻)_5}^{P,d} HO⁻(Mg²⁺)_m}$^{P\,d}$ (m = 1, 3–5)^e	SCF/DZP+dif p(O²⁻)	binding energies and activation energies of dissociative chemisorption	349, 350
H on MgO(111) microsurface region	(Mg²⁺O²⁻)₃, (Mg⁺O⁻)₃, H–(Mg²⁺O²⁻)₃, H–(Mg⁺O⁻)₃	UHF/VDZ+P	electronic structure of (111) surface atoms, binding energy	351
H–D exchange on irregularities of MgO(001) surfaces (kinks and steps)	(MgO)₂–H (planar),^{f} (MgO)₃–H (step site),^{f} (MgO)₂–HD₂, (MgO)₃–HD₂	SCF/3-21G MP3/3-21G^g	equilibrium geometry, binding energies, reaction path of H–D exchange	352
H₂ chemisorption on MgO surface, Mg vacancy (V center)	pc (¹/₆+, ²/₆+)	SCF/STO-3G	valence electron levels, OH stretching frequency, potential curve for H₂ dissociation	353
H₂ dissociation on MgO surface, Mg vacancy (V center)	{(O⁻⋯O⁻)(O₂²⁻)₃}^{P} {(⁻OH⋯HO⁻)(O₂²⁻)₃}^{P}	MR-S-CI/[4,2] MR-S-CI/[4,2] MR-SD-CI/[5,3,1/3,1]	symmetric reaction path of H₂, transition structure, reaction barrier	75
H₂O dissociation on the MgO(100) surface	{Mg²⁺}^{S,h} {O²}^{S,h} {(Mg²⁺)H₂O}^{S,h} {(O²⁻)H₂O}^{S,h} {(Mg²⁺)OH⁻}^{S,h} {(O²⁻)H⁺}$^{S\,h}$	SCF/[4,2/3,2,1/21]	mechanism of formation and properties of surface hydroxyls	354
chemisorption of H on NiO(001) perfect surfaces, vacancies, substitutional defects	H–O²⁻Ni²⁺}^{P}, H–Ni²⁺(O²⁻)₄}^{P}, H–(O²⁻)₅}^{P} (vacancy), H–(Ni²⁺)₅}^{P} (vacancy), H–Ni²⁺(O²⁻)₄}^{P} (vacancy), H–O²⁺}^{P} (vacancy), H–Al²⁺(O²⁻)₅}^{P}, H–N²⁻(Ni²⁺)}^{P}, H–P²⁻(Ni²⁺)}^{P}	UHF,RHF,GVB/ [431] (Ni) MB+dif s(O)	equilibrium distance of ad-atom, binding energy for various electronic states	355, 356, 357
Physisorption				
CO adsorption of MgO(001) surfaces (nondefective and doped)	OC–X^{n+}}^{P,c} OC–X^{n+}(O²⁻)₅}$^{P\,d}$ (X = Mg²⁺, Li⁺, Na⁺, Al³⁺, Cu²⁺, Cu⁺, Zn²⁺); CO–O²⁻}^{P,c} CO–Mg²⁺O²⁻}^{P}, CO–(Mg²⁺O²⁻)₂}^{P}	SCF/DZP +dif p(O²⁻)	binding energies on different sites, equilibrium distance, influence of surface relaxation	359, 349, 350
adsorption of C₁ species on the MgO(001) surface and on impurity Cu⁺ ion therein	{O²⁻–Mg(A)–O²⁻}^{P} (M = Mg²⁺, Cu⁺; A = CO, HCO, HOC, H₂CO, HCOH, CH₂OH, CH₃O)	RHF/3-21G(A), 3-21+G(O²⁻), [4,1] (Mg), [5,2,1] (Cu)	equilibrium distance of ad-molecule, binding energies	360
alanine on the quartz (1010) surface	H₂N·CH(CH₃)·COOH}^{P}, ⁺(H₃N)CH(CH₃)·COOH}^{P}, CO₂}^{P}, CO₂(Cl⁻)₂}^{P}, R·C=O}^{P}	SCF/STO-6G	binding energies of L and D forms	361
CO₂ and carbonyl compounds on the NiCl(100) surface	CO₂}^{P}, CO₂(Cl⁻)₂}^{P}, R·C=O}^{P}	SCF/STO-6G	energy and geometry of adsorption, ν₂ frequency splitting of CO₂	362
H₂O in A-type zeolites	H₂O–Na⁺, H₂O–Na⁺}$^{P\,c,i}$	SCF/4-31G	relative binding energy on different Na⁺ sites	363
He on different surface defects of LiH: H⁻ vac (100), Li⁺ vac (100), Li⁺–Li⁺ (110), Li⁺ (110), H⁻–H⁻ (110), H⁻ (110), H⁻ vac (110)	models contained all ions within 5-Å interaction radius (e.g., the surface layer contained 5x5 atoms for on-top sites and 4x4 or 4x6 atoms for interatomic sites)	SCF/FSGO^j	binding energy for adsorption on different sites	364
He on LiF surfaces	He–F⁻(Li⁺)₅}^{P,b} He–F⁻, HeLi⁺}^{P,a} F⁻}^{a}, F⁻(Li⁺)₅}$^{P\,b}$	SCF/[12,8,5/1,1/1,1]	pairwise-additive potential of ad-atom–surface interactions	344

^{a}}^{P} denotes embedding by an array of point charges. ^{b} See footnote b of Table XIV. ^{c} Single-ion model (SIM). ^{d} Nearest-neighbor model (NNM). ^{e} m = 5 refers to the planar surface. ^{f} An embedding point ion array is *not* used; hence, the cluster may lack ionicity. Cf. ref 359. ^{g} Note that correlation energy estimates employing this basis set are meaningless. ^{h}{}^{S} denotes embedding by a pseudopotential; cf. ref 272. ^{i} The Na⁺ ion is put on different sites with respect to the point charge array. ^{j} Floating spherical Gaussian orbitals. The basis set is similar to the minimal closed-shell model.[197,365]

their electrons and nuclei (ghost functions) are added. The energy obtained, $E_{A(B)}$, is lower than the energy E_A calculated with the basis functions of A only, and the difference is defined as basis set superposition error (BSSE):

$$\epsilon_A = E_A - E_{A(B)} \qquad (V.1)$$

There is also a BSSE for subsystem B:

$$\epsilon_B = E_B - E_{(A)B} \qquad (V.2)$$

Instead of the interaction energy

$$\Delta E_{AB} = E_{AB} - E_A - E_B \qquad (V.3)$$

a corrected interaction energy, $\Delta E_{AB}{}^c$, is defined com-

paring the energy of the complex, E_{AB}, with the energies of the separated subsystems, $E_{A(B)}$ and $E_{(A)B}$, obtained by ghost orbital calculations:

$$\Delta E_{AB}{}^c = E_{AB} - E_{A(B)} - E_{(A)B} \qquad (V.4)$$

Equation V.4 has the advantage that the difference is taken between energies that are obtained by the same basis set. From eq V.1–4 follows

$$\Delta E_{AB}{}^c = \Delta E_{AB} + \epsilon_A + \epsilon_B \qquad (V.5)$$

The only way to keep basis set superposition effects within tolerable limits (or small enough to render corrections according to eq V.5 meaningful) is to properly balance the basis sets of anions and cations when

dealing with clusters of them. In general, compared to standard atomic sets, additional diffuse functions on anions are mandatory while cations stabilize on exponent reoptimization for inner-shell orbitals. But, even if very carefully prepared basis sets are employed, the stability of the results with respect to the superposition of the orbitals of the other subsystems *must always* be checked by the Boys–Bernardi method.[369] There is no excuse not to do this. However, as far as the possibilities to eliminate the BSSE is concerned, the scientific community is split into roughly three parties. The first demands the basis set must be extended until the Boys–Bernardi estimate indicates that superposition effects are sufficiently small. (This is only rarely possible.) The second group says we will obtain a better approximation to the full basis set limit if the (full) Boys–Bernardi correction is applied to our result. (This view is based on vast empirical data and supported by arguments from intermolecular perturbation theory. I share this view.) The opinion of the third group is as follows: correction yes, but only part of the Boys–Bernardi estimate should be applied. (It is argued that part of the ghost functions are filled with electrons in the real complex.) The latter position was taken in the studies on "in-crystal" polarizabilities of anions[265,268] and on F^+ centers in MgO.[271]

The danger of BSSE is particularly large if standard minimal basis sets of atoms are employed for anions and cations. While all orbitals are occupied on the anion, on the cation a whole valence shell is empty. By necessity, the electrons of the anion will make use of them to lower their energy and charge will be artificially transferred. Hence, serious doubts emerge, e.g., as to the significance of the STO-3G study on the off-center instability in KCl:Li.[370] The stability curves of the Li^+ ion will be massively affected by the BSSE, and the charge transfer on which the model suggested in ref 218 is based will be largely an artifact. For example, the stabilization energy of the $(HO)_2PO_2^-\cdots Mg^{2+}$ complex (1445 kJ/mol from extended basis sets[271]) is heavily exaggerated by the STO-3G basis set (2080 kJ/mol)[372] that is due to the BSSE. We note that better balanced results for ionic complexes are obtained[373] by another minimal basis set, MINI-1.[59–62] For the complex mentioned, it yields 1390 kJ/mol and after correcting the BSSE only 1300 kJ/mol.[373] (The insufficient description of anion polarizabilities by minimal basis sets accounts for the difference to the extended basis set result.) An example of a small, but properly balanced, basis set is the "minimal closed-shell" model used in a CO study of LiH.[197] Just one orbital is employed for the electron pairs attributed to Li^+ and H^-. The optimum exponents (2.6875 and 0.772 42 for Li^+ and H^-, respectively) were determined for ions embedded in a point charge array.[365] The crystal field changed the exponent for the hydride ion from 0.6875 (free ion) to 0.772 42, while it had no effect on the lithium ion. This means that the latter is not polarized and is a point charge at this level of approximation.

Another computational problem concerns the lattice relaxations accompanying formation of surfaces, defects, and chemisorbates. They involve so many atoms that they can only be modeled by pair-type potentials. Hence, in the future it will be very important to combine ab initio techniques (which yield accurate energies in a localized region) with potential models (which allow relaxation of many atoms of the lattice) in a consistent way to make possible the theoretical determination of relaxed geometries over extended areas of the solid from the condition of vanishing forces on all nuclei of the lattice including the local region. An important step in this direction has been made by Vail et al.[271]

VI. Semiconductors and Insulators

A. Overview

The overwhelming majority of theoretical papers on semiconductors and insulators is devoted to bulk and surface band structures (see, e.g., the exhaustive review on semiconductor, especially silicon, surfaces[374]) and employ special techniques of solid-state physics (cf. sections I and III.D). Recent applications of "total energy" density functional methods that are able to make structure predictions have been mentioned in section III.D. In contrast, the number of "true" ab initio calculations (in the sense of exact-exchange calculations, which are the subject of this review) is modest. They mainly deal with local geometry, energetics and electronic structure of defects, impurities, and chemisorptive bonds.

Because of its prominent role in electronic devices, most effort was spent on silicon (Table 18). Charts 6 and 7 show models of surface and chemisorption sites for the (111) and (100) surfaces, respectively. Ab initio studies on silyl–diborane,[375] $H_3Si-B_2H_5$, and fluorinated silylboranes[376] were made to look into the mechanism of chemical vapor decomposition processes (CVD) by which gaseous silanes and silane/dopant gas mixtures decompose into amorphous silicon.

Carbon structures (Table 17), in particular diamond, are studied not only because of interest in these materials but also as a useful starting point for later investigations on silicon and germanium. The structural aspects of bonding in silicon carbide polytypes have also been studied.[377]

There are also some results on A^{III}–B^V semiconductors (Table 19).

B. Carbon Structures

We do not aim at an exhaustive review of the vast literature on carbon clusters, mention but rather two groups of papers of more general interest.

Fink et al.[278] propose a special embedding technique and apply it to investigate the electronic properties of graphite and diamond surface sites as well as the chemisorption and surface diffusion of hydrogen on the (100) surface of diamond.[385] Similar to Whitten (section IV.C), they divide the model in an interior part, C, and an exterior part, S. The wave function φ_C of the interior part is determined self-consistently, while for the exterior part a "frozen" solution φ_S is used that provides the proper potential for φ_C. In section IV.E we argued that in solids with covalent bonds and, hence, in diamond and graphite, overlap between atoms is crucial for bonding. It seems that a technique[278] treating this overlap in an approximate way could be more naturally applied to systems where overlap between interior and exterior parts is small as in molecular crystals (cf. ref 277) and ionic crystals. For solids with covalent bonds the recommendations of section IV.E should be fol-

TABLE 17. Calculations on Models of Diamond and Graphite: Bulk, Surface, and Chemisorption[a]

subject	model	method/basis set	aims	ref
graphite	C_6, C_{24}, C_{54} (high spin): C_6H_6, $C_{24}H_{12}$, $C_{54}H_{18}$, $C_{96}H_{24}$, $C_{150}H_{30}$	SCF/DZ	CC bond distance, stability, valence electron levels	378, 379
diamond	$C_{10}H_{16}$ (adamantane), $C_{35}H_{36}$, $C_{84}H_{64}$	SCF/DZ	CC bond distance, stability, valence electron levels	379
diamond	$C(CH_3)_4$	SCF/6-31G*	CC bond distance	377
C–C bond in bulk diamond	$C(CH_3)_4$	SCF/DZ	Compton profile	380
(111) surface relaxation	$\cdot C(CH_3)_3$,[b] $^+C(CH_3)_3$, $^-C(CH_3)_3$	SCF/STO-3G	position of surface atom, dangling bond IP[d]	381
(111) diamond surface relaxation and reconstruction	$\cdot C(CH_3)_3$,[b] $\cdot C_9H_{15}$[b]	SCF/4-31G SCF/6-31G* SCF/EC-DZ SCF/EC-DZP SCF/STO-3G	position of surface atoms	382
neutral vacancy in diamond	$(\cdot CH_3)_4$	GVB-CI/VDZ	electronic structure, relative energies of low-lying electronic states	383
chemisorption of O, O_2, and H on graphite	$C_{10}H_8$ (naphthalene), $O-C_{10}H_8$, $O_2-C_{10}H_8$, $H-C_{10}H_8$	UHF/STO-3G	equilibrium distance above surface, binding energy	384
H on (100) of diamond	$H-C_5$ embedded	SCF[c]	binding energy, activation energy of adsorption, surface diffusion barrier	385
H on (111) of diamond	$H-C(CH_3)_3$	SCF/STO-3G SCF/EC-DZP	equilibrium distance, binding energy, vibrational frequency of ad-atom	386
muonium in diamond	muonium-$C_{10}H_{16}$ (adamantane structure)	UHF/STO-3G	location (tetrahedral interstitial space), hyperfine interaction, vibrationally averaged spin density	387
muonium in diamond	muonium-$C_{10}H_{16}$, $H-C_{10}H_{16}$	UHF/STO-3G + 10s (muonium)	location (tetrahedral interstitial space, center of an extended C–C bond), hyperfine coupling constant	388

[a] Cf. ref 379 for additional references to theoretical investigations on carbon clusters. [b] Cf. Chart 6. [c] Basis not specified. [d] IP = ionization potential.

CHART 6. Different Models for (111) Surface Sites of Silicon and Diamond[a]
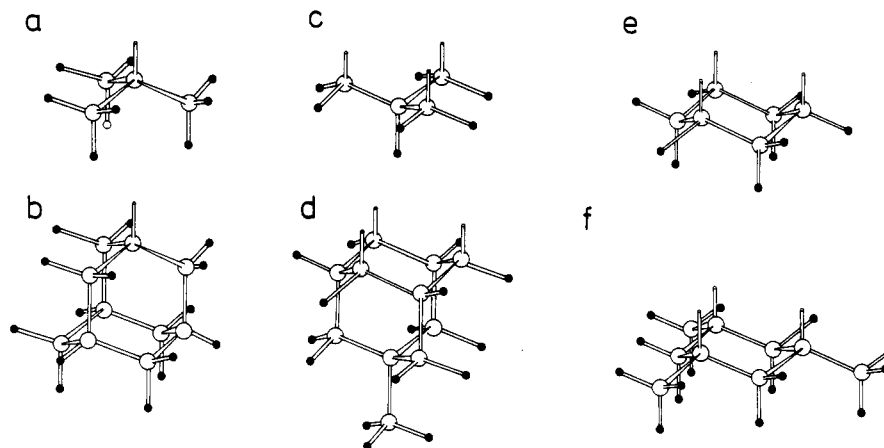
[a] Broken lines indicate dangling bond directions; small full circles are terminating hydrogen or siligen atoms. Key: (a) Si_4H_9, (b) Si_9H_{15}, (c) Si_4H_7, (d) $Si_{10}H_{15}$, (e) Si_6H_9, (f) Si_9H_{15}. In chemisorption studies (e.g., ref 401), (a) and (b) are used to model the on-top, (c) the eclipsed hollow site, and (d)–(f) the open hollow site approach.
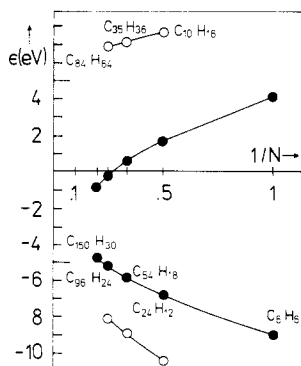

Figure 9. Dependence of the energies of the highest occupied and lowest unoccupied orbitals for models of graphite (full circles, $C_{6N^2}H_{6N}$) and diamond (open circles, $C_{n_C}H_{n_H}$, $n_C = N(4N^2 - 1)/3$, $n_H = 4N^2$) on N.[379]

lowed, namely to cut atoms rather than bonds. In summary, diamond and graphite do not seem to be favorable cases for application of Fink's technique, which did not prove superior to other (simpler) possibilities of terminating a model.

For carbon clusters probably some of the largest SCF calculations to date have been recently made[378,379] (cf. Table 17). Comparison was made of the spherical "Buckminster fullerene" (C_{60}) with planar, single-sheet graphite fragments with 6, 24, and 54 atoms (D_{6h} symmetry). For these "free-boundary" clusters the spins of the dangling bond electron (6, 12, and 18, respectively) can be paired in many ways. However, albeit not lowest in energy, the high-spin forms ($S = 3, 6,$ and 9, respectively) are most representative for graphite (a special case of "electronic" boundary conditions; cf.

TABLE 18. Calculations on Silicon (and Germanium): Bulk, Surface Sites, Chemisorption, Defects, and Impurities

subject	model	method/basis set	aims	ref
		(i) Bulk		
	$Si(SiH_3)_4$	SCF/3-21G	geometry	389
	$Si(SiH_3)_4$	SCF/6-31G*	geometry	377
	$Si(SiH_3)_4$	SCF/EC-DZ	variation of saturator Si–H bond lengths, band gap, charge density	390
parameters of a force field model of bulk Si	$Si(Si\overline{H}_3)_4{}^a$	GVB-CI/EC-DZ	harmonic force constants, phonon band structure	292
	$Si(Si\overline{H}_3)_4$	SCF/EC-DZ	optimum orbital exponent of siligens	291
		(ii) Surface[b]		
ab initio effective core potentials for silicon (111) surface relaxation	Si, Si_2, $H_3Si^{\cdot}$, $H_3SiO_2^{\cdot}$	SCF, GVB, GVB-CI/DZ, ECP-DZ	IP,[c] EA,[c] excitation energies	391
	$^{\cdot}Si(SiH_3)_3$, $^+Si(SiH_3)_3$, $^-Si(SiH_3)_3$	SCF/STO-3G, SCF/4-31G, SCF/EC-DZ	position of surface atom dangling bond IP[c]	79, 392, 393
(111) surface, parameters of a force field model	$^{\cdot}Si(SiH_3)_3$, $(^{\cdot}SiH_2)_3SiSiH_3$	SCF/EC-DZ	harmonic force constants of surface and subsurface atoms	394
(111)–(2x1) surface electronic nature and relaxation	$^{\cdot}Si(Si\overline{H}_3)_3$, $(\overline{H}_2Si^{\cdot})_2SiH_2$, $[-Si\overline{H}_2{}^{\cdot}Si(Si\overline{H}_3)-]_3{}^a$	GVB-CI/EC-DZ	position of surface atoms, dangling bond ionization potential, and energy dispersion curve, Si (^{2}p) core level shifts	76
(111)–(7x7) surface reconstruction	$^{\cdot}SiH_3$, Si_2H_6, $^{\cdot}Si_3H_3$, $(^{\cdot}SiH_2)_2$	SCF/4-31G (plus estimate of influence of correlation and polarization functions)	estimate of relative stability of different models of 7x7 reconstruction (Lander vacancy, milk stool)	395
steps on the (111) surface	$H_2\dot{S}i-\dot{S}i-SiH_3$ $H_2\dot{S}i-\dot{S}i-SiH_2$	GVB/EC-DZ(P) GVB-CI/EC-DZ(P)	electronic and geometric structure, excitation, and ionization energies	396
(100) surface reconstruction, relaxation, and electronic nature	$Si_9\overline{H}_{12}{}^a$	GVB-CI/ECP-DZ	surface geometry,[d] electronic state, Si (2p) core level shifts	77
		(iii) Chemisorption[b]		
H on Si(100), vibrational spectra of monohydrated and dihydrated surface atoms	Si_9H_{14} $H_2Si_2(SiH_3)_4$, $H_2Si_2H_4$ $H_2Si_2H_4$	SCF/3-21G SCF/3-21G$^{(*)}$, MP2/3-21G$^{(*)}$ SCF/6-31G**	surface geometry harmonic force constants, equilibrium geometry	397
	..., $Si^4OH_x{}^2Al^4$	SCF/6-31G*, MP2/3-21G	harmonic force constants	398
H on Si(111) (on-top site)	$H-SiH_3$, $H-Si(SiH_3)_3$ $H-Si(SiH_3)_3$	SCF/DZP^e SCF/EC-DZP,^{e} SCF/STO-3G	equilibrium distance, binding energy, vibrational frequency	399 386
H on Si(111) (3-fold open site)	$H-Si_{10}H_{13}$ $H-Si_6H_9$	SCF/VDZ(P)^f TC-SCF^g/VDZ	equilibrium distance, well depth, barrier height, vibrational frequency of motion normal to surface	400
F and Cl on Si(111) (on top, eclipsed, and open site)	$X-Si(SiH_3)_3$, $X-Si_{10}H_{15}$ (on top), $X-Si_4H_7$ (eclipsed), $X-Si_{10}H_{13}$ (open)	SCF/VDZ	equilibrium distance, binding energy, vibrational frequency	401, 402
F and Cl on Si(111) and Ge(111) (on top)	$X-Si_4H_7$, $X-Ge_4H_7$	SCF/EC-DZP,^{e,h} SCF/EC-DZP^e	equilibrium distance, vibrational frequency, binding energy	403, 404
O and O_2 on Si(111)	$\overline{H}_3SiO_2$,^{a} $\overline{H}_3SiOSi\overline{H}_3{}^a$ $\overline{H}_3SiO^{\cdot}{}^a$	SCF/EC-DZ GVB/EC-DZ	geometries of surface complexes Si (2p) and O (1s) core levels	291
O_2 on Si(111)	$H_3SiO_2^{\cdot}$, $H_2Si^{\cdot}-SiH_2-SiH_2O_2^{\cdot}$	GVB-CI/DZ	geometry of surface radical, IP,[c] excitation energies	293
O on Si(100), (on top, bridge, and center sites)	$O-Si(SiH_3)_2$, $(H_3Si)_2Si-O-Si(SiH_3)_2$, $O-Si_7H_8$	CASSCF/basis set not specified	equilibrium distance and vibrational frequency of O normal to the surface, binding energy, O (1s) core level shift	405, 406
		(iv) Defects and Impurities		
structure of the (450 °C) oxygen donor (interstitial oxygen silicon–oxygen ylide)	$Si(SiH_3)_4$ $Si(OSiH_3)(SiH_3)_3$, $O[Si(SiH_3)_2](SiH_3)_2$	SCF/3-21G MP3/3-21G	geometries, relative energies, ionization potentials	389
oxygen uptake by silicon	$(H_3Si)_3Si-Si(SiH_3)_3$, $(H_3Si)_3Si-O-Si(SiH_3)_3$	SCF/EC-MB	local geometry, electron distribution	407
fluorinated amorphous Si	SiH_3F, Si_2H_5F SiH_2F^+, SiH_3F^+ $[H_3Si-F-SiH_3]^+$	SCF/3-21G SCF/6-31G* MP3/6-31G*	geometries, vibrational frequencies, energetics	408
interstitial transition metals (M^0, M^+, M^{2+}) on T_d sites of undistorted Si lattice	$MSi_4Si_6H_{16}$	SCF/EC-DZ	impurity ionization energies, term orderings, term splittings	409
neutral vacancy	$\square(^{\cdot}SiH_3)_4$	GVB/MB, GVB-CI/VDZ	electronic structure, relative energies of low-lying electronic states (^1E, $^3T_1$, $^5A_2$)	299 383
neutral vacancy	$Si(Si\overline{Si}_3)_4$,^{i} $(^{\cdot}Si\overline{Si}_3)_4{}^i$	CI/EC-DZ, CI/EC-DZP	electronic structure, relative energies of low-lying electronic states	298

$^a\overline{H}$ denote siligens; cf. section IV.E.4.[291] ^{b}For model of (111) and (100) surface and chemisorption sites, see Charts 6 and 7, respectively. ^{c}IP = ionization potential; EA = electron affinity. ^{d}Geometric boundary conditions imposed. ^{e}DZ basis set only on terminating H atoms. ^{f}Polarization p function on the ad-hydrogen atom only. ^{g}TC-SCF = two-configuration SCF. ^{h}Polarization function on first-layer surface atoms and on the ad-atom only. $^i\overline{Si}$ denotes pseudoatoms; cf. section IV.E.6.

TABLE 19. Calculations on Surface and Chemisorption Sites of Semiconductors

subject	model	method/basis set	aim	ref
relaxation and reconstruction of the (110) surface of of a^{III}–b^V semiconductors (a = Ga, Al, B; b = As, P, N)	H_2abH_2 $(H_2a)_2bH$, $(H_2b)_2aH$, $H_2a \cdot bH \cdot aH \cdot bH_2$	SCF/EC-DZP SCF/EC-DZ	geometry parameters for surface atoms (surface strain, reconstruction angle)	410 411
oxidation of the GaAs(111) surface	H_3As, H_3Ga, H_2AsGaH_2 H_3AsO, H_3GaO, $H_2Ga \cdot H_2AsO$	SCF/EC-DZP GVB-CI/EC-DZP	geometries, vibrational frequencies, core level ionization potentials	411 392
oxidation of a^{III}–b^V semiconductors	Cl_3b=O (b = N, P, As, Sb)	GVB-CI/EC-DZP	length, vibrational frequency, dissociation energy of the b–O bond	412

TABLE 20. C–C Bond Distances (pm) in Graphite and Diamond: Convergence of Molecular Model Results[229] and Comparison with Crystal Orbital Calculations[192]

system	basis set	r_e^a	system	basis set	r_e^b	diff^c
C_6H_6	STO-3G	138.7^d	C_2H_6	STO-3G	153.8^d	15.1
C_6H_6	DZ	138.4^e	C_2H_6	DZ	153.0^f	14.6
C_6H_6	obsd	139.7^g	C_2H_6	obsd	152.6^h	12.9
graphite	CO/STO-3G	145^i $(146)^a$	diamond	CO/STO-3G	155.5^j $(154.3)^b$	10.5
$C_{24}H_{12}$	DZ	140.1^e $(141.4)^a$	$C_{10}H_{16}$	DZ	154.2^e $(153.8)^b$	14.1
$C_{54}H_{18}$	DZ	140.4^e $(141.7)^a$	$C_{35}H_{36}$	DZ	154.0^e $(153.6)^b$	13.6
$C_{96}H_{24}$	DZ	140.6^e $(141.9)^a$	$C_{84}H_{64}$	DZ	153.9^e $(153.5)^b$	13.3
graphite	obsd	142.1^h	diamond	obsd	154.5^h	12.4

^{a} Projected results ($r_e + \delta$) in parentheses; δ = obsd(C_6H_6) – calcd(C_6H_6). ^{b} Projected results ($r_e + \delta$) in parentheses, δ = obsd(C_2H_6) – calcd(C_2H_6). ^{c} r_e(diamond) – r_e(graphite). ^{d} Reference 7. ^{e} Reference 379. ^{f} Calculation for this review. ^{g} r_0 value (Langseth, A.; Stoicheff, B. P. *Can. J. Phys.* 1956, 34, 350). ^{h} For reference to experimental work, see quoted theoretical papers. ^{i} Reference 192. ^{j} Reference 145.

CHART 7. Different Models for (100) Surface Sites of Silicon and Diamond^a
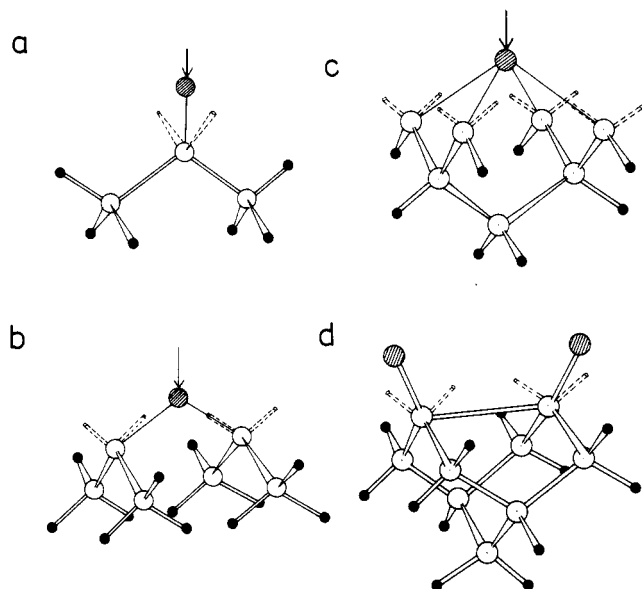
^{a} Broken lines indicate dangling bond directions; small full circles are terminating hydrogen or siligen atoms. The Si_3H_6 (a), Si_6H_{12} (b), and Si_7H_8 (c) models are used to study on-top, bridge and center sites of chemisorbed atoms (e.g., ref 405). The Si_9H_{12} model (d) is adopted for the monohydrated, reconstructed Si(100) surface.[397]

section IV.E). Nevertheless, hydrogen-saturated models of graphite and diamond (Table 20; Figure 9) are expected to converge more smoothly toward the bulk properties. The SCF calculations (DZ basis set) on the largest model studied, $C_{150}H_{30}$, involved 1560 contracted basis functions. As storage and rereading of the corresponding enormous amount of two-electron integrals would have been impossible, even on the CRAY-2 supercomputer employed, use was made of a so-called "direct" SCF program that recalculates the integrals in each iteration of the SCF process.

Thanks to these benchmark calculations there is the (rare) possibility to judge the convergence of the mo-

lecular approach in dealing with solids on results for models of increasing size. Table 20 and Figure 9 show some results.[378,379] The most important conclusion is that the convergence behavior of different properties is very different. While the geometry (CC bond distance, Table 20) certainly belongs to the properties that converge nicely, convergence of one-electron energy levels is very poor (Figure 9). The CC distance (Table 20) calculated for the adamantane model, $C_{10}H_{16}$ (X), of diamond changes by only 0.3 pm when passing to the largest model, $C_{84}H_{64}$, of the series. Similarly, the result for the $C_{24}H_{12}$ model of graphite changes by only 0.5 pm when passing to the $C_{96}H_{24}$ model. Note that the error due to the theoretical approach chosen, SCF/DZ basis set, is –0.7 pm as the calculation on C_6H_6 indicates; cf. Table 1. The projected bond lengths (obtained by adding an increment to correct for such errors; cf. section IV.G) are slightly shorter (by less than 1 pm) than the observed values.

Due to poor convergence of one-electron energy levels, even for the largest model of graphite, $C_{150}H_{30}$, the energy gap between occupied and unoccupied states is still about 4 eV (Figure 9). While the value of about 4 eV extrapolated from these calculations for the work function of graphite is in reasonable agreement with the observed value (4.9 eV), the extrapolated band gap of diamond (about 10 eV) is definitely larger than the experimental value of about 4.6 eV.[379] This discrepancy is attributed to neglect of electron correlation (cf. section III.C) which also prevents getting reasonable values for cohesive energies (cf. sections III.D and II.C).

C. Chemisorption Studies

Tables 21–23 illustrate the analogy between Si–H, Si–F, Ge–F, Si–Cl, and Ge–Cl bonds on surfaces and in molecules. The linear Si–H molecule (Table 21) is not an adequate model of a Si–H bond on a Si(111) surface since coordination of silicon and hybridization are totally different for both species. (Note, however, that low-valent silicon hydride[413] and silicon fluoride[414] species have attached great interest because of their role

TABLE 21. Molecules as Models of the H–Si(111) Bond and of the Si–Si Bulk Bond of Solid Silicon (Units: Equilibrium Distances (r_e), pm; Vibrational Frequencies (ω_e), cm^{-1}; Bond Dissociation Energies (D_e), kJ/mol)

		H–Si	$H\text{-}SiH_3$	$H\text{-}SiH_2\text{-}SiH_3$	$H\text{-}Si(SiH_3)_3$	H–Si(111) surface
r_e	6-31G*		147.5[a]	147.8[a]		
	DZP	153.1[b]	147.9[b]		148.6[b]	
	obsd	153.1[c]	148.1[a,d]	148.6[a,d]		
ω_e	DZP	2136[b]	2328[b,e]		2314[b,e]	
		(2099)[b]	(2288)[b,f]		(2274)[b,f]	
	obsd (harmonic)	2042[c]	2377[a,d]			
	obsd	1971[c]	2187[a,d]	2160[g]		2073[b,d]
D_e	6-31G*	210[h]	317[i]	305[h]		
	DZP	203[b]	317[b]		291[b]	
	obsd	295[c]	272,[i] 378[j]	361[j]		209–309[b,d]

		Si–Si	$(Si\text{-}Si)_3$[p]	$H_3Si\text{-}SiH_3$	$H_3Si\text{-}Si(SiH_3)_3$	crystal
r_e	obsd	224.6 $(^3\Sigma_g^-)$[k,d]		232.7[d,l]		235[d,m]
	STO-3G	210.5[n]	222.4[k]	224.3[l]		242[m]
	3-21G	231.6[n]		238.2[l]	238.3[o]	
	6-31G*	222.7[k]	232.8[k]	235.3[r]	236.5[q]	

[a] Reference 52. [b] Reference 399. [c] Bürger, H.; Eujen, R. *Top. Curr. Chem.* **1974**, *50*, 1. [d] For references to experimental work see the quoted theoretical papers. [e] Diatomic oscillator model, finite silicon mass (28). [f] Rigid-cluster model, infinitely large silicon mass; cf. ref 399. [g] Pfeiffer, M.; Spangenberg, H. J. *Z. Phys. Chem. (Leipzig)* **1966**, *232*, 47. [h] Calculated from energetics of ref 416. [i] Reference 415. [j] Walsh, R. *Acc. Chem. Res.* **1981**, *14*, 246. [k] Reference 300. [l] Reference 53. [m] Reference 146. [n] Reference 416. [o] Reference 389. [p] Cyclic structure. [q] Reference 377. [r] Reference 7.

TABLE 22. Results for Si–F and Si–Cl Bonds on Silicon Surfaces and in Molecules (Units: Equilibrium Distance (r_e), pm; Harmonic Vibrational Frequency (ω_e), cm^{-1}; Dissociation Energy (D_e), kJ/mol)

		$X_3Si\text{-}X$		$H_3Si\text{-}X$		$H_3Si\cdot H_2Si\text{-}X$	basis set	$(H_3Si)_3\text{-}X/H_{15}Si_{10}\text{-}X$	
	basis set	X = F	X = Cl	X = F	X = Cl	X = F		X = F	X = Cl
r_e	3-21G	158.4[a]		163.5[a]	219[h]	164.4[i]			
	6-31G	162.5[e]		168.2	219[j]		VDZ	168/168[b]	224/224[b]
	6-31G*	155.7[a,e]		159.4	207[h]	160.3[i]			
	EC-DZ(P)[j,k]			157.7[j]	204[j]		EC-DZ(P)[c,k]	161[c]	209[c]
	obsd[f]	155.2[a]	204[b]	159.3[a]	205[h]				203[c]
								$m = 28$[l] $m = \infty$[m]	$m = 28$[l] $m = \infty$[m]
ω_e	3-21G	845[a]		943[a]		925[i]			
	6-31G	757[e]					VDZ	784 605[b]	489 326[b]
	6-31G*	849[e]		952[j,p]	588[j,p]		EC-DZ(P)[c,k]	917 708[c]	543 362[c]
	obsd[f]	801[a]		875[j]	551[j]				
D_e	3-21G	484[a]		390[a]		264[g]			
	VDZ	328[b]	104[b]				VDZ	314/311[b]	160/158[b]
	6-31G*	535[a]		466[a]	340[g]	447	EC-DZ(P)[c,k]	425[c]	350[c]
	obsd[f]	600, 686[a]		643[a]					

[a] Reference 415. [b] Reference 401. [c] Reference 403. [e] Reference 417. [f] For references to experimental data, see quoted theoretical papers. [g] Calculated from energies of ref 415 and 52. [h] Reference 52. [i] Reference 418. [j] Reference 419. [k] No polarization functions on hydrogen atoms. [l] Diatomic oscillator model, finite silicon mass (28). [m] Rigid-cluster model, infinitely large silicon mass; cf. ref 401. [p] EC-DZ(P) calculation.

TABLE 23. Results for Ge–F and Ge–Cl Bonds in Molecules and on Ge(111) Surfaces[403,419] (Units: Equilibrium Distances (r_e), pm; Vibrational Frequencies (ω_e), cm^{-1})

		$H_3Ge\text{-}F$[b]	$Ge_4H_9\text{-}F$[c]	$H_3Ge\text{-}Cl$[b]	$Ge_4H_9\text{-}Cl$[c]
r_e	calcd[a]	169.7	177	215.5	221
	obsd[d]	173.5		215.0	207 ± 3

		$H_3Ge\text{-}F$[b]	$Ge_4H_9\text{-}F$[c]		$H_3Ge\text{-}Cl$[b]	$Ge_2H_9\text{-}Cl$[c]	
			$m = 74$[e]	$m = \infty$[f]		$m = 74$[e]	$m = \infty$[f]
ω_e	calcd[a,g]	752	728	649	440	420	346
	obsd[d] (extrap)	689	(667)	(595)	423	(404)	(333)

[a] SCF/EC-DZ(P); no polarization functions on hydrogen atoms. Note that calculations on H_3GeX molecules[419] and on Ge_4H_9-X models,[403] although at the same level, differ in details such as type of core potential and exponents of polarization functions. [b] Reference 419 (d exponents on F and Cl equal 0.8 and 0.75, respectively). [c] Reference 403 (d exponents on F and Cl equal 1.62 and 0.56, respectively). [d] For references to experimental work, see quoted theoretical papers. [e] Diatomic oscillator model, finite germanium mass (74). [f] Rigid-cluster model, infinitely large germanium mass; cf. ref 403. [g] Harmonic.

in the silicon chemical vapor deposition and surface etching processes; cf. ref 413 for a comprehensive study of geometries, force constants, and vibrational spectra of SiH, SiH_2, SiH_3, and SiH_4 and ref 414 for a study on SiF, SiF^+, SiF^-, SiF_2, SiF_2^+, $SiH_3\text{-}F$, $SiF_3\text{-}F$, $SiH_3\text{-}SiH_3$, $SiH_3\text{-}SiF_3$). In contrast, observed data for molecules like SiH_4, Si_2H_6, SiH_3X, and SiX_4 (X = F, Cl) are a valuable source of information for surface species

without making any calculation. It belongs without doubt to the appealing features of the molecular approach that models are obtained that really exist and can be investigated by experiments. Furthermore, calculations on such molecules can tell a lot about reliability and failure of a particular quantum chemical method. The specific results for different basis sets and models presented in Tables 21–23 detail the general comments on the performance of different levels of methods made in section II.B (Table 1) and II.C and are an example of the "hierarchic" approach to solid-state problems (section IV.G). When chemisorption of F and Cl on Si(111) surfaces was studied, it was possible to treat a model as large as $X-Si_{10}H_{15}$ when the basis set quality was limited to valence double-ζ (VDZ).[401] For the smaller $X-Si(SiH_3)_3$ cluster, virtually the same results were obtained but significant changes occurred on passing to a basis set including polarization functions.[403] Parallel changes are observed for the SiX_4, SiH_3X, and Si_2H_5X molecules when passing from split-valence (3-21G, 6-31G) to polarization-type basis sets (6-31G*). In accord with common experience (section II.B, Table 1), the latter types of basis sets (EC-DZP, 6-31G*(*)) yield reliable results for equilibrium distances and harmonic vibrational frequencies. When the vibrational frequencies of chemisorbed H, F, and Cl atoms were calculated perpendicular to the Si-(111) and Ge(111) surfaces, the ad-atom was assumed to vibrate against the rigid surface; i.e., the surface atom was given an infinitely large mass (rigid cluster model).[399,401,403] Comparison with results of a diatomic oscillator model using the genuine masses of Si and Ge, 28 and 74, respectively (albeit it still neglects coupling with adjacent Si–Si and Ge–Ge bonds, respectively) shows that the assumptions of the dynamical model sensibly affect the results. Note (i) that the force constants were the same for both frequency estimates and (ii) that these constants were obtained by quantum chemical ab initio calculations on much larger models, e.g. $(H_3Si)_3Si-X$. For chemisorbed hydrogen, due to its low relative mass, the rigid-cluster approximation seems justified. Nevertheless, for finer details better models are needed.

To assist assignment of high-resolution infrared data of Si(100) surfaces covered with H atoms, ab initio calculations were made of the Si–H (and Si–D) frequency splitting.[397,398] The monohydride phase involving vicinal >SiH–SiH< pairs and the dihydride phase involving geminal >SiH$_2$ species were considered. Force constants were evaluated for the $H_3Si-SiH_3$ and $H_3Si-SiH_2-SiH_3$ models, respectively. To suppress in the frequency calculation (GF method) undue coupling with motions of saturator H atoms a different mass (m_D = 2) was assumed for the latter, i.e. the saturator atoms were deuterium atoms (Figure 10). In turn, when deuterium adsorbates were considered, the saturator atoms were hydrogen atoms. A much larger model was adopted in molecular dynamics simulations of the infrared line shapes for the dihydride phase:[420] a slab containing 16 H atoms, 16 first-layer Si atoms, and 12 second-layer Si atoms (Figure 10). The Si–H force constants were transferred from the much smaller $H_3Si-SiH_3$ model. The Si–Si force constants in principle could be obtained from ab initio calculations of suitable bulk models as $Si(SiH_3)_4$ (cf. ref 292). Actually,

monohydride   dihydride

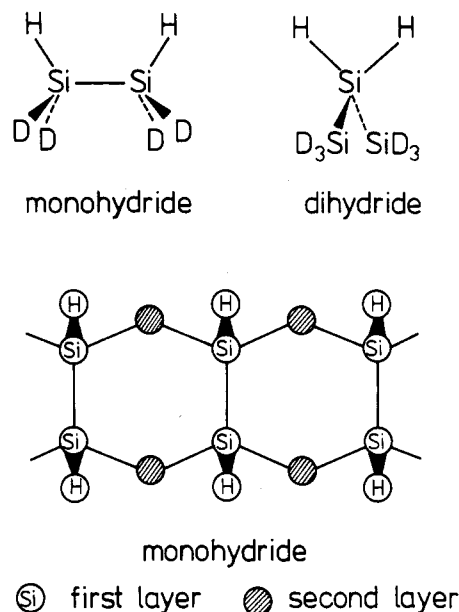monohydride

Ⓢ first layer   ◍ second layer

Figure 10. Models for monohydride and dihydride phases of hydrogen-loaded Si(100) surfaces.[397,398,420]

they were taken from an empirical bulk force field.[420]

As expected (sections II.B and II.C), the calculated dissociation energies for surface Si–H and Si–F bonds (Tables 21 and 22) are in error by over 50 and 100–200 kJ/mol, respectively. Only on inclusion of correlation does the error drop to acceptable limits (about ±20 kJ/mol at the simple MP2 level) as work on SiH_4, SiH_3F, SiF_4, and Si_2H_5F indicates.[415,418] We mention also a related study on H_2 dissociation on boron surfaces modeled by B_6 clusters.[421] Although the theoretical approach chosen (RHF/DZ basis set) does not yield reliable information on bond dissociation energies (sections II.B and II.C), conclusions are drawn on the mechanism of reactions involved in the growth of solid boron by the chemical vapor deposition technique. A more natural way to deal with bond-breaking processes is a multireference ansatz as in the generalized valence-bond (GVB) or two-configuration SCF (TC-SCF) methods (cf. section II.C). Table 18 includes further examples of striking failures of the SCF method: chemisorption of oxygen,[291] barrier for penetration of chemisorbed H atoms through the Si(111) surface,[400] and (2 × 1) reconstruction of Si(111) and Si(100) surfaces.[76-79]

In the near future substantial progress can be expected with an adequate description of electron correlation effects for chemisorption problems for two reasons. It not only emerges from Tables 21–23 that models including only very few surface atoms will provide the basic answer, but there are also suggestions[401,404] on how molecular orbitals of a model that are not involved in the chemisorptive bond can be identified, namely by a corresponding orbital transformation with respect to the cluster without the ad-atom.[401] Computational work of a correlation energy calculation can be reduced by excluding these orbitals already from the integral transformation step.[404] Note that a similar idea has been implemented in Whittens technique (section IV.C).

When compared with reactions of molecules in the gas phase, the present stage of chemisorption studies looks premature not only because of a very approximate

wave function but also because of the still rather primitive treatment of nuclear degrees of freedom. For molecules it is now generally accepted that a meaningful comparison of energies can only be made for completely optimized structures. In contrast, most chemisorption studies use rigid surface geometries (Tables 21–23). Even for naked surfaces only partial geometry optimizations were reported (Tables 17–19). The main problem when relaxing geometry parameters of models of surface sites, chemisorbates, defects, etc., is the boundary to the bulk (cf. the remarks at the end of section V.C). A final answer can only be expected when the coordinates of a very large region of bulk atoms are relaxed. This is only possible by force field type potentials[292,394] whose parameters are ideally derived from calculations of the same type as employed for the small model investigated.

VII. Zeolites, Silica, and Related Materials

A. Introduction

Silica[422] and silicates,[423] the most abundant chemical compounds on earth, are as important a subject for basic research in mineralogy and solid-state chemistry as is SiO_2, an ingredient of many electronic devices, in solid-state physics.[424] Zeolites, the microporous three-dimensional alumosilicate networks,[425] have found wide industrial applications as ion exchangers, molecular sieves, and catalysts.[426–428] The (not yet understood) role of oxides as supports of metal catalysts should be also mentioned.[429]

In these oxides, the electropositive component, i.e., most frequently silicon or aluminum, is tetrahedrally coordinated by oxygen atoms and the corresponding TO_4 tetrahedra (T = Si, Al, ...) are the primary building units of their complex structures. Higher coordinations of the central atoms (predominantly six, but also five or eight) play a minor role. The negatively charged aluminosilicate frameworks of zeolites are (hypothetically) formed when Si atoms of a SiO_2 network are isoelectronically replaced by Al^- ions. Framework-excluded metal cations (or protons) are necessary to compensate the framework charge, and the general formula of zeolites is $M_{x/n}[(AlO_2)_x (SiO_2)_y]\cdot zH_2O$. The Si/Al ratio of zeolite frameworks can range from 1 to infinity, and virtually pure SiO_2 micropore structures may be obtained. These materials, which may be considered as microporous silica modifications rather than as high-silica zeolites, proved very efficient catalysts, in particular for the conversion of methanol into hydrocarbons. An example is ZSM-5.[430] Figure 11 shows the formation of its channel system by a particular connectivity pattern of SiO_4 tetrahedra. First, 12 SiO_4 tetrahedra are linked together to the secondary building unit (SBU) shown in Figure 11a. The ZSM-5 framework structure can be completely assembled by applying symmetry operations to this SBU. The individual SBUs in a chain (Figure 11b) are related by a 2-fold screw axis, and neighbored chains of a layer (Figure 11c) are related by mirrors. The 10-membered silicate rings formed this way constitute the walls of channels. There are two types of channels (straight and sinusoidal) that intersect at right angles (Figure 11d).

Since there are many different types of secondary building units and connectivity patterns, a large number
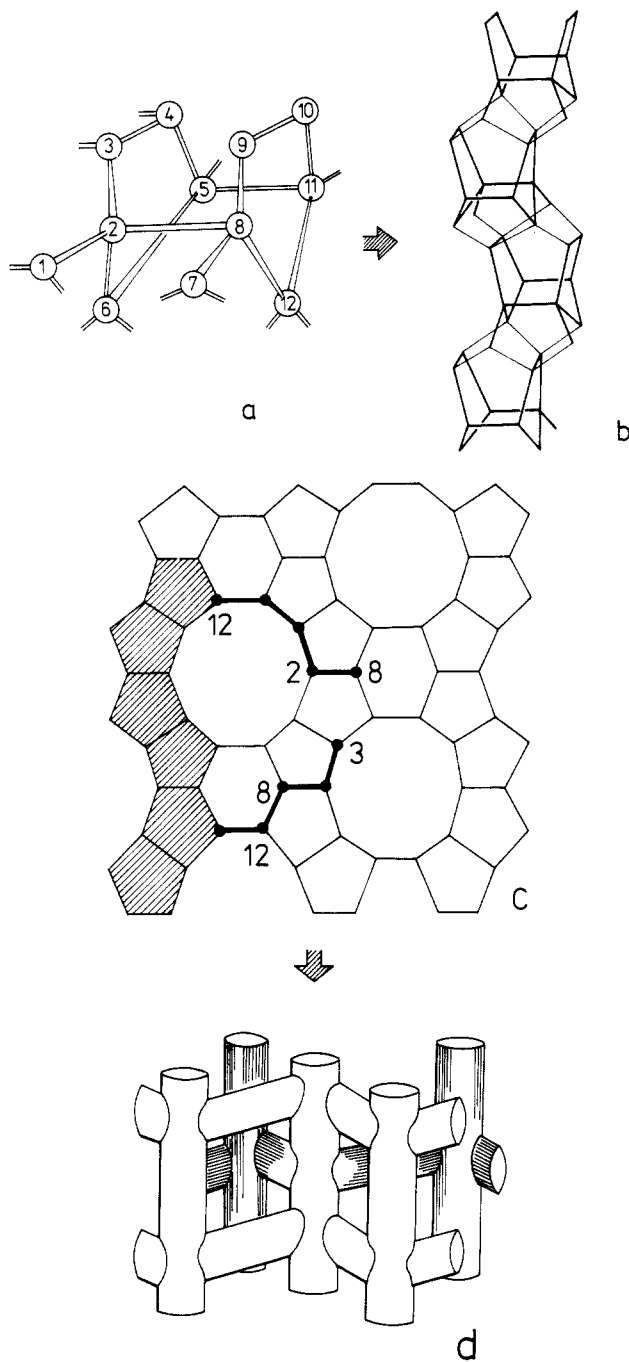
Figure 11. Framework structure of ZSM-5 type zeolites.[430] The positions of the tetrahedral Si atoms are shown only. Lines represent T–O–T linkages with the O atoms not shown. (a) Secondary building unit. (b) Chain of secondary building units. (c) Layer consisting of annealed chains and formation of ten-membered ring openings. Two five-membered chains of TO_4 tetrahedra investigated in the model calculations of ref 288 are marked. (d) System of straight and "zigzag" channels.

of framework types can be designed. This as well as variations of the Si/Al ratio and cation content explains the vast variety of zeolites found in nature or prepared in the laboratory.[431] Synthesis of new framework types, of high-silica forms of zeolites, and of a broad variety of zeolite analogues containing elements like Be, B, Mg, Al, P, Ge, Sn, and Fe have renewed the interest in structure–property relationships of such catalysts.[427,428] Examples are microporous aluminum phosphates (AlPO₄) and MAPOs, e.g., SAPO (metal- or silicium-substituted aluminum phosphates).[432]

CHART 8. Different Molecular Models of Silicate (or Related) Networks[a]

a

b

c

d

e

f
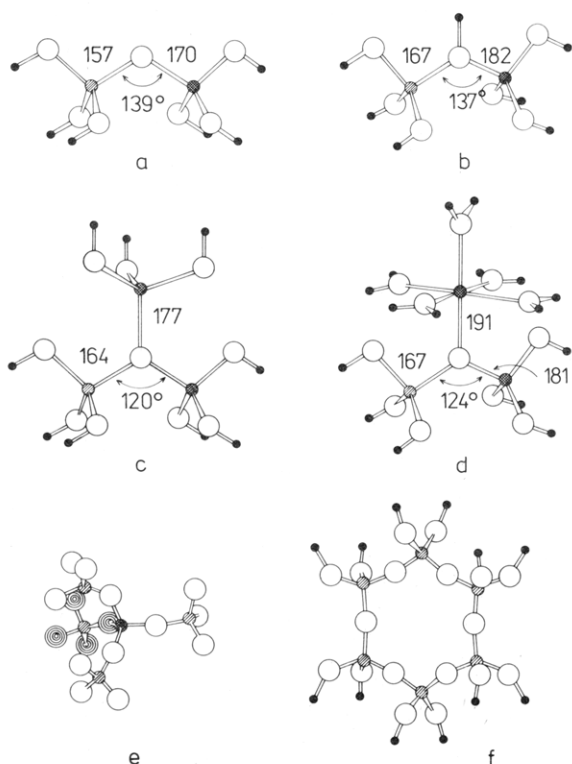
[a] Key: (a) Two linked tetrahedra; (b) T–O–T bond of (a) protonated; (c) T–O–T bond of (a) coordinated by an X(OH)$_3$ group;[282] (d) T–O–T bond of (a) coordinated by an [X(OH$_2$)$_5$]$^{n+}$ ion[282] (X is, e.g., Al with $n = 3$); (e) model consisting of five tetrahedra (terminating hydrogen atoms not shown);[287,288,444] (f) six-membered silicate ring.[287] Large open circles symbolize oxygen atoms, medium-sized circles tetrahedral atoms (Si or Al), and small filled circles terminating hydrogen atoms. Bond length and angles specified are STO-3G results.[280,282]

Nonempirical calculations on models of silica and zeolites have been reviewed in 1981 by Gibbs et al.,[281] in 1982 by Gibbs,[280] and in 1984 by Sauer and Zahradnik[433] and Mezey.[434] Inferences from these as well as from calculations on related framework structures for minerals, glasses, and melts are considered by Navrotsky et al. (1985)[435] and Gibbs and Boisen (1985).[436]

For calculations on models of oxide catalysts by semiempirical[26] or density functional methods,[437] see the pertinent review articles.[26,437] Applications of Anderson's ASED method[211] are described in ref 438–440.

B. Models and Methods

The TO$_4$ and TOT structure fragments were subjects of the first nonempirical studies[441,442] made as early as 1972/1973. A fast development started with the works of Zupan and Buh,[283] Sauer and Zurawski,[307] and Newton and Gibbs.[295] The first ab initio studies on models of zeolites also go back to 1980.[363,443] Since then, on the one hand, models of growing size involving, e.g., five or six TO$_4$ tetrahedra (cf. Chart 8),[287,288,444] have been studied employing the STO-3G basis sets. On the other hand, molecules like orthosilicic acid, Si(OH)$_4$, disiloxane, (H$_3$Si)$_2$O, and disilicic acid, (HO)$_3$Si$_2$O, have continued to serve as models in increasingly sophisticated ab initio studies,[129,130,445–450] some of which even include electron correlation at the MP2 level.[130,131]
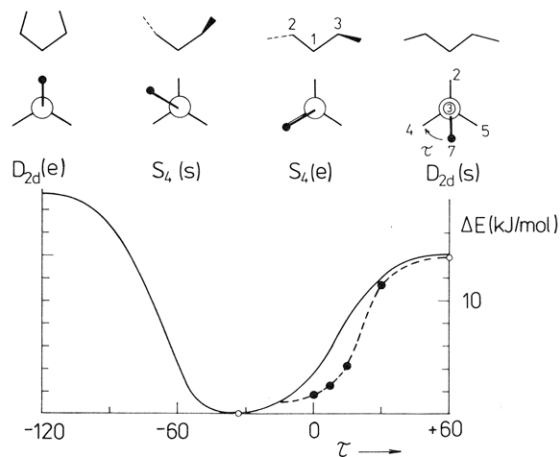
Figure 12. Selected conformations of Si(OH)$_4$ (D_{2d} or S_4 point groups). In the D_{2d} (s) structure all protons are staggered (s) and in the D_{2d} (e) structure all protons are eclipsed (e) with respect to the oxygen atoms. One structure can be converted to the other by synchroneous rotations of the four protons about the respective Si–O axis. All structures passed belong to the S_4 point group. A convenient symmetry coordinate to describe this motion is $\tau = {}^1/_4(\tau_{6215} + \tau_{7314} - \tau_{9513} - \tau_{8412})$ where τ_{abcd} is defined as the angle of planes abc and bcd (cf. Figure 13). Its sign is positive if the movement of the directed vector ba toward the directed vector cd involves a right-handed screw motion. There are two special S_4 structures: one with all four protons eclipsed, S_4 (e), and one with all four protons staggered, S_4 (s). The potential shown is schematical. Calculated are only the energies of the miminum[69,451] and of the D_{2d} (s) structure.[417] The broken line connects points calculated under the constraint of a regular SiO$_4$ tetrahedron.[454]
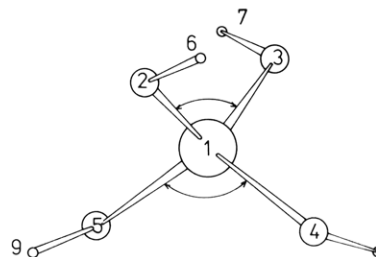
Figure 13. Equilibrium conformation of orthosilicic acid (6-31G* basis set).[69]

While the molecular structure of disiloxane was observed by electron diffraction, orthosilicic acid, due to its tendency to self-polymerize, has not yet been detected in experiments. Table 24 shows the results of geometry optimizations performed with basis sets of increasing quality for this molecule. The protons of Si(OH)$_4$ give rise to a wealth of possible conformations. Figure 12 shows the most symmetrical ones only (D_{2d} and S_4). The equilibrium geometry (S_4 point group; Figure 13) is found for a torsional angle of −33° (6-31G* basis set).[69] It has been shown to be a true minimum on the energy hypersurface (all eigenvalues of the matrix of second derivatives were positive)[451] while the D_{2d} (staggered) structure is a saddle point (one negative eigenvalue).[417] The rotational barrier (energy difference between the D_{2d} (staggered) and the equilibrium structure) amounts to 13.8 kJ/mol[451] (6-31G*). On further extension of the basis set by adding p-type polarization functions on hydrogen atoms (6-31G**), one gets virtually the same value (13.4 kJ/mol).[129] Basis sets smaller than 6-31G* also correctly predict the S_4 structure to be more stable and yield rotational barriers of 7.5 kJ/mol (STO-3G),[452] 5.4 kJ/mol (STO-3G$^{(*)}$),[452]

TABLE 24. Molecular Structure of Orthosilicic Acid: Results of Geometry Optimizations (SCF Calculations) for Basis Sets of Increasing Quality

basis set	year	ref	point group	O–H	SiOH	SiO	OSiO (4×)	OSiO (2×)	τ	type of optimizn	harmonic force const calcd?[a]
STO-3G	1980	296	D_{2d}	(96)[b]	(109.5)[b]	165.3	(109.47)[b]		(60)[b]	energy	no
STO-3G	1983	454	D_{2d}	98.1	109	165.7	(109.47)[b]		(60)[b]	energy	no
STO-3G	1984	452	D_{2d}	98.3	109.1	165.5	112.4	103.8	(60)[b]	gradient	no
STO-3G	1986	417	D_{2d}	98.3	109.1	165.5	112.4	103.7	(60)[b]	gradient	yes (M)[c]
STO-3G	1981	281	S_4	98.1	108.8	165.4	107.1	114.2	-38	gradient	no
	1984	452	S_4	98.1	109.6	165.2	107.1	114.4	-25.3	gradient	no
STO-3G*	1980	296	D_{2d}	(96)[b]	(109.5)[b]	160.5	(109.47)[b]		(60)[b]	energy	no
	1984	452	D_{2d}	98.4	110.7	160.3	113.5	101.6	(60)[b]	gradient	no
	1984	452	S_4	98.3	111.4	160.2	106.4	115.8	-12.3	gradient	no
4-31G	1983	454	D_{2d}	93.8	140	163.0	(109.47)[b]		(60)[b]	energy	no
3-21G	1986	417	D_{2d}	95.7	128.4	164.2	111.5	105.5	(60)[b]	gradient	yes (S)
6-31G	1986	417	D_{2d}	94.1	134.6	166.2	111.9	104.8	(60)[b]	gradient	yes (S)
3-21G	1987	455	S_4	95.8	127.0	164.1	107.2	114.1	-30.4	gradient	no
DZ	1987	456	S_4	95.1	135.5	164.2	(109.47)[b]			gradient	no
3(4)-21G[(*)d]	1985	453	D_{2d}	96.0	114.5	161.8	112.3	103.9	(60)[b]	gradient	no
3(4)-21G[(*) d]	1985	453	S_4	95.8	114.5	161.7	109.5	109.4	8.4	gradient	no
6-31G*	1986	417	D_{2d}	94.7	117.2	162.9	112.6	103.3	(60)[b]	gradient	yes (S)
6-31G**	1987	129	D_{2d}	94.2	118.3	162.7	112.6	103.4	(60)[b]	gradient	no
6-31G[(*)]	1986	302	$S_4{}^e$	94.5	129.5	162.2	107.1	114.3	f	gradient	no
6-31G*	1983	454	S_4	94.7	116.5	163.5	(109.47)[b]		-15.8	energy	no
6-31G*	1987	69	S_4	94.7	117.2	162.9	106.4	115.8	-33	gradient	yes (M)
6-31G*	1987	451	S_4	94.7	117.1	162.9	106.4	115.8	f	gradient	yes (M)
6-31G**	1987	129	S_4	94.2	118.8	162.6	106.6	115.4	f	gradient	yes (M)

[a] M = minimum; S = saddle point. [b] Parameter fixed in optimization. [c] We doubt this finding since the S_4 structure has a lower energy[452] and the D_{2d} structure should be a saddle point. [d] Combination of 4-21G basis set on O and 33-21G basis set on Si; d functions on Si and O. [e] In the original paper the point group was by error reported as D_{2d}; cf. ref 2 of ref 451. [f] Not reported.

and 4.8 kJ/mol ((4)3-21G*).[453] No calculations for torsional angles below -60° have been reported so far. One may expect that the D_{2d} (eclipsed) structure also corresponds to a saddle point with an even higher energy than the D_{2d} (staggered) form.

Table 24 reveals an interesting correlation of the conformation and the distortion of the SiO$_4$ tetrahedron: For the D_{2d} (staggered) conformation (Figure 12) the two opposite OSiO angles (within the symmetry planes) are *smaller* than the remaining four OSiO angles. The SiO$_4$ tetrahedron is elongated along the S_4 axis. The opposite is true for the equilibrium S_4 structures (τ <0), where the two opposite OSiO angles have the *larger* values and the tetrahedron is flattened (Figure 13). The results calculated for Si(OH)$_4$ agree nicely with the electron diffraction data for the related Si(OCH$_3$)$_4$ molecule.[457] The two opposite OSiO angles are 115.5°, and the point group is S_4 with τ = -56°. Even the deviation between the observed Si–O bond length (161.4 pm) and the 6-31G* result (Table 24) lies within the typical limits of ±2.2 pm for this basis set (cf. Table 1). Other T(XH)$_4$-type models studied by nonempirical calculations are [Zn(OH)$_4$]$^{2-}$,[458] [Al(O-H)$_4$]$^{-}$,[452] and all the eight T(XH)$_4$ molecules with T = C, Si, Ge, and Sn and X = O and S.[129]

In contrast to the lack of experimental data for TO$_4$ groups in molecules, the structure of TXT fragments (T = Si, Ge, Sn; X = O, S) in the H$_3$TXTH$_3$ gas-phase molecules has been observed. The striking similarities with the structures of corresponding fragments in crystals[129,281] support the use of hydrogen atoms for saturating the dangling bonds of fragments that have been cut out of solids. This procedure has now become standard in calculations on oxidic materials such as silica and zeolites. The reason that these naive molecular models perform so well is that both "T/4" and "X/2" pseudoatoms, which are formed following the fractional atom scheme of section IV.E, are neutral for

T = Si, Ge, and Sn and X = O and S. It has also been pointed out in section IV.E.3 that for atoms from other groups of the periodic table (e.g., Al or P in AlO$_4^-$ and PO$_4^+$ tetrahedra) pseudoatoms with modified effective nuclear charges and modified orbital exponents are preferable. This applies also to other coordination numbers, e.g., to 6-coordinated Si in SiO$_2$ (stishovite; section IV.E.5).

In establishing models for calculations on solids, a lot of ideas have been implemented. For example, the following model has been suggested to simulate high pressure on SiO$_2$:[459] To the (HO)$_3$SiOSi(OH)$_3$ model (cf. Chart 8) two helium atoms were added and placed along the Si–O bridging bonds. To increase the pressure, the helium atoms were symmetrically stepped toward the Si atoms, keeping the Si–O$_{br}$ distance constant. At a particular Si–He distance the equilibrium positions and force constants of the Si–O$_{br}$ bond and the Si–O$_{br}$–Si angle were determined from pointwise energy calculations.

Very different from the molecules considered so far are the models suggested by Shluger.[460,461] He starts from the idea that the equivalence of the Si–O bonds in SiO$_2$ and other silicates is a fundamental property and that the natural building units of these materials are SiO$_2$ molecules. Correspondingly, clusters of SiO$_2$ molecules may serve as models of bulk silica or silicates (Figure 14). However, SiO$_2$ molecules are known to be linear.[462] To model tetrahedral sites appropriately it is necessary that the energy gained in cluster formation is sufficient to bend the molecules. Shluger refers to a second minimum he found in the O–Si–O bending potential at an angle of 55°. The calculations used a minimum basis set only (STO-6G). It is very doubtful that the minimum persists when passing to larger basis sets, and inclusion of electron correlation is inevitable to settle this problem definitely. With other compounds the situation may be more favorable. For example, a
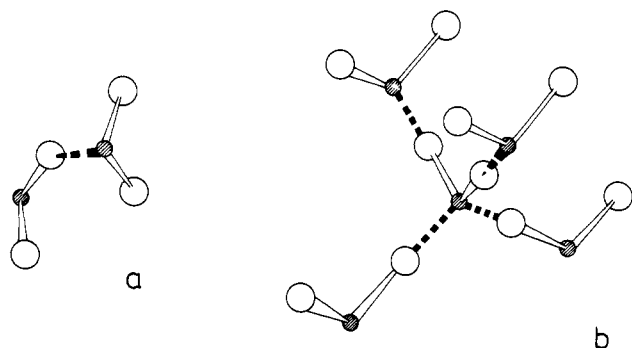
Figure 14. (a) Cluster of two TeO_2 molecules used to model the TeOTe bond of paratellurite[463] and (b) cluster of five SiO_2 molecules used to model the idealized β-cristobalite.[460,461]

dimer of TeO_2 molecules was used as a model of the Te–O–Te bond in paratellurite, which shows also "long" and "short" Te–O bonds (Figure 14).[463] The equilibrium O–Te–O bond angle calculated for the gas-phase molecule is between 112° and 122° depending on the basis set used while the value observed for the paratellurite crystal is 102°.

Another argument put forward in favor of the model is that the valence band edge in the electronic states is correctly described. Since the valence band edge is formed by nonbonding oxygen atoms, this, however, will always be true as long as the model contains any oxygen atoms with lone pairs only. The defect of such clusters of SiO_2 molecules as models of bulk SiO_2 is that only a small fraction of the atoms is properly coordinated (in the pentamer model (Figure 14) only the central silicon atom and four of the ten oxygen atoms). That means the models do not ensure proper hybridization on oxygen atoms and, hence, will always exhibit too short terminal Si–O bonds with double-bond character.

C. Framework

1. Introduction

Table 25 summarizes calculations on models of oxides and related minerals. In what follows we will comment only on silicates and zeolites. For a detailed discussion of other materials we refer to the pertinent reviews.[280,281,435,436] The degree of complexity of silicate models for which calculations are feasible (Chart 8) does not allow to distinguish directly between different framework structures. Such differences can be incorporated into the models only indirectly, i.e. by making use of atomic coordinates observed for a given zeolite type.[287,288,444,464] The virtue of the theoretical approach is that a number of problems can be addressed that can not be easily solved by experiments. Some of them will be considered in this and the following sections:

(1) X-ray diffraction is usually unable to distinguish between Si and Al atoms in aluminosilicate structures and theoretical information on how the local structures of SiOSi and SiOAl⁻ linkages differ are highly welcome. Further, there is interest in the local structures of framework hydroxyls, ≡SiOH·Al≡, that form the active sites of acidic catalysts. X-ray diffraction can not localize protons, and even when using neutron diffraction very crude data are obtained unless the experiments can be made on very large single crystals, which is rarely the case.

(2) Knowledge of force fields of silicates[465] is particularly poor. Attempts at theoretical interpretations of IR and Raman spectra of silicates mostly employed simple diagonal force fields that neglect coupling (nondiagonal) terms and frequently make additional assumptions on bending force constants.[466,467] Virtually nothing is known on differences between Si–O and Al–O bonds.

(3) The Al distribution in zeolite frameworks is a key feature for understanding the catalytic properties of zeolites. The difficulties of classical diffraction methods in this respect have been already mentioned, and it is only recently that inferences can be made from ^{29}Si MAS-NMR spectroscopy.[2] For frameworks with crystallographically different positions the question is whether there are sites of preferred Al substitution.

(4) Surface sites such as hydroxyls and defects are also not accessible by diffraction methods because of low concentration and lack of periodicity. Interpretation of spectroscopic results needs support from calculations.

2. Local Structures

Crucial for structure and bonding of the systems considered is the T–O–T link between two corner-sharing tetrahedra, $-(-O)_3T-O-T-(O-)_3-$. Newton and Gibbs[296] showed that the geometry of disilicic acid mimics nicely the Si–O bond length and Si–O–Si bond angle variations in silicates and, moreover, that the wide range of Si–O–Si angles observed for silica glass and silicates is related to the broad and shallow shape of the potential curve calculated for disilicic acid as a function of the Si–O–Si angle, i.e., to the weak Si–O–Si bending potential.[280,281,468] Extending these calculations to Al-substituted models (Chart 8a) narrower T–O–T angles have been found, namely 139° for Si–O–Al and 137° for Si–OH·Al.[280,496] The protonated bridge, SiOH·Al, shows a substantially increased barrier to linearity.[280] Compared with the Si–O bond in SiOSi, the Al–O bond in SiOAl and both the Si–O and Al–O bonds in the protonated SiOH·Al linkages are significantly longer:[280,282,496,497]

$$
\begin{array}{cc}
157 \quad 170 & 167 \quad 182 \\
& H \\
Si-O-Al & Si-O\cdots Al \\
159\pm1 \quad 171.5\pm2.5 & 168.5\pm3 \quad 194\pm5
\end{array}
$$

While the upper line gives directly the STO-3G results, the lower line gives recommended estimates based also on better calculations on smaller models[68,69] (cf. section IV.G). The difference between the recommended estimates of Si–O and Al–O bonds in SiOAl bridges, 12.5 ± 2.5 pm, gains support from the Si–O and Al–O distances resolved for zeolite Na–A (160 and 173 pm).[498]

3. Force Constants

The similarity of local force fields of the disiloxy groups in disilicic acid and quartz crystals emerges from the result of Newton et al.[469] that the bulk modulus of α-quartz can be reproduced by force constants calculated for this molecule. While this study used the STO-3G basis set, later 6-31G* calculations[468] yielded more reliable force constants. Valuable force constant data for the angle deformation and nondiagonal coupling terms in SiO_4 tetrahedra were obtained from 6-

TABLE 25. Calculations on Oxides (Including Silica and Zeolites) and Related Minerals

subject	model	method[a]/basis set	aim	ref
	(i) Silica and Silicates[b]			
local structure of silica	$H_3SiOSiH_3$	6-31G**, DZ+2P MP2/6-31G**, MP2/DZ+2P	bond lengths and angles	130, 131
	$(HO)_3SiOSi(OH)_3$	6-31G[(*)], 6-31G[(*)]+d(O_{br})	bond lengths and angles, force constants	302, 468
	$(HO)_3SiOSi(OH)_3$	STO-3G	bond lengths and angles, force constants	296, 301, 302, 448, 469
small rings in silicates	$(H_2SiO)_2$	test of various basis sets	geometry	470
	$[(HO)_2SiO]_n$	STO-3G, 6-31G[(*)], 6-31G*	geometry	471
	$(H_2SiO)_n$ (n = 3, 4)	3-21G	geometry	472
	$(H_2SiO)_n$ (n = 3, 4)	6-31G[(*)]	geometry	67
"silica-w"	$(HO)_2SiO_2SiO_2SiO_2Si(OH)_2$	STO-3G	geometry	471
stishovite	$Si(O[^2/_3H]_2)_6$ (T_h) $Si_2(OH)_2F_8{}^{2-}$	STO-3G	geometry	295
	$Si(OH)_4(OH_2)_2$	6-31G[(*)]	Si–O bond length	473
structure of silica and silicates	$Si(OH)_4$, $(HO)_3SiOSi(OH)_3$, $[(HO)_2SiOH]_2$	STO-3G 6-31G[(*)]	force field parameters for molecular mechanics	473
nature of SiO bond	$SiO_4{}^{4-}$, $Si(OH)_4$, $H_3SiOSiH_3$	[6,5,1/4,3,1/3,1]	NMR chemical shift, O nuclear quadrupole coupling constants	474
silicon oxides and fluorides	$SiO_4{}^{4-}$, SiF_4, $SiF_5{}^-$, $SiF_6{}^{2-}$	[6,5,3/4,3,1]	^{29}Si NMR chemical shifts	475
	(ii) Aluminosilicates (Zeolites)[c] and Related Oxides			
relative stability of Al–O–Al pairs	$(HO)_3SiOSi(OH)_3$, {$(HO)_3SiOAl(OH)_3{}^-$}[P,d] {$(HO)_3AlOAl(OH)_3{}^{2-}$}[P,d]	STO-3G	geometry, relative energy	301
	$(HO)_3T^1OT^2(OH)_3\cdot M$ (T^1, T^2 = Si, Al[-]; M = Li^{+}, Na^{+}),	STO-3G	relative energies	434, 476
	$[H_2TO]_4{}^{n-}\cdot M$ (M = Li^{+}, Be[2+]; one or two T atoms are Al)	STO-3G	relative energies	434, 477
[29]Si chemical shift	$[Si(OSiH_3)_{4-n}(OAlH_3)_n]^{n-}$	STO-3G	atomic charge on Si	285
local structure of SiOBe bonds	$(HO)_3SiOBe(OH)_3{}^{2-}$, $(HO)_3SiOH\cdot Be(OH)_3{}^-$	STO-3G	bond lengths and angles	478
local structure of TOT bands	$(HO)_3TO(H)T(OH)_3{}^e$ (T = Si, Al, B, Be, Mg), $(HO)_3TO[T(OH)_3]\cdot X(OH)_3$ (T = Si, Al; X = Li, Be, B, C, Na, Mg, Si, Al), $(HO)_3TO[T(OH)_3]\cdot x(OH)_5$ (T = Si, Al; X = Li, Na, Mg, Al)	STO-3G	bond lengths and angles	282
bond length–bond strength relaxation in oxides	$X(OH)_m(OH_2)_n$ (n = 3, 5;[f] X = Li, Na, Al, Si), $MgO(OH_2)_n$ (n = 3, 5), $NO_2(OH)_n$ (n = 1, 3), $SO_2(OH)_2$, $(HO)O_2SOSO_2(OH)$	6-31G[(*)], 6-31G*	bond lengths	479
	(iii) Defects			
AlO_4 centers in α-quartz	$[T(OH)_4]$,[n] $[T(OH)_2(OSiH_3)_2]^n$ (T = Si (n = 0), T = Al (n = 0, +1, -1))	STO-3G	local structure, spin density, hyperfine tensor	480, 482
$[AlO_4/M^+]$ centers in α-quartz (M^+ = H^{+}, Li^{+}, Na^{+})	$M^+[Al(OH)_4]^n$ (n = 1, 0), $M^+[Al(OSiH_3)_4]^n$ (n = -1, 0), $Mg^+[O(SiH_3)_2]$, $O(SiH_3)_2$	STO-3G	local structure, spin density, hyperfine tensor	481, 482
E_4' center of α-quartz	$(HO)_3Si\cdots H\text{-}Si(OH)_3$	STO-3G	local structure, spin density	483
defects in amorphous silica (Si=O double bond, four-membered rings)	$(HO)_2Si{=}O$, planar $Si(OH)_4$, $H_2Si_2O_5$, $SiH_2(OH)_2$, $[(HO)_2Si\text{-}O]_2$ (4-ring), $[H_2Si\text{-}O]_3$ (6-ring)	6-31G[(*)]	local structure, stability	67
defects and surface sites of silica	H_2SiO, $(HO)HSiO$, $(HO)_2SiH$	3-21G, DZP	local structure, vibrational frequencies	484
electronic structure of silica and origin of surface states (E_s' center, Si=O double bond)	SiO_4, $SiOSi$ + point charges (bulk), $\cdot Si(OSi)_2$ + point charges, $O{=}Si(OSi)_2$ + point charges	EC-MB	energy levels	485
nonclosed SiOSi links in high-silica zeolites precursor of NBOHC[h] defects in SiO_2	$(H_3SiOH)_2$	3-21G	local structure, deprotonation energy	486
V_0 center in paratellurite	molecules TeO_2, Te_2O_4,[g] bulk $(HO)_3TeOTe(OH)_3$, defect site $[(HO)_3Te\ Te(OH)_3]^{\cdot+}$	SCF/STO-3G + d(Te) + dif. s (vacancy)	charges, geometry of the defect site, EPR parameters	463
	(iv) Phosphates and Aluminum Phosphates			
	H_3PO_4	STO-3G, STO-3G[(*)]	geometry	452
	$(HO)_2OPOPO(OH)_2$	STO-3G, STO-3G[(*)], STO-3G, STO-3G[(*)], 6-31G[(*)], 6-31G*+d(O_{br})	geometry	302
	$(HO)_3POP(OH)_3{}^{2+}$	6-31G[(*)]	geometry	302
	$P(OH)_4{}^+$, H_3PO_4, $H_2PO_4{}^-$, $PO_4{}^{3-}$	6-31G[(*)]	geometry	302
	$PO_3{}^-$, HPO_3, $P(OH)_5$	6-31G[(*)]	geometry	302
nature of $\equiv P^+OAl^-\equiv$ bonds	$P(OH)_4{}^+$, $(HO)_3POAl(CH)_3$	STO-3G	geometry, charge distribution	289

TABLE 25 (Continued)

subject	model	method[a]/basis set	aim	ref
	(v) Borates			
triangles and tetrahedra, dimer	$B(OH)_3$, $B(OH)_4^-$, $B(OH)_3 \cdot H_2O$ $(HO)_2BOB(OH)_2$	6-31G* STO-3G, 4-31G, 6-31G, 6-31G*	geometry, deformation electron density	487
dimers	$H_2O(HO)_2BOB(OH)_2OH_2$ $[(HO)_3BOB(OH)_2]^-$	STO-3G STO-3G	geometry	487
cyclic trimers	$B_3O_6H_3$, $B_3O_6H_2^-$, $B_3O_6H^{2-}$	STO-3G		
monomers and dimers	BO_3^{3-}, $B(OH)_3$, H_2BOBH_2, $(HO)_2BOB(OH)_2$	STO-3G, 4-31G	geometry, BOB bond angle	488
cyclic trimers	$[OBO]_3^{3-}$, $[(HO)BO]_3$	STO-3G, 4-31G	geometry	488
dimer	$(HO)_2BOB(OH)_2$	DZ	electron density differences	488
	BO_3^{3-}, $B(OH)_3$, BO_4^{5-}, $B(OH)_4^-$	MB	electron density differences, B–O stretch vibrational frequencies	489
monomers and dimers	$HB(OH)_2$, H_2BOBH_2	DZ+d(O)	geometry	490
monomer	$B(OH)_3$	$[5,4,1/2,1]^i$	electric field gradient tensor	491
dimer, cyclic trimer	$[B(OH)_3]_2$, $[(HO)BO]_3$	[4,1/2]		
tetraborate anion	$B_4O_9H_4^{2-}$	[4,1/2]		
monomers and dimers	$HB(OH)_2$, H_2BOBH_2	DZ+d(O)	geometry	338
	(vi) Analogues of Oxides			
thiosilicates	$Si(SH)_4$, $(H_3Si)_2S$ $[(HS)_2HSi]_2S$	STO-3G	geometry	492
	$(H_2SiY)_2$ (Y = O, S)	3-21G, 6-31G*	electron density	472
germanates, stannates, and their thioanalogues	$T(YH)_4$, H_3TYTH_3 (T = C, Si, Ge, Sn; Y = O, S) $Ge(OH)_4(OH_2)_2$	6-31G** (T = C, Si), 3-21G^{(*)} (T = Ge, Sn)	geometry, force constants	129
silicon nitrides	$H_3Si–NH_2$	SCF/6-31G*, MP2/6-31G*	geometry, nitrogen inversion barrier	493
	$H_3Si–NH_2$	SCF/TZ+2P		
	$H_3Si–NH_2$, $Si(NH_2)_4$, $N(SiH_3)_3$, $NH(SiH_3)_2$, $[(H_2N)_3Si]_2NH$	STO-3G, 6-31G^{(*)}, 6-31G	geometry	494
	$[(H_2N)_2HSi]_2NH$	STO-3G	geometry	492

[a] If not otherwise noted, SCF method is used. [b] For calculations on the $Si(OH)_4$ model of SiO_4 tetrahedra employing various basis sets, see Table 24. [c] See also Tables 26 and 28. [d] { }^P denotes embedding by a point ion array. [e] The proton (H) may be or may be not present. This as well as the particular choice of T determines the residual charge. [f] m is chosen such that the models are neutral. [g] Cf. Figure 14a. [h] Nonbridging oxygen hole center.[495] [i] CI-SD calculations were also performed.
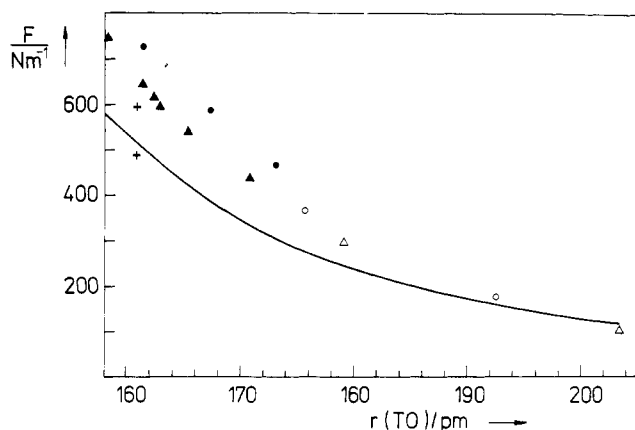
Figure 15. Harmonic stretching force constants of T–O bonds in aluminosilicates derived from ab initio calculations on (H-O)$_3$SiOSi(OH)$_3$,[468] Si(OH)$_4$,[417] H$_3$SiOH and H$_3$SiOH·AlH$_3$,[499] and [H$_3$SiO·AlH$_3$]$^-$.[500] Full and open symbols refer to Si–O and Al–O bonds, respectively, while circles and triangles refer to 3-21G and 6-31G* basis sets, respectively. The line indicates the particular Badger–Bauer relation, which proved successful in describing observed zeolite lattice vibrations.[466,467] The crosses refer to two different experimental force fields for SiO$_2$ (see ref 417 for the original references).

31G* calculations on orthosilicic acid.[417] Figure 15 shows the Si–O bond stretching force constants from these studies[417,468] together with 6-31G* and 3-21G results for the Si–O and Al–O bonds in the H$_3$SiOH, H$_3$SiOH·AlH$_3$,[499] and H$_3$SiOAlH$_3^-$ models.[500] Comparison is made with a simple empirical force field fitting observed vibrational frequencies of zeolite frameworks.[466,467] It is based on the assumption that differences between Si–O and Al–O bonds as well as differ-

ences between bonds of one type, but with different lengths, can be reduced to the Badger Bauer relation between bond lengths (r) and force constants:[466,467]

$$f_{ii}(r) = A_i/(r - b_i)^3 \qquad (VII.1)$$

I.e., there is only one set of constants A and b for both Si–O and Al–O bonds.

The figure shows that the calculated force constants are larger than the values that fit the experiment. The common experience is that 6-31G* and 3-21G basis sets yield force constants that are too large by about 25% (cf. Table 1). Nevertheless, the calculated force constants also follow the Badger Bauer relation. It is a significant result that differences between Si–O and Al–O bond stretching force constants can be reduced to bond length differences since the justification of this assumption was very uncertain. Typical lengths of Si–O and Al–O bonds in zeolites, 160 and 173 pm, respectively,[498] correspond to stretching force constants of 532 and 310 N m^{-1}, respectively.

The influence of variations in framework composition (measured by Sanderson's average electronegativity) on Si–O and Al–O bond stretching frequencies has been studied by Datka et al.[501] Gibbs et al. calculated the stretching force constants of the TX bonds in T(XH)$_4$ molecules (T = C, Si, Ge, Sn; X = O, S) and showed that their distance dependence follows the relation[129]

$$f_{ii}(r) = (c_i/r)^n \qquad (VII.2)$$

with $n = 2.45$. Force constants of framework and sur-

TABLE 26. Model Calculations of Relative Stabilities of Al–O–Al and Al–O–Si–O–Al Pairs in Aluminosilicate and Zeolites

model equilibria considered[a]	cation (X$^+$)[b]	ΔE, kJ/mol
(a) $2[\text{Al, Si}]^-\text{X}^+ \rightleftharpoons [\text{Al, Al}]^{2-}\text{X}^+ + [\text{Si, Si}]\text{X}^+$	non	490,[301] 485[476]
	non	380–455[464]
	pc	460[301]
	Li$^+$	440[476]
(b) $2[\text{Al, Si}]^-\text{X}^+ \rightleftharpoons [\text{Al, Al}]^{2-}\text{X}^{2+} + [\text{Si, Si}]$	six distributed	120[301]
	pc ($^1/_6+$, $^2/_6+$)	
	pc (1+, 2+)	−330[301]
Ring-Type Models		
(c) $[\text{Al, Si, Al, Si}]^{2-}\text{X}^{n+} \rightleftharpoons [\text{Al, Al, Si, Si}]^{2-}\text{X}^{2+}$	non	135,[477] 120[444]
	Li$^+$	90[477]
	Be^{2+}	60[477]
	2 H$^+$	50[444]
$[\text{Al, Si, Al, Si, Si, Si}]^{2-} \rightleftharpoons [\text{Al, Al, Si, Si, Si, Si}]^{2-}$	non	170[287]
(d) $[\text{Al, Si, Si, Al, Si, Si}]^{2-} \rightleftharpoons [\text{Al, Si, Al, Si, Si, Si}]^{2-}$	non	15–50[287]

[a] Only the central T atoms of TO$_4$ tetrahedra are specified in square brackets; i.e. [T, T] denotes the (HO)$_3$TOT(OH)$_3$ model. [b] pc = point charge.

face hydroxyl groups[68,499,501–503] are mentioned in section VII.D.

4. Si–Al Ordering and Siting

It is commonly accepted that Loewenstein's rule controls the distribution of Al in aluminosilicate frameworks. This rule excludes the existence of Al–O–Al pairs. Table 26 shows model equilibria considered in theoretical studies of the limits of validity of this rule. For type (a) models (pairs of linked tetrahedra) the Al–O–Al pairs are highly unstable. In larger models (c), four- or six-membered rings, the instability of these pairs is largely reduced, in particular when the models are made more realistic by adding charge-compensating metal cations or protons. The essential feature of type (b) equilibria is that only neutral models are involved. The results indicate that Al–O–Al pairs may occur provided that they are stabilized by strong local electric fields created by nearby cations. The general conclusion is that cation effects should not be ignored. The results for type (d) equilibria show that Al–O–Si–O–Al pairs are destabilized by 15–50 kJ/mol. Dempsey's rule states that also such pairs are avoided whenever the Si/Al ratio allows this. In conclusion, both Loewenstein's and Dempsey's rules, which were based on simple electrostatic arguments, can be rationalized by quantum chemical results.

The problem of Al siting in frameworks with crystallographically distinguishable positions has been theoretically studied by André, Fripiat, and Derouane et al.[287,288,444,464] in a number of papers. Knowledge of the preferred sites for Al substitution (if there are any) would allow one to make suggestions for the location of the active framework hydroxyls within the channel system of a catalyst. The basic idea was that the local structures of the different sites will be differently suited to accommodate an Al atom. From what has been said in section VII.C.2, it emerges that the best suited sites would be those with the longest T–O bonds and smallest T–O–T angles. A way to check whether a given local structure is optimal for accommodating Al is to perform quantum chemical calculations of an Al(OH)$_4^-$ model adopting the observed atomic coordinates. The difference of the obtained energy and the energy of the corresponding Si(OH)$_4$ model at the same geometry yields the substitution energy.

For selected positions, calculations have been completed (STO-3G basis set) on much larger models:

pentameric Al[OSi(OH)$_3$]$_4$ models (Chart 8e), pentameric chains in ZSM-5 (cf. Chart 8e), and four- and six-membered rings (Chart 8f) in mordenite and ferrierite, respectively. The authors reached the conclusion[287,288,444,464] that the preferred sites of Al substitution are located in the six-membered rings (T2) of the ferrierite framework, the four-membered rings (T3 and T4) of the mordenite framework, and the five-membered ring (T12 and T2) of the ZSM-5 framework.

There are some problems that may affect the reliability of the results:

(1) The atomic coordinates are not always accurately enough known to render calculated energy differences significant. For example, the ZSM-5 structure data[430] for which the calculations[288,464] were performed show variations of the average T–O bond length for the individual tetrahedra between 163 (T12) and 156 pm (T8). In contrast, a more refined structure (single-crystal data) yields average T–O distances for the 12 different tetrahedra that vary between 160 (T10) and 157.5 (T8) only.[504] (The standard deviation is 2 pm.)

(2) Cations may affect the relative substitution energies significantly.[288] For example, the energy changes observed on protonation of models are of the same magnitude as the differences between the sites and may change the order of relative substitution energies.

(3) Zeolites are metastable systems, and their Al distribution may also depend on kinetic aspects. Nevertheless, it would be certainly a significant progess if we knew the energetically most favorable Al siting for a given framework, and the quoted studies[287,288,444,464] made an important step toward the proper solution. It seems that we will not get a definitive answer unless we include the effect of cations (protons), optimize the local geometry, and allow for relaxation of the surrounding lattice. This is a task by far too demanding for a direct ab initio calculation, and this the more as minimal or other small basis sets will not be sufficient for this purpose. Semiempirical methods[438,439] or electrostatic lattice energy calculations yield also too crude results[440] and hope focuses on ab initio derived potential functions, either within an ionic model[505] or within a covalent force field model.[473]

D. Framework and Surface Hydroxyls (Acidic Sites)

The outer surfaces of microcrystallites of three-di-

TABLE 27. Molecules as Models of Surface Hydroxyls: Comparison of O–H Stretching Frequencies (cm⁻¹) Observed on Surfaces with Gas-Phase Data for Molecules

type of silanol group	surface	molecules		calculations[j] (molecular models)
		gas	solution	
single (≡SiOH)	3749[a,b]		3700 [Me₂(Me₃SiO)SiO]₃SiOH[c]	3840[j] (4025) (HO)₃SiOH[f]
			3705 [Me₃SiO]₃SiOH[c]	
			3698 (MeO)₃Si–OH[c]	
			3695 Me₃Si–OH[c]	
		3740 Me₃SiOH[d]	3688 Me₃Si–OH[e]	3811[j] (3995) H₃SiOH[g]
geminal 3742[b]			3686 Me₂Si(OH)₂[e]	ref 543
vicinal	3720[a]		3700 Et₃Si–OH[i]	3778[j] (3960)
	3550[a]		3500 (Et₃SiOH)₂[i]	3598[j] (3771) (H₃SiOH)₂[h]
bridged	3665			3750[j] (3931) H₃SiOH·AlH₃

[a] Reference 508. [b] References 509 and 510. [c] 0.01 m solution in CCl_4.[511,512] [d] Reference 513. [e] Diluted CCl_4 solution.[513,514] [f] Reference 417. [g] References 68 and 499. [h] Reference 486. [i] 0.033 m solution in cyclohexane.[515] [j] Scaled SCF/3-21G frequencies (calculated harmonic frequencies in parentheses). Scale factors derived from calculated and observed frequencies for H_2O and CH_3OH.[68]

mensional zeolite or silica networks are terminated by surface hydroxyls called "terminal" hydroxyls (XIa).
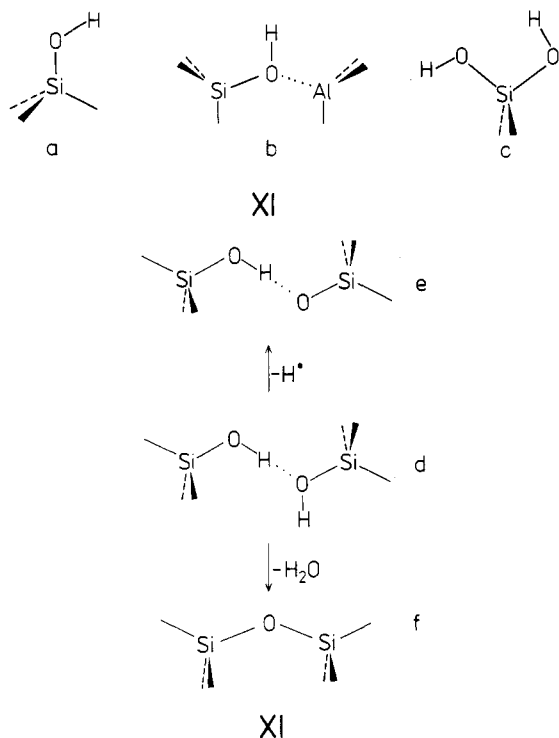
When protons are attached to SiOAl bridges of aluminosilicate frameworks, to compensate their negative charge, "framework" or "bridged" hydroxyls (XIb) are created that are the origin of Brønsted acidity of zeolites.[68] In contrast, terminal hydroxyls are only weakly acidic. Besides "isolated" terminal hydroxyls, geminal (XIc) or adjacent pairs (XId) of hydroxyls may occur on silica surfaces.[506,507] Recently, it has been suggested that adjacent hydroxyl pairs may be present as defects (unclosed SiOSi links) in high-silica zeolites (ZSM-5).[486] Such unclosed SiOSi links are also believed to form the precursors of so-called "nonbridging oxygen hole centers" (XIe) in SiO_2.[495]

A common means for identification of surface hydroxyls is IR spectroscopy of the OH vibration.[507] Comparison of observed frequencies (Table 27) demonstrates that molecules in the gas phase or in solution can successfully model different types of hydroxyls on solids. Results of calculations are also given.

Figure 8 in section IV.G shows predictions for the local geometry of protons in framework hydroxyls,

≡SiOH·Al≡, and terminal hydroxyls on the outer surface of crystals, ≡SiOH.[69] (Results for hydroxyls in solid sodium hydroxide[259] have been mentioned in section V.B). The OH vibrational properties were first studied on the basis of 3-21G calculations.[68] Calculations on $H_3SiOH·AlH_3$ models in which the H atoms on Si and/or Al were gradually replaced by F confirmed that the OH vibrational frequency varies linearly with Sanderson's average electronegativity.[502] Thus, the ab initio calculations on molecular models give theoretical support for correlations of various IR spectroscopic parameters and the acid strength of hydroxyl groups with a parameter describing the composition of the catalyst. However, STO-3G calculations on $H_3SiOH·AlH_3$ models[516] produced evidence that structural factors, i.e., the differences of T–O bond lengths and SiOH bond angles between the individual sites of zeolite frameworks may also account for observed shifts of OH frequencies. It turned out that the OH bond properties are much more sensitive to changes in composition when the hydroxyl group interacts with an electron donor, H_2O. Frequency shifts on interaction of hydroxyls with electron donors (CO, NH_3, H_2O) for the bridging groups are found at least double those of the terminal ones, which agrees with experimental IR spectral data.[517] Comparing different groups, these shifts follow more closely the acidity strength than the OH frequencies of the unperturbed groups. To estimate the effect of isomorphous substitution on surface hydroxyls, the above-mentioned studies on the $H_3SiO-H·AlH_3$ model[68,517] were extended by calculations of local geometries, OH vibrational frequencies as well as their shifts on formation of complexes with CO and NH_3 for the $H_3T^{(1)}OHT^{(2)}H_3$ models with $T^{(1)}$ = Si, $T^{(2)}$ = B, Al, Ga and $T^{(1)}$ = Ge, $T^{(2)}$ = Al.[518] The characteristics of the Brønsted sites were predicted to vary in the order ≡SiOH < ≡SiOH·B≡ < ≡SiOH·Ga≡ ≲ ≡GeOH·Al≡ ≲ ≡SiOH·Al≡ in agreement with experimental observations.

Recent calculations on the complete force field of ≡SiOH·Al≡ groups[499] revealed that the SiOH deformation frequency undergoes much larger shifts between different types of hydroxyls and confirmed an earlier suggestion[519,520] to look at this mode when trying to identify surface hydroxyls. Model calculations also showed[516] that the SiOH deformation is more sensitive to changes of the local structure of SiOH·Al sites than the OH vibration.

Unfortunately, this band is hidden by framework vibrations and can only be uniquely identified as a

TABLE 28. Models of Brønsted Sites on Oxidic Catalysts (Including Zeolites): Deprotonation Energies, ΔE_{DP} (kJ/mol), Net Charge on the Acidic Proton, q_H (au), and Estimated^a Gas-Phase Acidities, $\Delta H_{DP}{}^\circ(0)$ (kJ/mol), from SCF/STO-3G Calculations

model	geometry, site	ΔE_{DP}	q_H	$\Delta H_{DP}{}^\circ(0)^a$	ref
$H_aOSi(OH)_3$	optimized	2090	0.106	1470	496
$(HO)_3SiOH_a \cdot Al(OH)_3$	optimized	1740	0.26	1225	496
$(HO)_3SiOH_a \cdot [Al(OH)_3]_2$	optimized	1510 ± 30		1065 ± 50	496
$H_aOSi[OSi(OH)_3](OH)_2$	standard (quartz)	2190	0.18	1540	521
$(HO)_3SiOH_aAl(OH)_3$	standard (quartz)	1690	0.29	1190	521
$H_aO[Al(O-)_5]_3$	standard (alumina)	2036	0.32	1435	522
$HOH_a \cdot Al[OSi(OH)_3](OH)_2$	standard (quartz)	1740	0.30	1225	521
$(HO)_2AlOH_a \cdot [Al(OH)_3]_2$	standard (alumina)	1563	0.25	1100	522
$(HO)_3SiOH_aAl(OH)_3$	ZSM5,^{b} $Si^1OH_aAl^4$	1761	0.25	1240	464
	ZSM5,^{b} $Si^6OH_aAl^2$	1610	0.26	1135	464
	ZSM5,^{b} $Si^{12}OH_aAl^{12}$	1556	0.30	1100	464
$(HO)_3SiOH_aAl[OSi(OH)_3]_3{}^c$	ZSM5,^{b} $Si^{12}OH_aAl^{12}$	1571	0.29	1105	288
$trans$-$[Si_4Al]$-$H_a{}^d$	ZSM5,^{b} $Si^{12}OH_aAl^{12}$	1553		1095	288
cis-$[Si_4Al]$-$H_a{}^d$	ZSM5,^{b} $Si^{12}OH_aAl^{12}$	1576		1110	288
cis-$[Si_3Al_2]$-$H_a{}^1H_a{}^2$	ZSM5,^{b} $Si^{12}OH_a{}^1Al^{12}$	1516		1070	288
	..., $Si^3OH_a{}^2Al^{2\,e}$	1917^e		1350	288
$[Si, Si, Si, Al]$-$H_a{}^f$	MOR, $Si^4OH_aAl^4$	1585		1115	444
$[Si, Si, Si, Al]$-$H_a{}^f$	MOR, $Si^3OH_aAl^3$	1593		1120	444
$[Si, Al, Si, Al]$-$H_a{}^1H_a{}^{2\,f}$	MOR, $Si^3OH_a{}^1Al^3$	1620		1140	444
	..., $Si^4OH_a{}^2Al^4$	1896		1335	444
$(HO)_3SiOH_a \cdot Al(OH)_3$	standard	1690	0.29	1190	523
$(HO)_3SiOH_a \cdot Al(OH)_3$	standard	1640		1155	524
$(HO)_3SiOH_a \cdot Al(OH)_3$	partially optimized	1680		1185	282
$(HO)_3SiOH_a \cdot B(OH)_3$	partially optimized	1680		1185	282

^{a} $\Delta H_{DP}{}^\circ(0) \approx f \cdot \Delta E_{DP}(STO\text{-}3G)$, $f = 0.704 \pm 0.015$ (see text). ^{b} Atomic coordinates observed for the specified crystallographic positions have been used. ^{c} Cf. Chart 8e. ^{d} Pentameric chain of five TO_4 tetrahedra; cf. Figure 11c. ^{e} Second deprotonation step (bifunctional acid). ^{f} Four-membered ring model of mordenite.

combination band with the O–H stretch in the near-IR region (diffuse reflectance technique).[519,520] Interpretation of the spectra requires knowledge of anharmonicity constants of the vibrations that have been provided by ab initio calculations.[503]

A direct measure of the intrinsic acidity strength of an individual surface site is the heat of deprotonation at 0 K, $\Delta H_{DP}{}^\circ(0)$:[68,496]

$$\Delta H_{DP}{}^\circ(0) = \Delta E_{DP} + \Delta E^{ZP} \qquad (VII.3)$$

This is a straightforward extension of definitions introduced for gas-phase molecules. Since anions are formed on deprotonation, accurate calculations of the deprotonation energy, ΔE_{DP}, require extended basis sets (diffuse functions) and inclusion of electron correlation. Nevertheless, one may still get correct *relative* values of deprotonation energies from small basis set SCF calculations—the only ones that can be completed for reasonably large models of surface sites. Since the change of the zero-point vibrational energy, ΔE^{ZP}, is a minor correction frequently assumed to vary linearly with ΔE_{DP}, an estimate of $\Delta H_{DP}{}^\circ(0)$ may be obtained from calculations employing even minimal STO-3G basis sets:

$$\Delta H_{DP}{}^\circ(0)^{est} \approx f\Delta E_{DP}(SCF/STO\text{-}3G) \qquad (VII.4)$$

The scale factor f is derived from calculations on H_2O and CH_3OH since for these molecules $\Delta H_{DP}{}^\circ(0)$ is known from experiments. Table 28 shows results for models of different hydroxyl sites on zeolites and related catalysts. The following inferences can be made:

(1) Bridged hydroxyls are significantly more acidic than terminal hydroxyls. Generally, the acidity strength is higher the larger the coordination number of the hydroxyl oxygen atom and the lower the coordination numbers of the neighbored cations are.[521,522,525] This is clearly seen from the calculations for different hydroxyls

on alumina (coordinated by one, two, or three aluminum atoms in a trigonal, tetrahedral, or octahedral environment).[522,525]

(2) Changes of local geometry as observed between different frameworks and between different sites of a given framework may cause major acidity changes (see also ref 524 and 526).

(3) The acidity strength of the second proton in paired $\equiv$SiOH·Al$\equiv$ sites is lower than that of the first proton.[288] This is expected since multiple $\equiv$SiOH·Al$\equiv$ sites interacting through the framework correspond to polyfunctional acids.

(4) The acidity strength of $\equiv$SiOH$_a$·B$\equiv$ sites that may be present in B-modified zeolites is not higher than that of $\equiv$SiOH$_a$·Al$\equiv$ sites (cf. ref 518).

Brønsted acidity and Lewis acidity as well as basicity have been discussed as complementary principles for composite metal oxides (silica–alumina, silica–magnesia),[521] magnesium oxide,[527] and different types of alumina.[522,525,528]

Other calculations of deprotonation energies[68,486,529] used the 3-21G basis set (cf. section II). Except the simple H_3SiOH, $H_3SiOH \cdot AlH_3$, and $(H_3SiOH)_2$ models of sites XIa, b, and d[68,486] $\{O_3SiOH \cdot AlO_3{}^{6-}\}^P$ models embedded in an array of 82 point ions (charges of 2+ and 1– on Si and O, respectively) were studied.[529] The calculations used the observed atomic coordinates of ZSM-5.[430] The deprotonation energies of about 2650 kJ/mol reported[529] are much larger than the 1430 kJ/mol obtained, e.g., for the $H_3SiOH \cdot AlH_3$ model.[68] A possible explanation is that the model adopted in ref 529 is *not neutral* as the point charge array is terminated by oxygen ions.

Theoretical studies of the acidity strength of complex catalysts as, e.g., supported transition-metal oxides,[530] require calculations on models such as XII that are very large for a decent quantum chemical ab initio treatment. Calculations of the deprotonation energies of

models XIIa–c were completed[530] within the local density approximation in combination with effective-core potentials (cf. section II.D). They successfully explained the experimentally observed acitivity trends for supported catalysts, namely $TiO_x \ll NbO_x < WO_x$. In

HO\ /OH   O\ /OH
   \Ti/   \Nb/
  O/ \O   O/ \O
  | | | |
  Al   Al   Al   Al
 / \ / \   / \ / \
HO   O   OH   HO   O   OH

      a   b

        O
        ‖
      O\ / \OH
       W
      O/   \
      | H
      | O   c
      Al   Al
     / \   / \
   HO   O   OH

XII
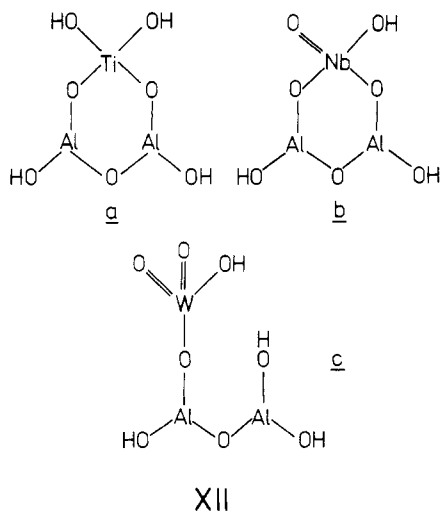
addition to the studies already mentioned, Akarenkov et al.[354] investigated the formation of surface hydroxyls on adsorption of H_2O on the MgO(100) surface. Bauschlicher considered Ni_5OH, CuOH, and AgOH as models of hydroxyls on metal surfaces[531] that may form on dissociation of H_2O on metals in the presence of preadsorbed K or O atoms.

E. Surface Complexes

The interaction of molecules with surfaces of silica, aluminosilicates, or zeolites can be understood in terms of intermolecular interactions of these molecules with surface groups such as hydroxyls, SiOT bridges (T = Si, Al⁻), or cations.[433,443,532] Gas-phase cation–molecule complexes provide the first information on the binding of molecules on the respective cations in zeolites.[533,534] Of particular interest are hydrocarbons as they are involved in catalytic transformations. Among the molecules studied are benzene, isobutene, and ethene.[58,373,533,534] The calculated IR frequency shifts (MINI-1 basis set) for the Na^+–C_2H_4 complex compared with free C_2H_4 explains the IR band shifts observed on adsorption of C_2H_4 in Na–X as well as in Ca–X and Ca–Y zeolites.[58]

This example shows that methods suited to study intermolecular complexes,[321,322] e.g., ion–molecule or hydrogen-bonded complexes, can be readily applied to surface complexes provided that appropriate molecular models of the surface sites can be found.[433,532] Molecular electrostatic potentials (MEP) not only provide qualitative information on the bonding ability of different surface sites of silica[535,536] but also are the data from which meaningful point charges can be derived[263] (cf. section IV.D). The desire to study large (and hopefully more realistic) models has tempted some researchers to employ the minimal STO-3G basis set. Examples are surface complexes of H_2O,[537,538] NH_3,[538] N_2, and O_2[539] on Lewis acidic sites in aluminosilicates ($Al(OH)_3$ models) and hydrogen-bonded complexes of NH_3[540] and H_2O[541] with terminal[540,541] and bridged[541] hydroxyl groups.

However the STO-3G basis set has its weakest performance just with intermolecular interactions (unhealty large BSSE; cf. section V.C). It has been shown many times[322] that other small basis sets like 4-31G or MINI-1 (see, e.g., ref 57 and 373) are better suited for studying intermolecular interactions provided that corrections are made (i) for the basis set superposition error (BSSE), (ii) for the overestimated dipole moments with the 4-31G basis set, and (iii) for neglected intermolecular correlation contributions. The latter can be achieved by adding a semiempirical estimate of the dispersion energy to the corrected SCF result. These prescriptions were followed in the investigation of the binding of water molecules on different surface sites of silica, zeolites, and aluminosilicates by Sauer et al.[263,363,433,443,542–544]

The sites considered include Na^+ ions attached to zeolite A frameworks,[363,433,443] isolated[263,542,543] (XIa) and geminal (XIc)[543] terminal hydroxyls, bridged hydroxyls (XIb),[544] SiOSi bridges (XIf),[263,443,542] Lewis sites (3-fold-coordinated Al modeled by $Al(OH)_3$),[544] and Al^{3+} cations.[373,544]

The bonding of H_2O, NH_3, and CO on terminal (XIa) and bridged hydroxyls (XIc) was also compared on calculations using the 3-21G basis set.[517] Note that much too large binding energies are obtained with this basis set[545] because of a large BSSE and overestimated electrostatic interactions. Calculations on complexes of one and two H_2O molecules with silanol, H_3SiOH, were performed using the 6-31G$^{(*)}$ basis set.[546]

Entropy changes accompanying the formation of surface complexes should not be neglected when comparing the bonding ability of different types of sites.[433,542,543] Specifically, the hydrophobicity of dehydroxylated silica surfaces and high-silica zeolites is caused by the fact that the heat of adsorption released is not sufficient to compensate the loss of entropy when H_2O binds on SiOSi surface sites.[433,532] In contrast, the energy of binding of H_2O on bridged hydroxyls, XIb, is a multiple of that on siloxan bridges, SiOSi.[544] This finding supports the view that in silicium-rich zeolites bridging hydroxyls act as hydrophylic sites within an environment of hydrophobic siloxan bridges.

On surfaces, molecules "feel" the potential of large parts of the solid and they can interact with more than one site. This is particularly true for the micropores of zeolites that have "molecular" dimensions. For example, H_2O is found to bond with its two hydrogen atoms to two SiOSi linkages.[532,543] There is definitely no way to peform directly nonempirical calculations on models that include many surface sites and reflect their arrangement on realistically shaped surfaces. Therefore, the suggestions of Clementi,[547] Beveridge,[548,549] and others for molecules in aqueous solution and biopolymers were adopted and an analytical transferable site–site potential (QPEN,[548,549] quantum mechanical potential based on electrons and nuclei) was derived for water–silica interactions from ab initio calculations on small models.[263,543]

The same aim is pursued by Vigne-Maeder,[550] but a different approach is employed based on the theory of Claverie[551] for intermolecular interactions between large molecules. Potentials have been calculated for the adsorption of H_2O, CH_4, and CH_3OH inside the ZSM-5 channels. Present Monte Carlo[552–554] or molecular dy-

namics[555-557] simulations on zeolitic water[554-557] and gases adsorbed in zeolites[552,553] to obtain structures,[554-557] vibrational spectra,[555-557] energies,[552-557] and thermodynamic functions[552,553] exclusively employ empirical potentials. Ab initio derived potentials could elevate them onto a nonempirical level.

All the studies mentioned so far presume that under common chemical conditions ideally ionic surfaces do not exist. Such surfaces would be (hypothetically) formed when cleaving, e.g., a quartz crystal by heterolytic fission of all affected SiO bonds:

$$\equiv Si-O-Si\equiv \rightarrow Si^+ + {}^-OSi$$
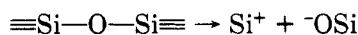
They would either reconstruct and form additional strained SiOSi linkages (i.e., SiO_4 tetrahedra will be linked by common edges) or, in the presence of traces of water, would immediately cover with hydroxyls. Hence, the assumption of a pure ideally ionic ($10\bar{1}0$) surface of quartz made by Julg et al.[361] seems to be not very realistic, at least not for the situation they are going to model, namely the chiral discrimination between an alanine molecule and a quartz surface during the formation of peptides.[558]

Different from the progress made in theoretically modeling adsorption phenomena, the theoretical treatment of chemical reactions on active surface sites is still premature. The few studies published are limited to analyzing charge distributions of possible reactant, intermediate, or product states obtained by very simple ab initio methods. Charge distributions and valence electron levels (STO-3G basis set) were considered for sites formed on dehydroxylation of aluminosilicates[523] and for ethoxyl groups bonded to zeolite frameworks.[537]

To explore the initial step of the photooxidation of propane over vanadium oxide catalysts supported by silica, calculations have been made for separate and coadsorption of ethene and oxygen on $(HO)_3VO$ models.[559] Different modes of approach were considered,
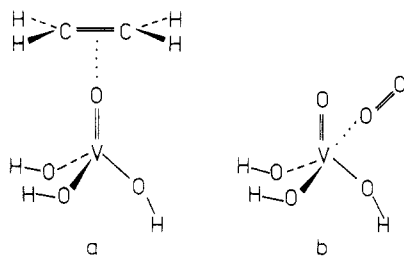
XIII

but restrictions were imposed on geometry parameters and assumptions made for the structure of the $(HO)_3VO$ model. The calculations used the 3-21G basis set for C, O, and H and a [5s3p2d] basis set for V. The V-O-Si linkages between the vanadium oxide and its support were replaced by the terminating hydrogen atoms. The differences between the singlet and triplet states of the active site and the mechanism of coadsorption (synergetic effect) is discussed.

F. Metal–Support Interactions

A few nonempirical studies are devoted to this key problem of catalysis.[429] The conclusions they reach largely depend on the model adopted for the support

surface. For the Cu–MgO catalyst (converts CO to methanol) it has been confirmed by ab initio calculations[560] that Cu can stably stay in a Mg vacancy on the surface of MgO. A Cu atom donates two electrons to the cluster and a Cu^+ ion donates one electron, both yielding a Cu^{2+} ion. Table 16 quotes calculations on the MgO (111) surface[351] showing that these types of oxide surfaces, which consist of oxygen ions only, are stabilized by a reduced net charge on the surface oxygens. They can be represented as O^- instead of O^{2-} in MgO. Similarly, when an Al_2O_3 (corundum) surface model is adopted that contains in the surface layer only oxygen atoms, the charge distribution found in calculations is O^-.[561] When a nickel atom is added to such surface model, about 1.5 electrons are transferred to the surface atoms; i.e., nickel oxide is formed, and nickel is present as nickel ion.[562] This finding seems to be in contradiction with the experimental results indicating that the catalytic action of nickel on alumina is the same as that of Ni by itself.[562] In the previous paragraph it has been pointed out that under the conditions of common catalyst preparation oxide surfaces either are covered by surface hydroxyls or reconstruct and form additional oxygen bridges. Typical sites of such stabilized surfaces of silica or aluminosilicates, or of the ideal "internal" zeolite surfaces, are SiOSi and $SiOAl^-$ oxygen bridges and SiOH and AlOH surface hydroxyls. Sauer et al.[87,563] addressed the problem of the nature of the interaction of transition-metal atoms with such sites. The binding state of oxygen in these sites is the same as in the water molecule and, therefore, transition-metal atom–water complexes may serve as the most primitive model to understand the basic mechanism of interaction. These complexes appear to be weak van der Waals adducts,[87,89,564] and extension of the study to the larger $H_3SiOAlH_3$ model does not change this finding.[563] The weakness of the interaction explains that metal atoms nearly freely move in zeolites until they are trapped by a site of stronger interaction (e.g., a cation, a defect, or another metal atom).[565] Moreover, no pronounced electronic effects occur, and, hence, the catalytic properties of metal species within zeolite cavities should be understandable by considering the electronic properties of these species alone.

VIII. Prospects

Substantial progress is being made with applications of quantum chemical methods in various fields. This is not primarily due to new ideas emerging or new methods but rather to the revolution in scientific computation we witness presently. (1) Supercomputers become accessible to a substantial proportion of the scientific community and become more and more powerful. (2) There is a proliferation of super-microcomputers and work stations, bringing the power of previous main-frame computers into the laboratories. This development has lead to a mass production of results based on ideas and obtained by computational procedures produced in the past but not fully exploited due to computational limitations. Some special problems connected with applications of quantum chemical methods to solids and ways to solve them have been reviewed here. Supercomputers will allow us to complete crystal orbital calculations (section III) for solids with larger and larger unit cells[165,166] and molecular

calculations on larger and larger models.[378,379] On the other hand, the dedicated computers in the laboratories of solid-state and surface chemists, in research institutes of catalysis or mineralogy, and in semiconductor physics departments will produce results for a vast variety of molecular models employing the whole spectrum of quantum chemical methods. The examples of applications presented in sections V–VII give only an idea of future possibilities. However, it is also clear that direct applications of ab initio methods either by crystal orbital techniques or by using molecular models will face limits that exclude important questions from the investigation. To mention only one example, the unit cell of ZSM-5 zeolite contains 96 SiO_4 tetrahedra and even the asymmetric unit includes 12 Si and 26 O atoms.[430] This means that approximations are unavoidable when trying to evaluate the relative stabilities of such complex structures. There are two possible ways to introduce approximations, which may be named the "Hamiltonian" versus the "potential" approach. In the former, one introduces approximations into the Hamiltonian in the way of semiempirical methods until it is simple enough that the Hartree–Fock equations can be solved for such complex systems. One inevitably ends up with a semiempirical method with all its virtues and all the known problems. In particular, this type of method will not be able to make reliable predictions of structures, relative energies, potential surfaces, and vibrational properties. In the latter approach one makes the approximation directly on the potential governing the equilibrium positions and the motion of the nuclei within the Born–Oppenheimer approximation. There are different types of potentials: (1) force field type potentials, which proved suitable in molecular mechanics calculations; (2) Born–Mayer-type potentials or other potentials, which are used to calculate the lattice properties of ionic crystals; (3) intermolecular potential functions, which are applied to gas-phase complexes, liquids, and molecular crystals. The point is that the parameters of the potentials are derived from ab initio calculations on small systems and may be transferred to large systems. The main problem is to find potentials that are transferable to a large extent. In this review first examples of nonempirical potentials of all three types have been mentioned, but the most experience has been accumulated with intermolecular potentials. The "potential" approach to ab initio calculations on complex (nonlocal) structures of solids is the direction I consider the most fruitful, particularly if it becomes possible to combine an explicit ab initio treatment of a small part of a solid (defect, active site, the site where the reaction occurs) with a potential for its environment consistent with the particular ab initio method employed. This is in fact a research program pursued with success in molecular biology.

References

(1) Fyfe, C. A. *Solid State NMR*; CFC: Guelph, 1983.
(2) Engelhardt, G.; Michel, D. *High-Resolution Solid-State NMR of Silicates and Zeolites*; Wiley: Chichester, 1987.
(3) Binnig, G.; Gerber, C.; Weibel, E. *Appl. Phys. Lett.* **1982**, *40*, 178. Binnig, G.; Rohrer, H.; Gerber, C.; Weibel, E. *Phys. Rev. Lett.* **1982**, *49*, 57. Binnig, G.; Rohrer, H.; Gerber, C.; Weibel, E. *Phys. Rev. Lett.* **1983**, *50*, 120. Binnig, G.; Rohrer, H. *IBM J. Res. Dev.* **1986**, *30*, 355.
(4) Schaefer, H. F. *Methods of Electronic Structure Theory. Modern Theoretical Chemistry*; Plenum: New York, 1977; Vol. 3.
(5) Schaefer, H. F. *Applications of Electronic Structure Theory. Modern Theoretical Chemistry*; Plenum: New York, 1977; Vol. 4.
(6) Cársky, P.; Urban, M. *Ab Initio Calculations. Methods and Applications in Chemistry. Lect. Notes Chem.* **1980**, 16.
(7) Hehre, W. J.; Radom, L.; Schleyer, P. v. R.; Pople, J. A. *Ab Initio Molecular Orbital Theory*; Wiley: New York, 1986.
(8) Lawley, K.-P., Ed. *Ab Initio Methods in Quantum Chemistry-I*; Wiley: New York, 1987.
(9) Lawley, K.-P., Ed. *Ab Initio Methods in Quantum Chemistry-II*; Wiley: New York, 1987.
(10) O'Keeffe, M., Navrotsky, A., Eds. *Structure and Bonding in Crystals*; Academic: New York, 1981; Vol. 1 and 2.
(11) Devreese, J. T., Van Camp, P., Eds. *Electronic Structure, Dynamics, and Quantum Structural Properties of Condensed Matter*; Plenum: New York, 1985.
(12) Ladik, J., Suhai, S., Jr., Thomson, C., Eds. *Theor. Chem. (London)* **1981**, *4*, 49.
(13) Hoffmann, R. *Angew. Chem. Int. Ed. Engl.* **1987**, *26*, 846.
(14) Dahl, J. P., Avery, J., Eds. *Local Density Approximations in Quantum Chemistry and Solid State Physics*; Plenum: New York, 1984.
(15) Dreizler, R. M., da Providencia, J., Eds. *Density Functional Methods in Physics*; Plenum: New York, 1985.
(16) Jones, R. O. In Reference 8, p 413.
(17) Salahub, D. R. In Reference 9, p 447.
(18) Dunlap, B. I. In Reference 9, p 287.
(19) Martin, R. M. In *Advances in Solid State Physics*; Grosse, P., Ed.; Vieweg: Braunschweig, 1985.
(20) Louie, S. G. *J. Phys. Colloq.* **1985**, *46*, C4-335.
(21) Cohen, M. L. *Institute of Physics London Conf. Ser., No. 75*, **1985**, 1.
(22) Srivastava, G. P.; Weaire, D. *Adv. Phys.* **1987**, *36*, 463.
(23) Messmer, R. P., Ed. *The Molecular Cluster Approach to Some Solid-State Problems*; Plenum: New York, 1977; Vol. 8, p 215.
(24) Simonetta, M.; Gavezzotti, A. *Adv. Quantum Chem.* **1980**, *12*, 103.
(25) Simonetta, M. *Int. J. Quantum Chem.* **1986**, *29*, 1555.
(26) Zhidomirov, G. M.; Kazansky, V. V. *Adv. Catal.* **1986**, *34*, 131.
(27) Johnson, K. H. *Annu. Rev. Phys. Chem.* **1975**, *26*, 39.
(28) Bullett, D. W. *Solid State Phys.* **1980**, *35*, 129.
(29) Cohen, M. L. *Phys. Today* **1979**, *32*, 40.
(30) Cohen, M. L.; Louie, S. G. *Annu. Rev. Phys. Chem.* **1984**, *35*, 537.
(31) McWeeny, R.; Sutcliffe, B. T. *Methods of Molecular Quantum Mechanics*; Academic: London, New York, 1969.
(32) Roothaan, C. C. J. *Rev. Mod. Phys.* **1951**, *23*, 69.
(33) Boys, S. F. *Proc. R. Soc. London A* **1950**, *A200*, 542.
(34) Dunning, T. H., Jr.; Hay, P. J. In Reference 4, p 1.
(35) Ahlrichs, R.; Taylor, P. R. *J. Chim. Phys. Phys.-Chim. Biol.* **1981**, *78*, 315.
(36) Huzinaga, S. *Comp. Phys. Rep.* **1985**, *2*, 279.
(37) Davidson, E. R.; Feller, D. *Chem. Rev.* **1986**, *86*, 681.
(38) Koutecky, J.; Fantucci, P. *Chem. Rev.* **1986**, *86*, 539.
(39) Pulay, P. In Reference 5, p 153.
(40) Schlegel, H. B. In Reference 8, p 249.
(41) Pulay, P. In Reference 9, p 241.
(42) Gaw, J. F.; Handy, N. C. *Annu. Rep. C, Chem. Soc.* **1984**, *81*, 291.
(43) Binkley, J. S.; Frisch, M.; Raghavachari, K.; DeFrees, D.; Schlegel, H. B.; Whiteside, R.; Fluder, E.; Seeger, R.; Pople, J. A. *GAUSSIAN 82*; Carnegie-Mellon University: Pittsburgh, 1982.
(44) Binkley, J. S.; Frisch, M.; Raghavachari, K.; De Frees, D.; Schlegel, H. B.; Whiteside, R.; Fluder, E.; Seeger, R.; Fox, D. J.; Head-Gordon, M.; Topiol, S. *GAUSSIAN 86, Release C*; Carnegie-Mellon University: Pittsburgh, 1987.
(45) Fogarasi, G.; Pulay, P. *Annu. Rev. Phys. Chem.* **1984**, *35*, 191.
(46) Hess, B. A., Jr.; Schaad, L. J.; Cársky, P.; Zahradnik, R. *Chem. Rev.* **1986**, *86*, 709.
(47) Amos, R. D. *The Cambridge Analytical Derivatives Package*, CCP1/84/4; Computational Science Group, SERC: Daresbury, 1984.
(48) Dupuis, M.; Watts, J. D.; Villar, H. O.; Hurst, G. J. B. *HONDO*, Version 7.0, KGN-169; IBM: Kingston, 1988.
(49) Iwata, S. In *Quantum Chemistry Literature Data Base*; Ohno, K., Morokuma, K., Eds.; Elsevier: Amsterdam, 1982.
(50) Pople, J. A. *Ber. Bunsen-Ges. Phys. Chem.* **1982**, *86*, 806.
(51) De Frees, D. J.; Raghavachari, K.; Schlegel, H. B.; Pople, J. A. *J. Am. Chem. Soc.* **1982**, *104*, 5576.
(52) Francl, M. M.; Pietro, W. J.; Hehre, W. J.; Binkley, J. S.; Gordon, M. S.; De Frees, D. J.; Pople, J. A. *J. Chem. Phys.* **1982**, *77*, 3654.
(53) Gordon, M. S.; Binkley, J. S.; Pople, J. A.; Pietro, W. J.; Hehre, W. J. *J. Am. Chem. Soc.* **1982**, *104*, 2797.
(54) Dobbs, K. D.; Hehre, W. J. *J. Comput. Chem.* **1986**, *7*, 359; **1987**, *8*, 861; **1987**, *8*, 880.
(55) Pople, J. A.; Schlegel, H. B.; Krishnan, R.; De Frees, D. J.; Binkley, J. S.; Frisch, M. J.; Whiteside, R. A.; Hout, R. F.;

Hehre, W. J. *Int. J. Quantum Chem., Quantum Chem. Symp.* **1981**, *No. 15*, 269.

(56) Hout, R. F., Jr.; Levi, B. A.; Hehre, W. J. *J. Comput. Chem.* **1982**, *3*, 234.

(57) Hobza, P.; Sauer, J. *Theor. Chim. Acta* **1984**, *65*, 279.

(58) Sauer, J. *Z. Chem.* **1985**, *25*, 254.

(59) Tatewaki, H.; Huzinaga, S. *J. Comput. Chem.* **1980**, *1*, 205.

(60) Sakai, Y.; Tatewaki, H.; Huzinaga, S. *J. Comput. Chem.* **1981**, *2*, 100.

(61) Tatewaki, H.; Huzinaga, S. *J. Chem. Phys.* **1979**, *71*, 4339.

(62) Sakai, Y.; Tatewaki, H.; Huzinaga, S. *J. Comput. Chem.* **1982**, *3*, 6.

(63) Van Duijneveldt-van de Rijdt, J. G. C. M.; Van Duijneveldt, F. B. *J. Mol. Struct.* **1982**, *89*, 185.

(64) Sauer, J.; Jung, C. *Theor. Chim. Acta* **1975**, *40*, 129.

(65) Sauer, J.; Jung, C.; Jaffé, H. H.; Singerman, J. *J. Chem. Phys.* **1978**, *69*, 495.

(66) Kutzelnigg, W. *Top. Curr. Chem.* **1973**, *41*, 31.

(67) O'Keeffe, M.; Gibbs, G. V. *J. Chem. Phys.* **1984**, *81*, 876.

(68) Mortier, W. J.; Sauer, J.; Lercher, J. A.; Noller, H. *J. Phys. Chem.* **1984**, *88*, 905.

(69) Sauer, J. *J. Phys. Chem.* **1987**, *91*, 2315.

(70) Handy, N. C. *Faraday Symp. Chem. Soc.* **1984**, *No. 19*, 17.

(71) Bauschlicher, C. W., Jr.; Taylor, P. R. *J. Chem. Phys.* **1986**, *85*, 2779.

(72) Bobrowicz, F. W.; Goddard, W. A., III In Reference 5, p 79.

(73) Shepard, R. In Reference 9, p 63.

(74) Bernardi, F.; Robb, M. A. In Reference 8, p 155.

(75) Pope, S. A.; Guest, M. F.; Hillier, I. H.; Colbourn, E. A.; Mackrodt, W. C.; Kendrick, J. *Phys. Rev. B: Condens. Matter* **1983**, *B28*, 2191.

(76) Goddard, W. A., III; McGill, T. C. *J. Vac. Sci. Technol.* **1979**, *16*, 1308.

(77) Redondo, A.; Goddard, W. A., III *J. Vac. Sci. Technol.* **1982**, *21*, 344.

(78) Redondo, A.; Goddard, W. A., III; McGill, T. C. *Surf. Sci.* **1983**, *132*, 49.

(79) Redondo, A.; Goddard, W. A., III; McGill, T. C. *J. Vac. Sci. Technol.* **1982**, *21*, 649.

(80) Walch, S. P.; Bauschlicher, C. W.; Langhoff, S. R. *J. Chem. Phys.* **1985**, *83*, 5351.

(81) Roos, B. O. In Reference 9, p 399.

(82) Blomberg, M. R. A.; Brandemark, U. B.; Siegbahn, P. E. M.; Mathisen, K. B.; Karlström, G. *J. Phys. Chem.* **1985**, *89*, 2171.

(83) Siegbahn, P. E. M.; Almlöf, J.; Heiberg, A.; Roos, B. O. *J. Chem. Phys.* **1981**, *74*, 2384.

(84) Roos, B. O.; Taylor, P. R.; Siegbahn, P. E. M. *Chem. Phys.* **1980**, *48*, 157.

(85) Siegbahn, P. E. M. *Int. J. Quantum Chem.* **1983**, *23*, 1869.

(86) Veillard, A., Ed. *Quantum Chemistry: The Challenge of Transition Metals and Coordination Chemistry*; Reidel: Dordrecht, 1986.

(87) Sauer, J.; Haberlandt, H.; Pacchioni, G. *J. Phys. Chem.* **1986**, *90*, 3051.

(88) Rossi, A.; Kochanski, E.; Veillard, A. *Chem. Phys. Lett.* **1979**, *66*, 13.

(89) Bauschlicher, C. W., Jr. *Chem. Phys. Lett.* **1987**, *142*, 71.

(90) Ahlrichs, R.; Scharf, P. In Reference 8, p 501.

(91) Pople, J. A.; Binkley, J. S.; Seeger, R. *Int. J. Quantum Chem., Symp.* **1976**, *S10*, 1.

(92) Buenker, R. J.; Peyerimhoff, S. D. *Theor. Chim. Acta* **1974**, *35*, 33.

(93) Buenker, R. J.; Peyerimhoff, S. D.; Butscher, W. *Mol. Phys.* **1978**, *35*, 771.

(94) King, H.; Dupuis, M.; Rys, J. *Natl. Resour. Comput. Chem. Software Cat.* **1980**, *1*; QCPE **1981**, *13*, 403.

(95) Čársky, P.; Hess, B. A., Jr.; Schaad, L. J. *J. Comput. Chem.* **1984**, *5*, 280.

(96) Handy, N. C.; Gaw, J. F.; Simandiras, E. D. *J. Chem. Soc., Faraday Trans. 2* **1987**, *83*(9), 1577.

(97) Newton, M. D.; Kestner, N. R. *Chem. Phys. Lett.* **1983**, *94*, 198.

(98) Szczȩśniak, M. M.; Scheiner, S. *J. Chem. Phys.* **1986**, *84*, 6328.

(99) Frisch, M. J.; DelBene, J. E.; Binkley, J. S.; Schaefer, H. F., III *J. Chem. Phys.* **1986**, *84*, 2279.

(100) Sauer, J.; Hobza, P.; Čársky, P.; Zahradník, R. *Chem. Phys. Lett.* **1987**, *134*, 553.

(101) Hobza, P.; Schneider, B.; Sauer, J.; Čársky, P. *Chem. Phys. Lett.* **1987**, *134*, 423.

(102) Sauer, J.; Kathan, B.; Ahlrichs, R. *Chem. Phys. Lett.* **1987**, *113*, 201.

(103) Hohenberg, P.; Kohn, W. *Phys. Rev.* **1964**, *136*, B864.

(104) Kohn, W.; Sham, L. J. *Phys. Rev.* **1965**, *140*, A1133.

(105) Slater, J. C. *Adv. Quantum Chem.* **1972**, *6*, 1.

(106) von Barth, U.; Hedin, L. *J. Phys. C* **1972**, *5*, 2064.

(107) Gunnarson, O.; Lundqvist, B. I. *Phys. Rev. B: Solid State* **1976**, *B13*, 4274.

(108) Vosko, S. H.; Wilk, L.; Nusair, M. *Can. J. Phys.* **1980**, *58*, 1200.

(109) Perdew, J. P.; Zunger, A. *Phys. Rev. B: Condens. Matter* **1981**, *B23*, 5048.

(110) Ceperley, D. M.; Alder, B. J. *Phys. Rev. Lett.* **1980**, *45*, 566.

(111) Baerends, E. J.; Ellis, D. E.; Ros, P. *Chem. Phys.* **1973**, *2*, 41.

(112) Müller, J. E.; Jones, R. O.; Harris, J. *J. Chem. Phys.* **1983**, *79*, 1874.

(113) Sambe, H.; Felton, R. H. *J. Chem. Phys.* **1975**, *62*, 1122.

(114) Koller, J.; Zaucer, M.; Azman, A. *Z. Naturforsch. A: Phys., Phys. Chem., Kosmophys.* **1976**, *31A*, 1022.

(115) Kitaura, K.; Satoko, C.; Morokuma, K. *Chem. Phys. Lett.* **1979**, *65*, 206.

(116) Painter, G. S.; Averill, F. W. *Phys. Rev. B: Condens. Matter* **1982**, *B26*, 1781.

(117) Dunlap, B. I.; Connolly, J. W. D.; Sabin, J. R. *J. Chem. Phys.* **1979**, *71*, 3386, 4993.

(118) Andzelm, J.; Radzio, E.; Salahub, D. R. *J. Chem. Phys.* **1985**, *83*, 4573.

(119) Jones, R.; Sayyash, A. *J. Phys. C* **1986**, *C19*, L653.

(120) Versluis, L.; Ziegler, T. *J. Chem. Phys.* **1988**, *88*, 322.

(121) Radzio, E.; Salahub, D. R. *Int. J. Quantum Chem.* **1986**, *29*, 241.

(122) Painter, G. S. *J. Phys. Chem.* **1986**, *90*, 5530.

(123) Dunlap, B. I. *J. Phys. Chem.* **1986**, *90*, 5524.

(124) Satoko, C. *Chem. Phys. Lett.* **1981**, *83*, 111.

(125) Satoko, C. *Phys. Rev. B: Condens. Matter* **1984**, *30*, 1754.

(126) Andzelm, J.; Radzio, E.; Salahub, D. R. *J. Chem. Phys.* **1985**, *83*, 4573.

(127) Andzelm, J.; Radzio, E.; Salahub, D. R. *J. Comput. Chem.* **1985**, *6*, 520. Radzio, E.; Andzelm, J.; Salahub, D. R. *J. Comput. Chem.* **1985**, *6*, 533.

(128) Heggie, M.; Jones, R. *Philos. Mag. Lett.* **1987**, *55*, 47.

(129) Gibbs, G. V.; D'Arco, P.; Boisen, M. B., Jr. *J. Phys. Chem.* **1987**, *91*, 5347.

(130) Gibbs, G. V.; Lasaga, A. C.; Gordon, M. S., to be submitted for publication.

(131) Gibbs, G. V., personal communication.

(132) McLean, A. D.; Chandler, G. S. *J. Chem. Phys.* **1980**, *72*, 5639.

(133) Ribarsky, M. W.; Luedtke, W. D.; Landman, U. *Phys. Rev. B: Condens. Matter* **1985**, *B32*, 1430.

(134) Jörg, H.; Rösch, N. *Chem. Phys. Lett.* **1985**, *120*, 359.

(135) Čársky, P.; Dedieu, A. *Chem. Phys.* **1986**, *103*, 265.

(136) Broer, R.; Batra, I. P.; Bagus, P. S. *Philos. Mag. B* **1985**, *51*, 243.

(137) Simandiras, E. D.; Amos, R. D.; Handy, N. C. *Chem. Phys.* **1987**, *114*, 9.

(138) Ermler, W. C.; Rosenberg, B. J.; Shavitt, I. In *Comparison of Ab Initio Quantum Chemistry with Experiment for Small Molecules*; Bartlett, R. J., Ed.; Reidel: Dordrecht, 1985; p 171.

(139) Kemister, G. *J. Chem. Phys.* **1987**, *86*, 4507.

(140) Krijn, M. P. C. M.; Feil, D. *J. Chem. Phys.* **1986**, *85*, 319.

(141) Stoll, H.; Pavlidou, C. M. E.; Preuss, H. *Theor. Chim. Acta* **1978**, *49*, 143.

(142) Savin, A.; Stoll, H.; Preuss, H. In Reference 14, p 263.

(143) Lie, G. C.; Clementi, E. *J. Chem. Phys.* **1976**, *64*, 5308.

(144) Colle, R.; Salvetti, O. *Theor. Chim. Acta* **1975**, *37*, 329; **1979**, *53*, 55. *J. Chem. Phys.* **1983**, *79*, 1404.

(145) Dovesi, R.; Pisani, C.; Ricca, F.; Roetti, C. *Phys. Rev. B: Condens. Matter* **1980**, *22*, 5936.

(146) Dovesi, R.; Causà, M.; Angonoa, G. *Phys. Rev. B: Condens. Matter* **1981**, *24*, 4177.

(147) Kemister, G.; Nordholm, S. *J. Chem. Phys.* **1985**, *83*, 5163.

(148) Carravetta, V.; Clementi, E. *J. Chem. Phys.* **1984**, *81*, 2646.

(149) Causa, M.; Dovesi, R.; Pisani, C.; Colle, R.; Fortunelli, A. *Phys. Rev. B: Condens. Matter* **1987**, *36*, 891.

(150) Bloch, F. *Z. Phys.* **1928**, *52*, 555.

(151) Cotton, F. A. *Chemical Applications of Group Theory*; Wiley-Interscience: New York, London, 1963.

(152) André, J.-M.; Bodard, V. P.; Brédas, J. L.; Delhalle, J.; Fripiat, J. G. In *Quantum Chemistry of Polymers-Solid State Aspects*; Ladik, J., Et al., Eds.; Reidel: Dordrecht, 1984; p 1.

(153) Piela, L.; Delhalle, J. *Int. J. Quantum Chem.* **1978**, *13*, 605.

(154) Delhalle, J.; Piela, L.; Bredas, J. L.; André, J. M. *Phys. Rev. B: Condens. Matter* **1980**, *22*, 6254.

(155) Dovesi, R.; Pisani, C.; Roetti, C.; Saunders, V. R. *Phys. Rev. B: Condens. Matter* **1983**, *28*, 5781.

(156) Upton, T. H.; Goddard, W. A., III *Phys. Rev. B: Condens. Matter* **1980**, *22*, 1534.

(157) I'Haya, Y. J.; Narita, S.; Fujita, Y.; Ujino, H. *Int. J. Quantum Chem., Quantum Chem. Symp.* **1984**, *No. 18*, 153.

(158) Silvi, B.; Dovesi, R., to be submitted for publication.

(159) Blumen, A.; Merkel, C. *Phys. Status Solidi B* **1977**, *B83*, 425.

(160) André, J. M.; Vercauteren, D. P.; Bodart, V. P.; Fripiat, J. G. *J. Comput. Chem.* **1984**, *5*, 535.

(161) Dovesi, R. *Int. J. Quantum Chem.* **1986**, *29*, 1755.

(162) Pisani, C.; Dovesi, R. *Int. J. Quantum Chem.* **1980**, *17*, 501.

(163) André, J. M.; Vercauteren, D. P.; Fripiat, J. G. *J. Comput. Chem.* **1984**, *5*, 349.

(164) Dovesi, R.; Pisani, C.; Ricca, F.; Roetti, C. *Phys. Rev. B: Condens. Matter* **1982**, *25*, 3731.
(165) Dovesi, R.; Pisani, C.; Roetti, C.; Silvi, B. *J. Chem. Phys.* **1987**, *86*, 6967.
(166) Causa, M.; Dovesi, R.; Roetti, C.; Kotomin, E.; Saunders, V. R. *Chem. Phys. Lett.* **1987**, *140*, 120.
(167) Teramae, H.; Yamabe, T.; Satoko, C.; Imamura, A. *Chem. Phys. Lett.* **1983**, *101*, 149.
(168) Teramae, H. *J. Chem. Phys.* **1986**, *85*, 990.
(169) Ladik, J.; André, J. M.; Seel, M., Eds. *Quantum Chemistry of Polymers-Solid State Aspects*; Reidel: Dordrecht, 1984.
(170) Karpfen, A. *Chem. Phys.* **1984**, *88*, 415.
(171) Beyer, A.; Karpfen, A. *Chem. Phys.* **1984**, *64*, 343.
(172) Karpfen, A. *Chem. Phys.* **1983**, *79*, 211.
(173) Karpfen, A.; Schuster, P. *Can. J. Chem.* **1985**, *63*, 809.
(174) Suhai, S. *Chem. Phys. Lett.* **1983**, *96*, 619.
(175) Suhai, S. *Phys. Rev. B: Condens. Matter* **1983**, *27*, 3506.
(176) Suhai, S. *Int. J. Quantum Chem.* **1983**, *23*, 1239.
(177) Liegener, C.-M.; Ladik, J. *Phys. Rev. B: Condens. Matter* **1987**, *35*, 6403.
(178) Kunz, A. B. In Reference 169, p 83.
(179) Inkson, J. C. *Many Body Theory of Solids*; Plenum: New York, 1984; p 13.
(180) Delhalle, J.; Calais, J. L. *J. Chem. Phys.* **1986**, *85*, 5286.
(181) Delhalle, J.; Calais, J. L. *Int. J. Quantum Chem., Quantum Chem. Symp.* **1987**, *No. 21*, 115.
(182) Delhalle, J.; Calais, J. L. *Phys. Rev. B: Condens. Matter* **1987**, *35*, 9460.
(183) Delhalle, J.; Brédas, J. L.; André, J.-M. *Chem. Phys. Lett.* **1981**, *78*, 93.
(184) Angonoa, G.; Koutecký, J.; Ermoshkin, A. N. *Surf. Sci.* **1984**, *138*, 51.
(185) Dovesi, R.; Pisani, C.; Roetti, C. *Chem. Phys. Lett.* **1981**, *81*, 498.
(186) Seel, M. *Int. J. Quantum Chem.* **1984**, *26*, 753.
(187) Otto, P.; Bakhshi, A. K.; Ladik, J. *THEOCHEM* **1986**, *28*, 209.
(188) Otto, P.; Dupuis, M. *J. Chcm. Phys.* **1987**, *86*, 6309.
(189) Karpfen, A. In *Photoreaktive Festkörper*; Sixl, H., Ed.; Wahl-Verlag: Karlsruhe, 1984.
(190) Karpfen, A. *Chem. Phys.* **1980**, *47*, 401.
(191) Otto, P.; Steinborn, E. O. *Solid State Commun.* **1986**, *58*, 281.
(192) Dovesi, R.; Pisani, C.; Roetti, C. *Int. J. Quantum Chem.* **1980**, *17*, 517.
(193) Angonoa, G.; Koutecký, J.; Pisani, C. *Surf. Sci.* **1982**, *122*, 355.
(194) Surrat, G. T.; Euwema, R. N.; Wilhite, D. L. *Phys. Rev. B: Condens. Matter* **1973**, *8*, 4019.
(195) Euwema, R. N.; Greene, R. L. *J. Chem. Phys.* **1975**, *62*, 4455.
(196) Dovesi, R.; Pisani, C.; Roetti, C.; Dellarole, P. *Phys. Rev. B: Condens. Matter* **1981**, *24*, 4170.
(197) Dovesi, R.; Ermondi, C.; Ferrero, E.; Pisani, C.; Roetti, C. *Phys. Rev. B: Condens. Matter* **1984**, *29*, 3591.
(198) Dovesi, R.; Pisani, C.; Ricca, F.; Roetti, C.; Saunders, V. R. *Phys. Rev. B: Condens. Matter* **1984**, *30*, 972.
(199) Dovesi, R. *Solid State Commun.* **1985**, *54*, 183.
(200) Causà, M.; Dovesi, R.; Pisani, C.; Roetti, C. *Phys. Rev. B: Condens. Matter* **1986**, *33*, 1308.
(201) Causà, M.; Dovesi, R.; Pisani, C.; Roetti, C. *Surf. Sci.* **1986**, *175*, 551.
(202) Causà, M.; Dovesi, R.; Kotomin, E.; Pisani, C. *J. Phys. C* **1987**, *C20*, 4983.
(203) Dovesi, R.; Orlando, R.; Ricca, F.; Roetti, C. *Surf. Sci.* **1987**, *186*, 267.
(204) Causà, M.; Kotomin, E.; Pisani, C.; Roetti, C. *J. Phys. C* **1987**, *C20*, 4991.
(205) Imamura, A. *J. Chem. Phys.* **1970**, *52*, 3168.
(206) Bleiber, A.; Jung, C.; Lange, R. *Phys. Status Solidi B*, in press.
(207) Imamura, A.; Fujita, H. *J. Chem. Phys.* **1974**, *61*, 115.
(208) Ricart, J. M.; Illas, F.; Dovesi, R.; Pisani, C.; Roetti, C. *Chem. Phys. Lett.* **1984**, *108*, 593.
(209) Dovesi, R.; Pisani, C.; Roetti, C.; Ricart, J. M.; Illas, F. *Surf. Sci.* **1984**, *148*, 225.
(210) Zonnevylle, M. C.; Hoffmann, R. *Langmuir* **1987**, *3*, 452. Silvestre, J.; Hoffmann, R. *Langmuir* **1985**, *1*, 621. Sung, S.-S.; Hoffmann, R. *J. Am. Chem. Soc.* **1985**, *107*, 578. Saillard, J.-Y.; Hoffmann, R. *J. Am. Chem. Soc.* **1984**, *106*, 2006.
(211) Anderson, A. B. *J. Chem. Phys.* **1975**, *63*, 4430.
(212) Ray, N. K.; Anderson, A. B. *Surf. Sci.* **1983**, *125*, 803. Anderson, A. B.; Mehandru, S. P.; Smialek, J. L. *J. Electrochem. Soc.* **1985**, *132*, 1695. Anderson, A. B.; Onwood, D. P. *Surf. Sci.* **1985**, *154*, L261. Mehandru, S. P.; Anderson, A. B. *J. Catal.* **1986**, *100*, 210. Mehandru, S. P.; Anderson, A. B. *Surf. Sci.* **1986**, *169*, L281. Anderson, A. B.; Ravimohan, C.; Mehandru, S. P. *Surf. Sci.* **1987**, *183*, 438. Anderson, A. B.; Dowd, D. Q. *J. Phys. Chem.* **1987**, *91*, 869.
(213) Holzschuh, E. *Phys. Rev. B: Condens. Matter* **1983**, *28*, 7346.
(214) Kunc, K.; Martin, R. M. *Physica B+C: (Amsterdam)* **1983**, *117B, 118B*, 511.
(215) Martin, R. M. In Reference 11, p 175.
(216) Kunc, K. In Reference 11, p 227.
(217) Louie, S. G. In Reference 11, p 335.
(218) Nielsen, O. H.; Martin, R. M. In Reference 11, p 313.
(219) Chon, M. Y.; Lam, P. K.; Cohen, M. L. *Solid State Commun.* **1982**, *42*, 861.
(220) Zunger, A.; Freeman, A. J. *Phys. Rev. B: Solid State* **1977**, *15*, 5049.
(221) Cohen, M. L. *Phys. Rep.* **1981**, *110*, 293.
(222) Euwema, R. N.; Surratt, G. T.; Wilhite, D. L.; Wepfer, G. G. *Philos. Mag.* **1974**, *29*, 1033.
(223) Zunger, A.; Freeman, A. J. *Int. J. Quantum Chem., Quantum Chem. Symp.* **1977**, *No. 11*, 539.
(224) Adams, W. H. *J. Chem. Phys.* **1962**, *37*, 2009.
(225) Gilbert, T. L. In *Molecular Orbitals in Chemistry, Physics and Biology*; Löwdin, P.-O., Pullman, P., Eds.; Academic: New York, 1964; p 405.
(226) Kunz, A. B.; Klein, D. L. *Phys. Rev. B: Condens. Matter* **1978**, *17*, 4614.
(227) Walch, S. P. *Surf. Sci.* **1984**, *143*, 188.
(228) Whitten, J. L.; Pakkanen, T. A. *Phys. Rev. B: Condens. Matter* **1980**, *21*, 4357.
(229) Whitten, J. L. *Phys. Rev. B: Condens. Matter* **1981**, *24*, 1810.
(230) Cremaschi, P.; Whitten, J. L. *Phys. Rev. Lett.* **1981**, *46*, 1242.
(231) Cremaschi, P.; Whitten, J. L. *Surf. Sci.* **1981**, *112*, 343.
(232) Madhaven, P. V.; Whitten, J. L. *Surf. Sci.* **1981**, *112*, 38.
(233) Madhaven, P.; Whitten, J. L. *J. Chem. Phys.* **1982**, *77*, 2673.
(234) Cremaschi, P.; Whitten, J. L. *Chem. Phys. Lett.* **1984**, *111*, 215.
(235) Beckmann, H. O. *J. Electron Spectrosc. Relat. Phenom.* **1983**, *29*, 77.
(236) Cremaschi, P.; Whitten, J. L. *Theor. Chim. Acta* **1987**, *72*, 485.
(237) Fischer, C. R.; Burke, L. A.; Whitten, J. L. *Phys. Rev. Lett.* **1982**, *49*, 344.
(238) Fischer, C. R.; Whitten, J. L. *Phys. Rev. B: Condens. Matter* **1984**, *30*, 6821.
(239) Cremaschi, P.; Whitten, J. L. *Surf. Sci.* **1985**, *149*, 273.
(240) Bagus, P. S.; Bauschlicher, C. W., Jr.; Nelin, C. J.; Laskowski, B. C.; Seel, M. *J. Chem. Phys.* **1984**, *81*, 3594; **1985**, *83*, 914.
(241) Hermann, K.; Bagus, P. S.; Nelin, C. J. *Phys. Rev. B: Condens. Matter* **1987**, *35*, 9467.
(242) Daudey, J. P. PS HONDO, a modified version of the HONDO program.
(243) Bagus, P. S.; Hermann, K.; Bauschlicher, C. W., Jr. *J. Chem. Phys.* **1984**, *81*, 1966.
(244) Avoiris, Ph.; Bagus, P. S.; Rossi, A. R. *J. Vac. Sci. Technol., B* **1985**, *3*, 1484.
(245) Hermann, K.; Bagus, P. S.; Bauschlicher, C. W., Jr. *Phys. Rev. B: Condens. Matter* **1984**, *30*, 7313.
(246) Hermann, K.; Bagus, P. S.; Bauschlicher, C. W., Jr. *Phys. Rev. B: Condens. Matter* **1985**, *31*, 6371.
(247) Nakatsuji, H.; Hada, M. *J. Am. Chem. Soc.* **1985**, *107*, 8264.
(248) Bagus, P. S.; Hermann, K.; Seel, M. *J. Vac. Sci. Technol.* **1981**, *18*, 435.
(249) Kao, C. M.; Messmer, R. P. *Phys. Rev. B: Condens. Matter* **1985**, *31*, 4835.
(250) Blomberg, M. R. A.; Brandemark, U. B.; Siegbahn, P. E. M. *Chem. Phys. Lett.* **1986**, *126*, 317.
(251) Bauschlicher, C. W., Jr. *J. Chem. Phys.* **1986**, *84*, 260.
(252) Bauschlicher, C. W., Jr. *Chem. Phys.* **1986**, *106*, 391.
(253) Ewald, P. P. *Ann. Phys. (Paris)* **1921**, *64*, 253.
(254) Tennyson, J.; Murrell, J. N. *Mol. Phys.* **1981**, *42*, 297.
(255) Murrel, J. N.; Tennyson, J.; Kamel, M. A. *Mol. Phys.* **1981**, *42*, 747.
(256) Winter, N. W.; Pitzer, R. M.; Temple, D. K. *J. Chem. Phys.* **1987**, *86*, 3549.
(257) Winter, N. W.; Pitzer, R. M.; Temple, D. K. *J. Chem. Phys.* **1987**, *87*, 2945.
(258) Kung, A. Y. S.; Kunz, A. B.; Vail, J. M. *Phys. Rev. B: Condens. Matter* **1982**, *26*, 3352.
(259) Saul, P.; Catlow, C. R. A.; Kendrick, J. *Philos. Mag. B* **1985**, *51*, 107.
(260) Momany, F. A. *J. Phys. Chem.* **1978**, *82*, 592.
(261) Smit, P. H.; Derissen, J. L.; Van Duijneveldt, F. B. *Mol. Phys.* **1979**, *37*, 521.
(262) Cox, S. R.; Williams, D. E. *J. Comput. Chem.* **1981**, *2*, 304.
(263) Sauer, J.; Morgeneyer, C.; Schröder, K.-P. *J. Phys. Chem.* **1984**, *88*, 6375.
(264) Singh, U. C.; Kollman, P. A. *J. Comput. Chem.* **1984**, *5*, 129.
(265) Fowler, P. W.; Madden, P. A. *Mol. Phys.* **1983**, *49*, 913.
(266) Fowler, P. W.; Madden, P. A. *Phys. Rev. B: Condens. Matter* **1984**, *29*, 1035.
(267) Fowler, P. W.; Pyper, N. C. *Proc. R. Soc. London, A* **1985**, *398*, 377.
(268) Fowler, P. W.; Madden, P. A. *J. Phys. Chem.* **1985**, *89*, 2581.
(269) Gutowski, M.; Kakol, M.; Piela, L. *Int. J. Quantum Chem.* **1983**, *23*, 1843.
(270) Murrel, J. N.; Tennyson, J. *Chem. Phys. Lett.* **1980**, *69*, 212.

(271) Vail, J. M.; Harker, A. H.; Harding, J. H.; Saul, P. *J. Phys. C* **1984**, *17*, 3401.

(272) Abarenkov, I. V.; Bratcev, V. F.; Tulub, A. V. *Solid State Phys.* **1982**, *24*, 272.

(273) Noell, J. O.; Morokuma, K. *J. Phys. Chem.* **1976**, *80*, 2675.

(274) Lunell, S. *J. Chem. Phys.* **1984**, *80*, 6185.

(275) Cummins, P. L.; Bacskay, G. B.; Hush, N. S.; Halle, B.; Engström, S. *J. Chem. Phys.* **1985**, *82*, 2002.

(276) Taurian, O. E.; Lunell, S. *J. Phys. Chem.* **1987**, *91*, 2249.

(277) Bridet, J.; Fliszar, S.; Odiot, S.; Pick, R. *Int. J. Quantum Chem.* **1983**, *24*, 687.

(278) Fink, W. H.; Butkus, A. M.; Lopez, J. P. *Int. J. Quantum Chem., Quantum Chem. Symp.* **1979**, *No. 13*, 331.

(279) Litinskii, A. O.; Zyubin, A. S. *Zh. Strukt. Khim.* **1984**, *25*(4), 11.

(280) Gibbs, G. V. *Am. Mineral.* **1982**, *67*, 421.

(281) Gibbs, G. V.; Meagher, E. P.; Newton, M. D.; Swanson, D. K. In Reference 10, Vol. 1, p 195.

(282) Geisinger, K. L.; Gibbs, G. V.; Navrotsky, A. *Phys. Chem. Miner.* **1985**, *11*, 266.

(283) Zupan, J.; Buh, M. *J. Non-Cryst. Solids* **1978**, *27*, 127.

(284) Sauer, J., calculations for this review.

(285) Wolff, R.; Radeglia, R.; Sauer, J. *THEOCHEM* **1986**, *139*, 113.

(286) Sauer, J.; Lange, R., to be submitted for publication.

(287) Fripiat, J. G.; Galet, P.; Delhalle, J.; André, J. M.; Nagy, J. B.; Derouane, E. G. *J. Phys. Chem.* **1985**, *89*, 1932.

(288) Derouane, E. G.; Fripiat, J. G. *Zeolites* **1985**, *5*, 165.

(289) Sauer, J., unpublished work. Cf. ref 563.

(290) Pauling, L. *The Nature of the Chemical Bond*, 3rd ed.; Cornell University: Ithaca, NY, 1960.

(291) Redondo, A.; Goddard, W. A., III; Swarts, C. A.; McGill, T. C. *J. Vac. Sci. Technol.* **1981**, *19*, 498.

(292) Zur, A.; McGill, T. C.; Goddard, W. A., III; *Thirteenth International Conference on Defects in Semiconductors*, Coronado, CA, Aug 12–17, 1984; AIME: Warrendale, PA, 1985; p 235.

(293) Goddard, W. A., III; Redondo, A.; McGill, T. C. *Solid State Commun.* **1976**, *18*, 981.

(294) Li, Y. P.; Ching, *Phys. Rev. B: Condens. Matter* **1985**, *31*, 2172.

(295) Newton, M. D.; Gibbs, G. V. *Phys. Chem. Miner.* **1980**, *6*, 221.

(296) Hill, R. J.; Newton, M.; Gibbs, G. V. *J. Solid State Chem.* **1983**, *47*, 185.

(297) Downs, J. W.; Hill, R. J.; Newton, M. D.; Tossell, J. A.; Gibbs, G. V. In *Electron Distribution and the Chemical Bond*; Coppens, D., Hall, M. B., Eds.; Plenum: New York, 1981; p 173.

(298) Malvido, J. C.; Whitten, J. L. *Phys. Rev. B: Condens. Matter* **1982**, *26*, 4458.

(299) Surratt, G. T.; Goddard, W. A., III *Phys. Rev. B: Condens. Matter* **1978**, *18*, 2831.

(300) Raghavachari, K. *J. Chem. Phys.* **1986**, *84*, 5672.

(301) Sauer, J.; Engelhardt, G. *Z. Naturforsch. A: Phys., Phys. Chem., Kosmophys.* **1982**, *37A*, 277.

(302) O'Keeffe, M.; Domengès, B.; Gibbs, G. V. *J. Phys. Chem.* **1985**, *89*, 2304.

(303) Čársky, P.; Hess, B. A., Jr.; Schaad, L. J. *J. Am. Chem. Soc.* **1983**, *105*, 396.

(304) Blom, C. E.; Altona, C. *Mol. Phys.* **1976**, *31*, 1377.

(305) Pulay, P.; Fogarasi, G.; Pang, F.; Boggs, J. E. *J. Am. Chem. Soc.* **1979**, *101*, 2550.

(306) Pulay, P.; Fogarasi, G.; Pongor, G.; Boggs, J. E.; Vargha, A. *J. Am. Chem. Soc.* **1983**, *105*, 7037.

(307) Sauer, J.; Zurawski, B. *Chem. Phys. Lett.* **1979**, *65*, 587.

(308) Griscom, D. L. *J. Non-Cryst. Solids* **1977**, *24*, 155.

(309) Piela, L.; Pietronero, L.; Resta, R. *Phys. Rev. B: Solid State* **1973**, *7*, 5321.

(310) Newton, M. D. *J. Phys. Chem.* **1983**, *87*, 4288.

(311) Andzelm, J.; Piela, L. *J. Phys. C* **1977**, *10*, 2269.

(312) Andzelm, J.; Piela, L. *J. Phys. C* **1978**, *11*, 2695.

(313) Pertsin, A. J.; Kitaigorodsky, A. I. *The Atom-Atom Potential Method. Applications to Organic Molecular Solids*; Springer Series in Chemical Physics; Springer-Verlag: Berlin, 1987; Vol. 43.

(314) Newton, M. D. *Acta Crystallogr. B: Struct. Sci.* **1983**, *39*, 104.

(315) Kim, K. S.; Dupuis, M.; Lie, G. C.; Clementi, E. *Chem. Phys. Lett.* **1986**, *131*, 451.

(316) Morse, M. D.; Rice, S. A. *J. Chem. Phys.* **1982**, *76*, 650.

(317) Yoon, B. J.; Morokuma, K.; Davidson, E. R. *J. Chem. Phys.* **1985**, *83*, 1223.

(318) Smit, P. H.; Derissen, J. L.; Van Duijneveldt, F. B. *Mol. Phys.* **1979**, *37*, 521.

(319) Scheiner, S.; Nagle, J. F. *J. Phys. Chem.* **1983**, *87*, 4267.

(320) Matsuoka, O.; Clementi, E.; Yoshimine, M. *J. Chem. Phys.* **1976**, *64*, 1351.

(321) Chałasinski, G.; Gutowski, M. *Chem. Rev.* **1988**, *88*, 943.

(322) Hobza, P.; Zahradnik, R. *Chem. Rev.* **1988**, *88*, 871.

(323) Kofranek, M.; Karpfen, A.; Lischka, H. *Chem. Phys.* **1987**, *113*, 53.

(324) O'Shea, S. F.; Santry, D. P. *Theor. Chim. Acta* **1975**, *37*, 1.

(325) Andersen, S. G.; Santry, D. P. *J. Chem. Phys.* **1981**, *74*, 5780.

(326) Raynor, S. *J. Chem. Phys.* **1987**, *87*, 2790.

(327) Raynor, S. *J. Chem. Phys.* **1987**, *87*, 2795.

(328) Löwdin, P. O. *Adv. Phys.* **1956**, *5*, 1.

(329) Plummer, P. L. M. *J. Phys. Colloq.* **1987**, *48*(C-1), 45.

(330) Cummins, P. L.; Bacskay, G. B.; Hush, N. S. *Mol. Phys.* **1987**, *61*, 795.

(331) Cummins, P. L.; Bacskay, G. B.; Hush, N. S. *Mol. Phys.* **1987**, *62*, 193.

(332) Fowler, P. W. *J. Chem. Soc., Faraday Trans. 2* **1986**, *82*, 61.

(333) Laaksonen, A.; Corongiu, G.; Clementi, E. *Int. J. Quantum Chem., Quantum Chem. Symp.* **1984**, *No. 18*, 131.

(334) Laaksonen, A.; Clementi, E. *Mol. Phys.* **1985**, *56*, 495.

(335) Harding, J. H.; Harker, A. H. *Philos. Mag. B* **1985**, *51*, 119.

(336) Surratt, G. T.; Kunz, A. B. *Solid State Commun.* **1977**, *23*, 555.

(337) Broughton, J. Q.; Bagus, P. S. *Phys. Rev. B: Condens. Matter* **1984**, *30*, 4761.

(338) Broughton, J. Q.; Bagus, P. S. *Phys. Rev. B: Condens. Matter* **1987**, *36*, 2813.

(339) Green, T. A.; Jennison, D. R.; Melius, C. F.; Binkley, J. S. *Phys. Rev. B: Condens. Matter* **1987**, *36*, 3469. Green, T. A.; Jennison, D. R. *Phys. Rev. B: Condens. Matter* **1987**, *36*, 6112.

(340) Shashkin, S. Y.; Goddard, W. A., III *Phys. Rev. B: Condens. Matter* **1986**, *33*, 1353. Shashkin, S. Y.; Goddard, W. A., III *J. Phys. Chem.* **1986**, *90*, 255.

(341) Janssen, G. J. M.; Nieuwpoort, W. C. *Solid State Ionics* **1985**, *16*, 29.

(342) Janssen, G. J. M.; Nieuwpoort, W. C. *Philos. Mag. B* **1985**, *B51*, 127.

(343) Johansen, H.; Andersen, N. K. *Mol. Phys.* **1986**, *58*, 965.

(344) Fowler, P. W.; Hutson, J. M. *Phys. Rev. B: Condens. Matter* **1986**, *33*, 3742.

(345) Catlow, C. R. A.; Mackrodt, W. C. Computer Simulation of Solids. *Lect. Notes Phys.* **1982**, *166*.

(346) Euwema, R. N.; Wepfer, G. G.; Surratt, G. T.; Wilhite, D. L. *Phys. Rev. B: Solid State* **1974**, *B9*, 5249.

(347) Campbell, J. C.; Hillier, I. H.; Mackrodt, W. C. Cited by: Catlow, C. R. A.; Dixon, M.; Mackrodt, W. C. In Reference 345, p 130.

(348) Chang, K. J.; Cohen, M. L. *Phys. Rev. B: Condens. Matter* **1984**, *30*, 4774.

(349) Colbourn, E. A.; Mackrodt, W. C. *Surf. Sci.* **1982**, *117*, 571.

(350) Colbourn, E. A.; Kendrick, J.; Mackrodt, W. C. *Surf. Sci.* **1983**, *126*, 550.

(351) (a) Kunz, A. B.; Guse, M. P.; Blint, R. J. *Int. J. Quantum Chem., Quantum Chem. Symp.* **1976**, *No. S10*, 283. (b) Kunz, A. B.; Guse, M. P. *Chem. Phys. Lett.* **1977**, *45*, 18.

(352) Fujioka, H.; Yamabe, S.; Yanagisawa, Y. *Surf. Sci.* **1985**, *149*, L53.

(353) Derouane, E. G.; Fripiat, J. G.; André, J. M. *Chem. Phys. Lett.* **1974**, *28*, 445. Derouane, E. G.; Fripiat, J. G.; André, J. M. *Chem. Phys. Lett.* **1975**, *35*, 525. Derouane, E. G.; Fripiat, J. G.; André, J. M. *Theor. Chim. Acta* **1977**, *43*, 239.

(354) Abarenkov, I. V.; Tretjak, V. M.; Tulub, A. V. *Khim. Fiz.* **1985**, *4*(7), 974.

(355) Surratt, G. T.; Kunz, A. B. *Phys. Rev. B: Solid State* **1979**, *19*, 2352.

(356) Surratt, G. T.; Kunz, A. B. *Phys. Rev. Lett.* **1978**, *40*, 347.

(357) Kunz, A. B. *Philos. Mag. B* **1985**, *B51*, 209.

(358) Wepfer, G. G.; Surratt, G. T.; Weidmen, R. S.; Kunz, A. B. *Phys. Rev. B: Condens. Matter* **1980**, *B21*, 2596.

(359) Colbourn, E. A.; Mackrodt, W. C. *Surf. Sci.* **1984**, *143*, 391.

(360) Pope, S. A.; Hillier, I. H.; Guest, M. F.; Colbourn, E. A.; Kendrick, J. *Surf. Sci.* **1984**, *139*, 299.

(361) Julg, A.; Favier, A.; Ozias, Y. *Surf. Sci.* **1986**, *165*, L53.

(362) (a) Deprick, B.; Julg, A. *Chem. Phys. Lett.* **1984**, *110*, 150. (b) Julg, A.; Deprick, B. *Croat. Chem. Acta* **1984**, *57*, 85.

(363) Sauer, J.; Fiedler, K.; Schirmer, W.; Zahradnik, R. *Proceedings of the Fifth International Conference on Zeolites*, Naples, Italy, June 2–6, 1980; Rees, L. C. V., Ed.; Heyden: London, 1980; p 501.

(364) Wood, J. C. *Surf. Sci.* **1978**, *71*, 548.

(365) Hurst, R. P. *Phys. Rev.* **1959**, *114*, 746.

(366) Gijzeman, O. L. J.; van Zandvoort, M. M. J. *J. Chem. Soc., Faraday Trans. 2* **1984**, *80*, 771.

(367) Gready, J. E.; Bacskay, G. B.; Hush, N. S. *J. Chem. Soc., Faraday Trans. 2* **1978**, *74*, 1430.

(368) Gready, J. E.; Bacskay, G. B.; Hush, N. S. *Chem. Phys.* **1978**, *31*, 375.

(369) Boys, S. F.; Bernardi, F. *Mol. Phys.* **1970**, *19*, 553.

(370) Yamada, H.; Kojima, T. *J. Phys. C* **1985**, *18*, 731.

(371) Liebmann, P.; Loew, G.; McLean, A. D.; Pack, G. R. *J. Am. Chem. Soc.* **1982**, *104*, 691.

(372) Marynick, D. S.; Schaefer, H. F., III *Proc. Natl. Acad. Sci. U.S.A.* **1975**, *72*, 3794.

(373) Sauer, J.; Hobza, P. *Theor. Chim. Acta* **1984**, *65*, 291.
(374) Lieske, N. P. *J. Phys. Chem. Solids* **1984**, *45*, 821.
(375) Bock, C. W.; Trachtman, M.; Maker, P. D.; Niki, H.; Mains, G. J. *J. Phys. Chem.* **1986**, *90*, 5669.
(376) Bock, C. W.; Trachtman, M.; Mains, G. J. *J. Phys. Chem.* **1988**, *92*, 294.
(377) Guth, J.; Petuskey, W. T. *J. Phys. Chem. Solids* **1987**, *48*, 541.
(378) Lüthi, H. P.; Almlöf, J. *Chem. Phys. Lett.* **1987**, *135*, 357.
(379) Almlöf, J.; Lüthi, H. P. *Theoretical Methods and Results for Electronic Structure Calculations on Very Large Systems: Carbon Clusters*; UMSI Report 82/20; University of Minnesota: Minneapolis, 1987.
(380) Reed, W. A.; Snyder, L. C.; Eisenberger, P.; Pinder, X. J.; Weber, T.; Wasserman, Z. *J. Chem. Phys.* **1977**, *67*, 143.
(381) Snyder, L. C.; Wasserman, Z. *Surf. Sci.* **1978**, *71*, 407.
(382) Barone, V.; Lelj, F.; Russo, N.; Toscano, M. *Surf. Sci.* **1985**, *162*, 169.
(383) Surratt, G. T.; Goddard, W. A., III *Solid State Commun.* **1977**, *22*, 413.
(384) (a) Barone, V.; Lelj, F.; Iacouis, E.; Illas, F.; Russo, N.; Jonnon, A. *THEOCHEM* **1986**, *136*, 313. (b) Barone, V.; Lelj, F.; Minichino, C.; Russo, N.; Toscano, M. *Surf. Sci.* **1987**, *189/190*, 185.
(385) Fink, W. H. *Appl. Surf. Sci.* **1982**, *11/12*, 677.
(386) Barone, V.; Lelj, F.; Russo, N.; Toscano, M.; Illas, R.; Rubio, J. *Phys. Rev. B: Condens. Matter* **1986**, *B34*, 7203.
(387) Sahoo, N.; Mishra, S. K.; Mishra, K. C.; Coker, A.; Das, T. P.; Mitra, C. K.; Snyder, L. C. *Phys. Rev. Lett.* **1983**, *50*, 913.
(388) Claxton, T. A.; Evans, A.; Symons, M. C. R. *J. Chem. Soc., Faraday Trans. 2* **1986**, *82*, 2031.
(389) Snyder, L. C.; Corbett, J. W. In *Thirteenth International Conference on Defects in Semiconductors, Coronado, CA, Aug 12–17, 1984*; TMS-AIME, Defense Advanced Research Projects Agency, NASA, Office of Naval Research, Metallurgical Society AIME: Warrendale, PA, 1985; p 693.
(390) Kenton, A. C.; Ribarsky, M. W. *Phys. Rev. B: Condens. Matter* **1981**, *23*, 2897.
(391) Redondo, A.; Goddard, W. A., III; McGill, T. C. *Phys. Rev. B: Solid State* **1977**, *15*, 5038.
(392) Goddard, W. A., III; Barton, J. J.; Redondo, A.; McGill, T. C. *J. Vac. Sci. Technol.* **1978**, *15*, 1274.
(393) Snyder, L. C.; Wasserman, Z. *Surf. Sci.* **1978**, *77*, 52.
(394) Zeiri, Y.; Low, J. J.; Goddard, W. A., III *J. Chem. Phys.* **1986**, *84*, 2408.
(395) Snyder, L. C.; Wasserman, Z.; Moskowitz, J. W. *J. Vac. Sci. Technol.* **1979**, *16*, 1266.
(396) Redondo, A.; Goddard, W. A., III; McGill, T. C. *Phys. Rev. B: Condens. Matter* **1981**, *24*, 6135.
(397) Chabal, Y. J.; Raghavachari, K. *Phys. Rev. Lett.* **1984**, *53*, 282.
(398) Chabal, Y. J.; Raghavachari, K. *Phys. Rev. Lett.* **1985**, *54*, 1055.
(399) Hermann, K.; Bagus, P. S. *Phys. Rev. B: Condens. Matter* **1979**, *20*, 1603.
(400) Seel, M.; Bagus, P. S. *Phys. Rev. B: Condens. Matter* **1981**, *23*, 5464.
(401) Seel, M.; Bagus, P. S. *Phys. Rev. B: Condens. Matter* **1983**, *28*, 2023.
(402) Seel, M. *Int. J. Quantum Chem.* **1981**, *19*, 1083.
(403) Illas, F.; Rubio, J.; Ricart, J. M. *Phys. Rev. B: Condens. Matter* **1985**, *31*, 8068.
(404) Masip, J.; Rubio, J.; Illas, F. *Chem. Phys. Lett.* **1985**, *120*, 513.
(405) Batra, I. P.; Bagus, P. S.; Hermann, K. *Phys. Rev. Lett.* **1984**, *52*, 384.
(406) Batra, I. P.; Bagus, P. S.; Hermann, K. *J. Vac. Sci. Technol. B* **1984**, *2*, 1075.
(407) Plans, J.; Diaz, G.; Martinez, E.; Yudurain, F. *Phys. Rev. B: Condens. Matter* **1987**, *B35*, 788. Martinez, E.; Plans, J.; Yudurain, F. *Phys. Rev. B: Condens. Matter* **1987**, *B36*, 8043. Ortega-Blake, I.; Taguena-Martinez, J.; Barrio, R. A.; Martinez, E.; Yudurain, F., submitted for publication in *Phys. Rev. B: Condens. Matter*.
(408) Ignacio, E. W.; Schlegel, H. B.; Bicerano, J. *Chem. Phys. Lett.* **1986**, *127*, 367.
(409) Broer, R.; Aissing, G.; Nieuwopoort, W. C.; Feiner, L. F. *Int. J. Quantum Chem.* **1986**, *29*, 1059.
(410) Sworts, C. A.; Goddard, W. A., III; McGill, T. C. *J. Vac. Sci. Technol.* **1980**, *17*, 982.
(411) Barton, J. J.; Goddard, W. A., III; McGill, T. C. *J. Vac. Sci. Technol.* **1979**, *16*, 1178.
(412) Chang, R.; Goddard, W. A., III *Surf. Sci.* **1985**, *149*, 341.
(413) Allen, W. D.; Schaefer, H. F., III *Chem. Phys.* **1986**, *108*, 243.
(414) Garrison, B. J.; Goddard, W. A., III *J. Chem. Phys.* **1987**, *87*, 1307.
(415) Schlegel, H. B. *J. Phys. Chem.* **1984**, *88*, 6254.
(416) Whiteside, R. A.; Frisch, M. J.; Pople, J. A. *The Carnegie-Mellon Quantum Chemistry Archive*, 3rd Ed.; Carnegie-Mellon University: Pittsburgh, 1983.

(417) Hess, A. C.; McMillan, P. F.; O'Keeffe, M. *J. Phys. Chem.* **1986**, *90*, 5661.
(418) Schlegel, H. B.; Sosa, C. *J. Phys. Chem.* **1985**, *89*, 537.
(419) Schneider, W.; Thiel, W. *J. Chem. Phys.* **1987**, *86*, 923.
(420) Tully, J. C.; Chabal, Y. J.; Raghavachari, K.; Bowman, J. M.; Lucchese, R. R. *Phys. Rev. B: Condens. Matter* **1985**, *31*, 1184.
(421) Sykja, B.; Lunell, S. *Surf. Sci.* **1984**, *141*, 199.
(422) Iler, R. K. *The Chemistry of Silica. Solubility, Polymerization, Colloid and Surface Properties, and Biochemistry*; Wiley: New York, 1979.
(423) Liebau, F. *Structural Chemistry of Silicates. Bonding and Classification*; Springer-Verlag: Berlin, 1985.
(424) Pantelides, S. T. *The Physics of SiO₂ and Its Interfaces*; Pergamon: New York, 1978.
(425) Breck, D. W. *Zeolite Molecular Sieves. Structure, Chemistry, and Use*; Wiley-Interscience: New York, 1974.
(426) Barrer, R. M. *Zeolites and Clay Minerals as Sorbents and Molecular Sieves*; Academic: London, 1978.
(427) Murakami, Y.; Iijima, A.; Ward, J. W. *New Developments in Zeolite Science and Technology*; Kodansha: Tokyo, 1986.
(428) Grobet, P. J.; Mortier, W. J.; Vansant, E. F.; Schulz-Ekloff, G., Eds. *Studies in Surface Science and Catalysis*; Elsevier: Amsterdam, 1988; Vol. 37.
(429) Imelik, B.; Et al., Eds. *Metal-Support and Metal-Additive Effects in Catalysis*; Elsevier: Amsterdam, 1982.
(430) Olson, D. H.; Kokotailo, G. T.; Lawton, S. W.; Meier, W. M. *J. Phys. Chem.* **1981**, *85*, 2238.
(431) Meier, W. M.; Olson, D. H. *Atlas of Zeolites Structure Types*; Juris Druck: Zürich and Polycrystal Book Service: Pittsburgh, 1978.
(432) Flanigen, E. M.; Lok, B. M.; Patton, R. L.; Wilson, S. T. In Reference 427, p 103.
(433) Sauer, J.; Zahradnik, R. *Int. J. Quantum Chem.* **1984**, *26*, 793.
(434) Mezey, P. G. In *Catalytic Materials: Relationship Between Structure and Reactivity*; ACS Symposium Series 248; Whyte, T. E., Jr., Betta, A. D., Derouane, E. G., Baker, R. T. K., Eds.; American Chemical Society: Washington, DC 1984; p 145.
(435) Navrotsky, A.; Geisinger, K. L.; McMillan, P.; Gibbs, G. V. *Phys. Chem. Miner.* **1985**, *11*, 284.
(436) Boisen, M. B., Jr.; Gibbs, G. V. *Phys. Chem. Miner.*, in press.
(437) Tsukada, M.; Adachi, H.; Satoko, C. *Prog. Surf. Sci.* **1983**, *14*, 113.
(438) Anderson, A. B. *Chem. Phys. Lett.* **1980**, *76*, 155.
(439) Ooms, G.; van Santen, R. A. *Recl.: J. R. Neth. Chem. Soc.* **1987**, *106*, 69. Ooms, G.; van Santen, R. A.; Jackson, R. A.; Catlow, C. R. A. In Reference 428, p 317.
(440) Van Santen, R. A.; Keijsper, J.; Ooms, G.; Kortbeek, A. G. T. G. In Reference 427, p 169.
(441) Gilbert, T. L.; Stevens, W. J.; Schrenk, H.; Yoshimine, M.; Bagus, P. S. *Phys. Rev. B: Solid State* **1973**, *B8*, 5977.
(442) Collins, G. A. D.; Cruickshank, D. W. J.; Breeze, A. *J. Chem. Soc., Faraday Trans. 2* **1972**, 1189.
(443) Sauer, J.; Hobza, P.; Zahradnik, R. *J. Phys. Chem.* **1980**, *84*, 3318.
(444) Derouane, E. G.; Fripiat, J. G. Proceedings, 6th International Zeolite Conference, Reno, 1983; p 717.
(445) Grigoras, S.; Lane, T. H. *J. Comput. Chem.* **1987**, *8*, 84.
(446) Meier, R.; Ha, T.-K. *Phys. Chem. Miner.* **1980**, *6*, 37.
(447) Roelandt, F. F.; Van de Vondel, D. F.; Van der Kelen, G. P. *THEOCHEM* **1981**, *76*, 187.
(448) Revesz, A. G.; Gibbs, G. V. Proceedings, Conference on the Physics of MOS Insulators, Raleigh, NC, June 1980.
(449) Oberhammer, H.; Boggs, J. E. *J. Am. Chem. Soc.* **1980**, *102*, 7241.
(450) Ernst, C. A.; Allred, A. L.; Ratner, M. A.; Newton, M. D.; Gibbs, G. V.; Moskowitz, J. W.; Topiol, S. *Chem. Phys. Lett.* **1981**, *81*, 424.
(451) Hess, A. C.; McMillan, P. F.; O'Keeffe, M. *J. Phys. Chem.* **1987**, *91*, 1395.
(452) Luke, B. T.; Gupta, A. G.; Loew, G. H.; Lawless, J. G.; White, D. H. *Int. J. Quantum Chem., Quantum Biol. Symp.* **1984**, *No. 11*, 117.
(453) Ignatjev, I. S.; Schegolev, B. F.; Lazarev, A. N. *Dokl. Acad. Nauk. SSSR* **1986**, *285*(5), 1140.
(454) Sauer, J. *Chem. Phys. Lett.* **1983**, *97*, 275.
(455) Sauer, J., calculation for this review.
(456) Dolin, S. P.; Schegolev, B F.; Lazarev, A. N. *Dokl. Acad. Nauk. SSSR* **1988**, *298*(1), 131.
(457) Boonstra, L. H.; Mijlhoff, F. C.; Renes, G.; Spelbos, A.; Hargittai, I. *J. Mol. Struct.* **1975**, *28*, 129.
(458) Lehn, J. M.; Wipff, G.; Demuynck, J. *Chem. Phys. Lett.* **1980**, *76*, 344.
(459) Ross, N. L.; Meagher, E. P. *Am. Mineral.* **1984**, *69*, 1145.
(460) Shluger, A. *J. Phys. Chem. Solids* **1986**, *47*, 659.
(461) Geisser, C.; Shluger, A. *Phys. Status Solidi B* **1986**, *135*, 669.
(462) Pacansky, J.; Hermann, K. *J. Chem. Phys.* **1978**, *69*, 963.
(463) Corradi, G.; Bartram, R. H.; Rossi, A. R.; Janszky, J. *J. Phys. Chem. Solids* **1987**, *48*, 675.

(464) Fripiat, J. G.; Berger-André, J.-M.; Derouane, E. G. *Zeolites* **1983**, *3*, 306.
(465) Lazarev, A. N. *Vibrational Spectra and Structure of Silicates*; Consultants Bureau: New York, 1972.
(466) Blackwell, C. S. *J. Phys. Chem.* **1979**, *83*, 3251.
(467) Blackwell, C. S. *J. Phys. Chem.* **1979**, *83*, 3257.
(468) O'Keeffe, M.; McMillan, P. F. *J. Phys. Chem.* **1986**, *90*, 541.
(469) Newton, M. D.; O'Keeffe, M.; Gibbs, G. V. *Phys. Chem. Miner.* **1980**, *6*, 305.
(470) Brenstein, R. J.; Scheiner, S. *Int. J. Quantum Chem.* **1986**, *29*, 1191.
(471) O'Keeffee, M.; Gibbs, G. V. *J. Phys. Chem.* **1985**, *89*, 4574.
(472) Kudo, T.; Nagase, S. *J. Am. Chem. Soc.* **1985**, *107*, 2589.
(473) Lasaga, A. C.; Gibbs, G. V. *Phys. Chem. Miner.* **1987**, *14*, 107.
(474) Tossell, J. A.; Lazzeretti, P. *Chem. Phys.* **1987**, *112*, 205.
(475) Tossell, J. A.; Lazzeretti, P. *J. Chem. Phys.* **1986**, *84*, 369.
(476) Hass, E. C.; Mezey, P. G.; Plath, P. J. *THEOCHEM* **1981**, *76*, 389.
(477) Hass, E. C.; Mezey, P. G.; Plath, P. J. *THEOCHEM* **1982**, *87*, 261.
(478) Downs, J. W.; Gibbs, G. V. *Am. Mineral.* **1981**, *66*, 819.
(479) Gibbs, G. V.; Finger, L. W.; Boisen, M. B., Jr. *Phys. Chem. Miner.* **1987**, *14*, 327.
(480) Mombourquette, M. J.; Weil, J. A.; Mezey, P. G. *Can. J. Phys.* **1984**, *62*, 21.
(481) Mombourquette, M. J.; Weil, J. A. *Can. J. Phys.* **1985**, *63*, 1282.
(482) Mombourquette, M. J.; Weil, J. A. *J. Magn. Reson.* **1986**, *66*, 105.
(483) Isoya, J.; Weil, J. A.; Halliburton, L. E. *J. Chem. Phys.* **1981**, *74*, 5436.
(484) Dixon, D. A.; Gole, J. L. *Chem. Phys. Lett.* **1986**, *125*, 179.
(485) Bedford, K. L.; Kunz, A. B. *Solid State Commun.* **1981**, *38*, 411.
(486) Sauer, J.; Bleiber, A. *Catal. Today* **1988**, *3*, 485.
(487) Zhang, Z. G.; Boisen, M. B., Jr.; Finger, L. W.; Gibbs, G. V. *Am. Mineral.* **1985**, *70*, 1238.
(488) Gupta, A.; Tossell, J. A. *Am. Mineral.* **1983**, *68*, 989.
(489) Gupta, A.; Tossell, J. A. *Phys. Chem. Miner.* **1981**, *7*, 159.
(490) Fjeldberg, T.; Gundersen, G.; Jonvik, T.; Seip, H. M.; Saebo, S. *Acta Chem. Scand., Ser. A* **1980**, *A34*, 547.
(491) Gajhede, M. *Chem. Phys. Lett.* **1985**, *120*, 266.
(492) Geisinger, K. L.; Gibbs, G. V. *Phys. Chem. Miner.* **1981**, *7*, 204.
(493) Lehn, J. M.; Munsch, B. *J. Chem. Soc. D* **1970**; 994. Gordon, M. S. *Chem. Phys. Lett.* **1986**, *126*, 451.
(494) Julian, M. M.; Gibbs, G. V. *J. Phys. Chem.* **1985**, *89*, 5476.
(495) Edwards, A. H.; Fowler, W. B. In *Structure and Bonding in Noncrystalline Solids*; Walrafen, G. E., Revesz, A. G., Eds.; Plenum: New York, 1986; p 139.
(496) Sauer, J.; Schirmer, W. In *Innovation in Zeolite Materials Science (Studies in Surface Science and Catalysis)*; Grobet, P. J., Mortier, W. J., Vansant, E. F., Schulz-Ekloff, G., Eds.; Elsevier: Amsterdam, 1988; p 323.
(497) Beran, S. *J. Phys. Chem.* **1988**, *92*, 766.
(498) Pluth, J. J.; Smith, J. V. *J. Am. Chem. Soc.* **1980**, *102*, 4704.
(499) Sauer, J.; Mix, H.; Pfeifer, H., unpublished results. Mix, H. Ph.D. Thesis, Karl Marx University, Leipzig, 1987.
(500) Hill, J.-R.; Sauer, J. *Z. Phys. Chem. (Leipzig)*, in press.
(501) Datka, J.; Geerlings, P.; Mortier, W.; Jacobs, P. *J. Phys. Chem.* **1985**, *89*, 3483.
(502) Datka, J.; Geerlings, P.; Mortier, W.; Jacobs, P. *J. Phys. Chem.* **1985**, *89*, 3488.
(503) Mix, H.; Sauer, J.; Schröder, K.-P.; Merkel, A. *Collect. Czech. Chem. Commun.* **1988**, *53*, 2191.
(504) Lermer, H.; Draeger, M.; Steffen, J.; Unger, K. K. *Zeolites* **1985**, *5*, 131.
(505) Catlow, C. R. A.; et al. Ab initio Potentials for Zeolites, mentioned by Prof. Clementi during his lecture at the WATOC'87 Meeting, Budapest, 1987.
(506) Knözinger, H. In *The Hydrogen Bond*; Schuster, P., Zundel, G., Sandorfy, C., Eds.; North-Holland: Amsterdam, 1976; Vol. 3, p 1263.
(507) Boehm, H. P.; Knözinger, H. In *Catalysis—Science and Technology*; Akademie-Verlag: Berlin, 1983; Vol. 4, Chapter 2, p 39.
(508) Van Roosmalen, A. J.; Mol, J. C. *J. Phys. Chem.* **1979**, *83*, 2485.
(509) Fink, P.; Plotzki, I. *Wiss. Z.-Friedrich-Schiller-Univ. Jena, Math.-Naturwiss. Reiche* **1980**, *29*, 809.
(510) Fink, P.; Müller, B. *Wiss. Z.-Friedrich-Schiller-Univ. Jena Math.-Naturwiss. Reiche* **1981**, *30*, 589.
(511) Popowski, E.; Holst, N.; Kelling, H. *Z. Anorg. Allg. Chem.* **1982**, *494*, 166.
(512) Holdt, H. J.; Popowski, E.; Kelling, H. *Z. Anorg. Allg. Chem.* **1984**, *519*, 233.

(513) West, R.; Baney, R. H. *J. Am. Chem. Soc.* **1959**, *81*, 6145.
(514) Harris, G. I. *J. Chem. Soc.* **1963**, 5978.
(515) Nillius, O.; Kriegsmann, H., unpublished results. Nillius, O. Ph.D. Thesis, Humboldt University, Berlin, 1965.
(516) Pelmenshchikov, A. G.; Pavlov, V. I.; Zhidomirov, G. M.; Beran, S. *J. Phys. Chem.* **1987**, *91*, 3325.
(517) Geerlings, P.; Tariel, N.; Botrel, A.; Lissillour, R.; Mortier, W. J. *J. Phys. Chem.* **1984**, *88*, 5752.
(518) O'Malley, P. J.; Dwyer, J. *Chem. Phys. Lett.* **1988**, *143*, 97.
(519) Kustov, L. M.; Borovkov, V. Y.; Kazansky, V. B. *J. Catal.* **1981**, *72*, 149.
(520) Kazansky, V. B.; Kustov, L. M.; Borovkov, V. Y. *Zeolites* **1983**, *3*, 77.
(521) Kawakami, H.; Yoshida, S.; Yonezawa, T. *J. Chem. Soc., Faraday Trans. 2* **1984**, *80*, 205.
(522) Kawakami, H.; Yoshida, S. *J. Chem. Soc., Faraday Trans. 2* **1985**, *81*, 1117.
(523) Senchenya, I. N.; Chuvylkin, N. D.; Kazansky, V. B. *Kinet. Katal.* **1986**, *23*, 87.
(524) Derouane, E. G.; Fripiat, J. G. *J. Phys. Chem.* **1987**, *91*, 145.
(525) Kawakami, H.; Yoshida, S. *J. Chem. Soc., Faraday Trans. 2* **1986**, *82*, 1385.
(526) Senchenya, I. N.; Kazansky, V. B.; Beran, S. *J. Phys. Chem.* **1986**, *90*, 4857.
(527) Kawakami, H.; Yoshida, S. *J. Chem. Soc., Faraday Trans. 2* **1984**, *80*, 921.
(528) Kawakami, H.; Yoshida, S. *J. Chem. Soc., Faraday Trans. 2* **1985**, *81*, 1129.
(529) Vetrivel, R.; Catlow, C. R. A.; Colbourn, E. A. In Reference 428, p 309.
(530) Bernholc, J.; Horsley, J. A.; Murrell, L. L.; Sherman, L. G.; Soled, S. *J. Phys. Chem.* **1987**, *91*, 1526.
(531) Bauschlicher, C. W., Jr. *Int. J. Quantum Chem., Quantum Chem. Symp.* **1986**, *No. 20*, 563.
(532) Sauer, J. Doctor of Science Thesis, Forschungsbereich Chemie, Academy of Sciences, Berlin, 1985.
(533) Sauer, J.; Deininger, D. *J. Phys. Chem.* **1982**, *86*, 1327.
(534) Sauer, J.; Deininger, D. *Zeolites* **1982**, *2*, 114.
(535) Ruelle, P.; Hö Nam-Tran; Buchmann, M.; Kesselring, U. W. *Theochem* **1984**, *109*, 177.
(536) Sauer, J.; Morgeneyer, C. *Stud. Biophys.* **1983**, *93*, 253.
(537) Senchenya, I. N.; Chuvylkin, N. D.; Kazansky, V. B. *Kinet. Katal.* **1985**, *26(5)*, 1073.
(538) Senchenya, I. N.; Mikheikin, I. D.; Zhidomirov, G. M.; Trokhimets, A. I. *Kinet. Katal.* **1983**, *24(1)*, 35.
(539) Senchenya, I. N.; Chuvylkin, N. D.; Kazansky, V. B. *Kinet. Katal.* **1986**, *27(3)*, 608.
(540) Senchenya, I. N.; Mikheikin, I. D.; Zhidomirov, G. M.; Kazansky, V. B. *Kinet. Katal.* **1981**, *22(5)*, 1174.
(541) Zelenkovskii, V. M.; Zhidomirov, G. M.; Kazansky, V. B. *React. Kinet. Catal. Lett.* **1984**, *24*, 15.
(542) Hobza, P.; Sauer, J.; Morgeneyer, C.; Hurych, J.; Zahradnik, R. *J. Phys. Chem.* **1981**, *85*, 4061.
(543) Sauer, J.; Schröder, K.-P. *Z. Phys. Chem. (Leipzig)* **1985**, *266*, 379.
(544) Sauer, J. *Acta Chim. Phys., Szeged* **1985**, *31*, 19.
(545) Hobza, P.; Zahradnik, R. *Chem. Phys. Lett.* **1981**, *82*, 473.
(546) Chakoumakos, B. C.; Gibbs, G. V. *J. Phys. Chem.* **1986**, *90*, 996.
(547) Clementi, E. Computational Aspects for Large Chemical Systems. *Lect. Notes Chem.* **1980**, *No. 19*.
(548) Marchese, F. T.; Mehrotra, P. K.; Beveridge, D. L. *J. Phys. Chem.* **1982**, *86*, 2592.
(549) Marchese, F. T.; Mehrotra, P. K.; Beveridge, D. L. *J. Phys. Chem.* **1981**, *85*, 1.
(550) Vigne-Maeder, F. *Chem. Phys. Lett.* **1987**, *133*, 337.
(551) Claverie, P. In *Intermolecular Interactions: From Diatomics to Biopolymers*; Pullman, B., Ed.; Wiley: New York, 1978; Chapter 2, p 69.
(552) Kono, H.; Takasaka, A. *J. Phys. Chem.* **1987**, *91*, 4044.
(553) Fiedler, K.; Grauert, B. *Adsorpt. Sci. Technol.* **1986**, *3*, 181.
(554) Leherte, L.; Vercauteren, D. P.; Derouane, E. G.; André, J. M. In Reference 428, p 293.
(555) Demontis, P.; Fois, E. S.; Gamba, A.; Manunza, B.; Suffritti, G. B. *Theochem* **1983**, *93*, 245.
(556) Demontis, P.; Suffritti, G. B.; Quartieri, S.; Fois, E. S.; Gamba, A. In *Dynamics of Molecular Crystals Proceedings of the 41st International Meeting of the Societe Francaise de Chimie, Division de Chimie Physique*; Lascombe, J., Ed.; Elsevier: Amsterdam, 1987; p 699.
(557) Demontis, P.; Suffritti, G. B.; Quartiery, S.; Fois, E. S.; Gamba, A. *J. Phys. Chem.* **1988**, *92*, 867.
(558) Vega, L.; Breton, J.; Girardet, C.; Galatry, L. *J. Chem. Phys.* **1986**, *84*, 5171.
(559) Kobayashi, H.; Yamaguchi, M.; Tanaka, T.; Yoshida, S. *J. Chem. Soc., Faraday Trans. 1* **1985**, *81*, 1513.
(560) Bacalis, N. C.; Kunz, A. B. *Phys. Rev. B: Condens. Matter* **1985**, *B32*, 4857.

(561) Zdetsis, A. D.; Kunz, A. B. *Phys. Rev. B: Condens. Matter* **1982**, *B26*, 4756.
(562) Zdetsis, A. D.; Kunz, A. B. *Phys. Rev. B: Condens. Matter* **1985**, *B32*, 6358.
(563) Sauer, J.; Haberlandt, H.; Schirmer, W. In *Structure and Reactivity of Modified Zeolites*; Jacobs, P. A., Et al., Eds.;

Elsevier: Amsterdam, 1984; p 313.
(564) Haberlandt, H.; Sauer, J.; Pacchioni, G. *Theochem* **1987**, *149*, 297.
(565) Jaeger, N. I.; Ryder, P.; Schulz-Eckloff, G. In *Structure and Reactivity of Modified Zeolites*; Jacobs, P. A., Et al., Eds.; Elsevier: Amsterdam, 1984; p 299.